ST. GEORGE ISLAND BRIDGE PILE TESTING

Principal Investigator:	H. R. (Trey) Hamilton III, P.E., Ph.D.
Graduate Research Assistants:	Eric Cannon, E.I. Claire Lewinger, E.I. Caesar Abi, Ph.D.
Project Manager:	Marcus Ansley, P.E.

Department of Civil & Coastal Engineering
College of Engineering
University of Florida
Gainesville, Florida 32611

Engineering and Industrial Experiment Station

DISCLAIMER

The opinions, findings, and conclusions expressed in this publication are those of the authors and not necessarily those of the State of Florida Department of Transportation.

Technical Report Documentation Page

1. Report No.	2. Government Accession No.	3. Recipient's Catalog No.
4. Title and Subtitle St. George Island Bridge Pile Testing		5. Report Date June 2006
		6. Performing Organization Code
7. Author(s) Eric Cannon, Claire Lewinger, Caesar Abi, and H. R. Hamilton III		8. Performing Organization Report No. 00051711
9. Performing Organization Name and Address University of Florida Department of Civil & Coastal Engineering P.O. Box 116580 Gainesville, FL 32611-6580		10. Work Unit No. (TRAIS)
		11. Contract or Grant No. BD545, RPWO#27
12. Sponsoring Agency Name and Address Florida Department of Transportation Research Management Center 605 Suwannee Street, MS 30 Tallahassee, FL 32301-8064		13. Type of Report and Period Covered Final Report
		14. Sponsoring Agency Code

15. Supplementary Notes

16. Abstract

This report presents the results of a series of tests aimed at evaluating the existing capacity of precast pretensioned concrete piles that had been in service in a harsh salt-water environment for approximately 40 years. In 2004 the Bryant Patton Bridge over Apalachicola Bay in the Florida panhandle was replaced. During demolition, twelve prestressed concrete piles with varying levels of corrosion damage were recovered. Two of the selected piles were equipped with a cathodic protection that had been installed in 1994 as part of a repair project involving most of the piles supporting the bridge. Flexural test results indicated that some of the piles had severe reduction in capacity while others had no loss of capacity when compared to the calculated capacity. For example, in the most extreme case, the pile was able to carry only 31% of its calculated capacity. Some piles, however, were able to sustain loads higher than the rated capacity. In 7 of the 12 piles (58%) the normalized visual rating was within 10% of the normalized moment capacity. In only one pile (8%) was the capacity overestimated and in the remainder of the piles (34%) the capacities were underestimated by the normalized visual ratings.

Corrosion potentials measured on selected piles were related to the flexural capacity. It was found that when the average corrosion potential was less than -350 mV$_{CSE}$ over an approximate height of 1 ft. above the MHW, then 100% of the pile capacity remained. In the case where the corrosion potential was less than -350 mV$_{CSE}$ for 5 ft. above the MHW, then approximately 32% of the pile capacity remained.

The prestressing strand from a third recovered cathodically protected pile was sampled for dissolved hydrogen to determine the potential for hydrogen embrittlement. The dissolved hydrogen content averaged 2.0 ppm for the outer wires and 1.4 ppm for the inner wires of prestressing strands from a cathodically protected pile. The hydrogen content of the outer wires of a strand from an unprotected pile averaged 0.92 ppm.

To investigate the effect of the elevated levels of hydrogen on the mechanical properties of the strand, a ductility factor for each pile was calculated from the flexural test results. These factors were used to compare the ductility of the cathodically protected piles with the unprotected piles to determine if the strands appeared to be susceptible to hydrogen embrittlement. One of the cathodically protected piles had a ductility factor greater than all but two unprotected piles, while the other had a ductility factor greater than only two of the unprotected piles. This same pile also had a comparable reduction in flexural capacity, which may have been due to severe corrosion occurring prior to the installation of cathodic protection. In summary, there is no clear trend indicating that hydrogen embrittlement had affected the capacity or ductility of these piles. Based on this comparison, there does not appear to have been a significant loss of ductility in the CP piles when compared with unprotected piles.

Three precast post-tensioned cylinder piles from the Escambia Bay bridge carrying route I-10 were also tested to determine flexural capacity. All three piles retained at least their calculated flexural capacity. No significant corrosion was noted on the prestressing wire during post-test excavation.

17. Key Word piling, prestressed, concrete, corrosion, inspection, pretensioned	18. Distribution Statement No restrictions. This document is available to the public through the National Technical Information Service, Springfield, VA, 22161		
19. Security Classif. (of this report) Unclassified	20. Security Classif. (of this page) Unclassified	21. No. of Pages 113	22. Price

Form DOT F 1700.7 (8-72)   Reproduction of completed page authorized

ACKNOWLEDGMENTS

EXECUTIVE SUMMARY

This report presents the results of a series of tests aimed at evaluating the existing capacity of precast pretensioned concrete piles that had been in service in a harsh salt-water environment for approximately 40 years. In 2004 the Bryant Patton Bridge over Apalachicola Bay in the Florida panhandle was replaced. During demolition, twelve prestressed concrete piles with varying levels of corrosion damage were recovered. Two of the selected piles were equipped with cathodic protection that had been installed in 1994 as part of a repair project involving most of the piles supporting the bridge. Flexural test results indicated that some of the piles had severe reduction in capacity while others had no loss of capacity when compared to the calculated capacity. For example, in the most extreme case, the pile was able to carry only 31% of its calculated capacity. Some piles, however, were able to sustain loads higher than the rated capacity.

Visual inspections were conducted by District Two Florida Department of Transportation (FDOT) divers on the selected piles before they were removed. Visual ratings were assigned to each pile by the researchers based on photographs and notes taken by FDOT district 2 field personnel during their site visit. These ratings were then normalized to allow comparison with the tested flexural capacities of the piles. In 7 of the 12 piles (58%) the normalized visual rating was within 10% of the normalized moment capacity. In only one pile (8%) was the capacity overestimated and in the remainder of the piles (34%) the capacities were underestimated by the normalized visual ratings.

Corrosion potentials measured on selected piles were related to the flexural capacity. It was found that when the average corrosion potential was less than -350 mV$_{CSE}$ over an approximate height of 1 ft. above the MHW, then 100% of the pile capacity remained. In the case where the corrosion potential was less than -350 mV$_{CSE}$ for 5 ft. above the MHW, then approximately 32% of the pile capacity remained.

The prestressing strand from a third recovered cathodically protected pile was sampled for dissolved hydrogen to determine the potential for hydrogen embrittlement. The dissolved hydrogen content averaged 2.0 ppm for the outer wires and 1.4 ppm for the inner wires of prestressing strands from a cathodically protected pile. The hydrogen content of the outer wires of a strand from an unprotected pile averaged 0.92 ppm.

To investigate the effect of the elevated levels of hydrogen on the mechanical properties of the strand, a ductility factor for each pile was calculated from the flexural test results. These factors were used to compare the ductility of the cathodically protected piles with that of the unprotected piles to determine if the strands appeared to be susceptible to hydrogen embrittlement. One of the cathodically protected piles had a ductility factor greater than all but two unprotected piles, while the other had a ductility factor greater than only two of the unprotected piles. The reduced ductility of pile 44-3CP is mirrored by the reduced flexural capacity, which may have been due to severe corrosion that occurred prior to the installation of cathodic protection. In summary, no clear trend was found indicating that hydrogen embrittlement had affected the capacity or ductility of the CP piles.

Three precast post-tensioned cylinder piles from the Escambia Bay bridge carrying route I-10 were also tested to determine flexural capacity. All three piles retained at least their calculated flexural capacity. No significant corrosion was noted on the prestressing wire during post-test excavation.

TABLE OF CONTENTS

1 INTRODUCTION

The Bryant Patton Bridge (also known as the St. George Island Bridge) was constructed in 1965 to link the mainland Florida panhandle to St. George Island (bridge numbers 4900003 and 4900004). In 2004, the Bridge was replaced to improve traffic flow and because many of piles on the existing bridge had been badly damaged by corrosion (Figure 1). Some piles were severely corroded in spite of relatively recent extensive repairs. To study the effect of long-term exposure of prestressed concrete piles to the severe coastal environment, twelve prestressed concrete piles with varying levels of corrosion damage were recovered and structurally tested after being inspected visually. Two of the selected piles were equipped with cathodic protection, which had been installed as part of the 1994 repairs. Water samples taken in 1995 by the Department showed chloride levels at 16730 ppm and sulfates at 2829 ppm.

Figure 1 – Corrosion Damaged Pile

This report details the selection, recovery and testing of the piles. During the recovery operation, after the piles were selected, in-situ visual inspections were conducted, which are reported herein. In addition, prestressing strands from a single pile that had been cathodically protected since 1994 were sampled for chemical composition and hydrogen content. Corrosion potentials were taken on selected piles prior to extraction and chloride samples were taken from selected piles after recovery but before structural testing. Details of the structural testing and results are presented and compared to the visual ratings of the piles.

Also presented in this report are the test details and results for precast, post-tensioned cylinder piles that were recovered from Route I-10 over Escambia Bay after Hurricane Ivan in 2004.

2 SCOPE AND OBJECTIVES

Rating bridges is primarily visual and requires judgment to quantify loss of capacity when the element has corrosion damage. Furthermore, very little information on the long-term effects of cathodic protection on the structural and mechanical properties of the concrete and prestressing steel are available. The data gathered as part of this research project can be used to improve visual and other rating systems of corrosion damaged elements and to confirm that cathodic protection does not cause long-term problems with structural capacity. The data and findings from this report have already been used by FDOT District Two to aid in their evaluation, maintenance, and planning with respect to pilings in salt water.

3 STRUCTURE DESCRIPTION

The causeway portion of the existing bridge carried two lanes of traffic with a narrow elevated sidewalk and concrete barrier on each side of the roadway. The concrete deck was supported by four AASHTO Type II prestressed concrete girders with spans varying between 30 and 50 ft. The girders were supported by prestressed pile bents with a cast-in-place cap beam.

Construction records indicated that the prestressed piles had a 20-in square cross-section and were prestressed with twenty 7/16-in. diameter stress-relieved prestressing strands (Figure 2). The records further indicated that each strand was prestressed to 18.9 kips and that the pile ends were reinforced with No. 5 gage spiral ties. Design clear cover over the prestressing strand was 3-in. Measurements of effective depth d were made at each end of the piles after extraction and are given in Section 7.
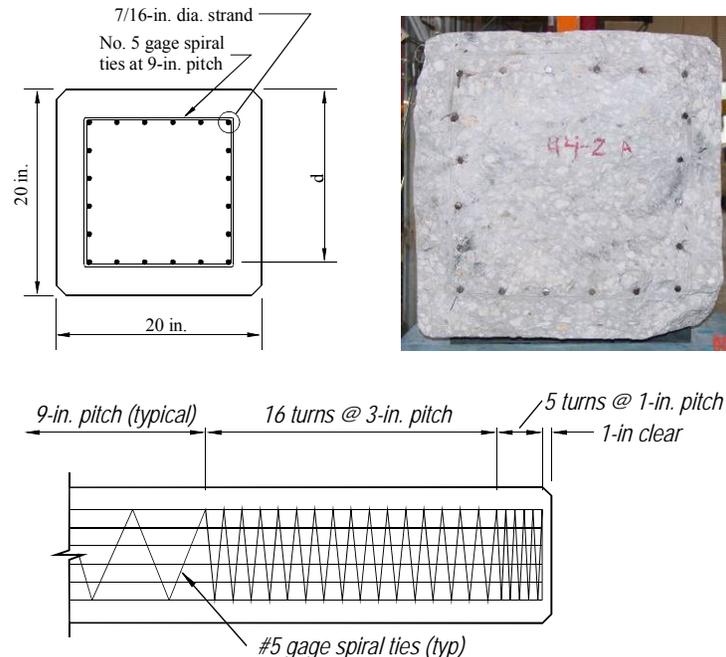
Figure 2 – Pile cross section and spiral details

The concrete specified on the construction drawings was a Class P. The 1959 Florida State Road Department standard specifications for road and bridge construction indicate that a

Class P concrete is for use in "all prestressed members and for concrete piles of all types." The 1959 specifications further indicate that a Class P mix had "been designed and tested in the Department's laboratory and has been shown to develop consistent cylinder strengths in excess of 5000psi at the age of 28 days." The mix proportions from the 1959 specifications are shown in Table 1.

Table 1 – Concrete specifications from 1959 FDOT specifications

Quantities per bag of cement		Theoretical Cement Factor in Barrels per yd^3	Slump Range (in.)	Air (%)
Maximum Water (gal)	Dry combined aggregates (lbs)			
4.8	473	1.625*	1-3	3-6

*This could be increased to 1.75 at the contractor's discretion

In 1994 extensive repairs were made to the prestressed piles including patching, installation of concrete jackets, and a galvanic cathodic protection system. In addition, a number of piles were so severely deteriorated that additional piles (termed "crutch" bents) were installed to share the bent loads. Figure 3a shows one such installation in which holes were cut in the deck to allow installation of the supplementary piles. Supporting cap beams were then cast under the existing cap beam to transfer load to the new piles. A three tiered galvanic cathodic protection was also installed as part of the repair process. Figure 3b shows the cathodic protection system in which the submerged portion of the pile was protected by a bulk zinc anode, the splash zone by a zinc mesh, and above the splash zone a sprayed zinc anode coating.

(a)   (b)

Figure 3 – Prestressed pile bents before bridge demolition. (a) "crutch bents" installed to relieve piles damaged by corrosion (b) cathodic protection system on existing piles

4   PILE RECOVERY AND SAMPLING

Figure 4 shows a plan layout of the bents from which the test piles were taken. The grid system shown in the figure is used to identify the piles in this report. The bent numbers match the official FDOT naming system in which the bents are numbered sequentially from south to north. The figure shows only those bents from which piles were recovered with the other intermediate bents omitted for clarity. Piles are identified by XX-X in which the first two digits

are the bent number and the last is the pile number. CP and J are added to the designations of piles with cathodic protection and jackets, respectively. Bents 31, 32, 33, and 40 also contain crutch bents, which are not considered in the naming system. Furthermore, bents 32 and 40 show piles in which the pile number does not match their location within the bent. Piles that were recovered for testing are identified along with piles fitted with cathodic protection; crutch bent piles; and piles that had been removed at the time of the district two inspection.
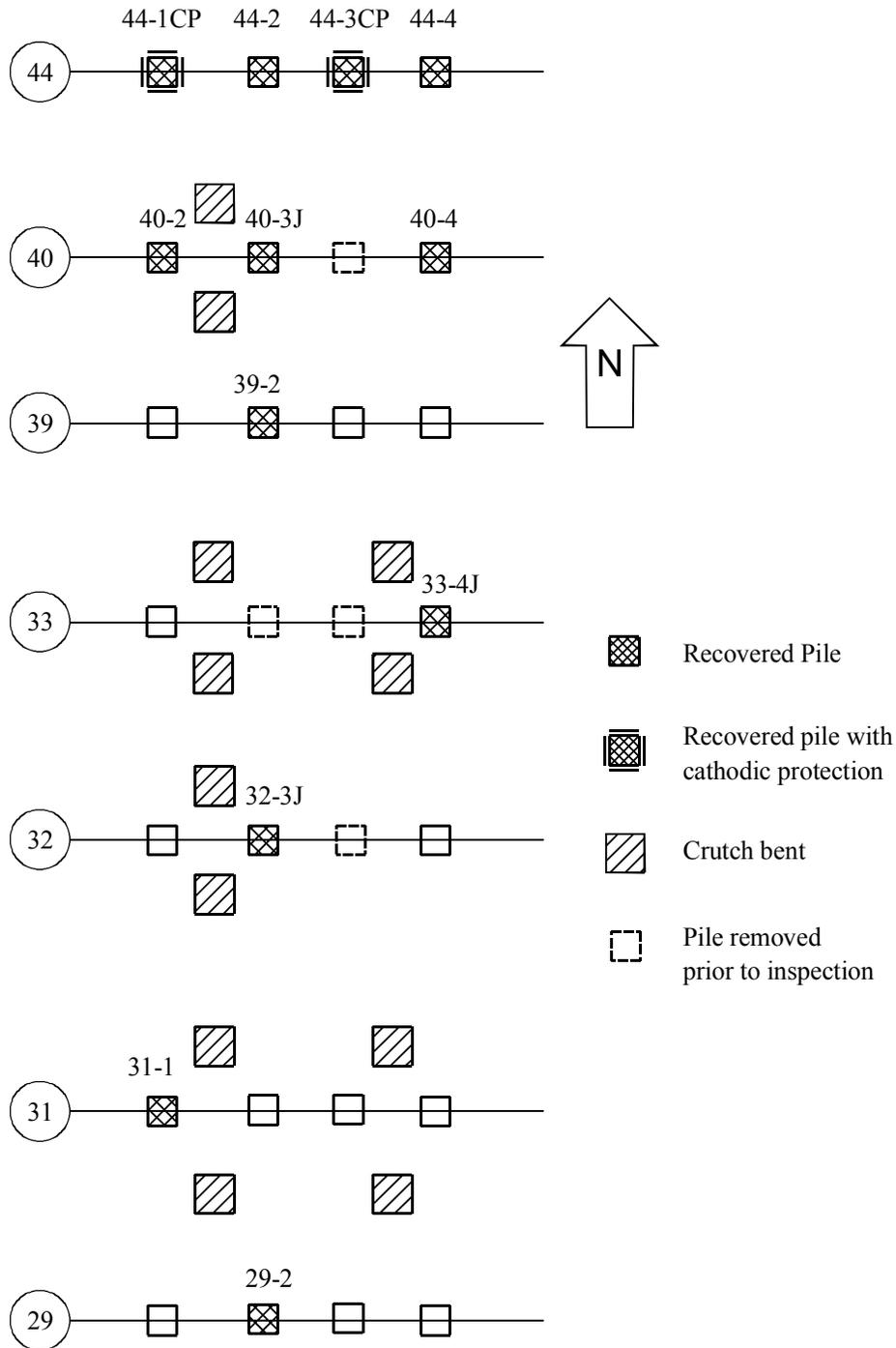
Figure 4 – Plan view of bents from which test piles were recovered

Table 2 shows the chronological steps taken from identification to destructive testing. Pile selection was made in December 2003. Before recovery began, several site visits were made. The first (March 2004) was by the University of Florida and the FDOT State Materials Office to check the operation of the cathodic protection system. At that time, potential measurements were taken on several randomly selected piles with CP to determine if the systems were still operating. The results of this testing are discussed in Section 4.1. The second site visit (May 2004) was conducted by FDOT District Two inspection personnel. The details of this inspection and pile conditions are included in Appendix A. The third visit was made by Concorr Florida, Inc. (under contract with FDOT) to conduct visual inspection, delamination survey, cover survey, and measure corrosion potentials. The results are included in Appendix B.

Table 2 – Chronology of pile recovery and testing

Date	Event	Purpose	Attending
12/23/03	Site visit	Select piles for Testing	UF, Boh Bros., FDOT
03/01/04	Site visit	Half cell potentials and instant off potentials, check operation of CP system	FDOT-SMO, UF
5/18/04	Pile Inspection	Independently evaluate in situ condition	FDOT District 2 Maintenance
5/19/04	Site visit	Visual inspection delamination survey cover survey corrosion potentials	Concorr Florida, Inc.
5/27/04	Site visit	Sample strands for dissolved hydrogen	UF, FDOT
5/2004 – 6/2004	Piles pulled and delivered to FDOT structures lab	N/A	Boh Bros., FDOT
7/15/04	Continuity survey of strands in FDOT structures lab	Confirm continuity of strands used in corrosion potential measurements	Concorr Florida, Inc.
10/20/04 – 11/03/04	Structural testing in FDOT Structures Lab		UF, FDOT
11/29/04	Chemistry sampled	Sample strands from non-CP pile for dissolved hydrogen	UF, FDOT
12/2/04	Cores taken	Samples for chloride content	Concorr Florida, Inc.

Recovery began in May and ended in June 2004. During recovery UF and FDOT personnel took strand samples from a CP pile for metallurgical evaluation. This pile was recovered from Bent 21 and is not shown on the pile plan figure. The details of this testing are given in Section 4.4. After piles were recovered and transported to the FDOT Structures Research Center in Tallahassee, Concorr Florida, Inc. checked continuity of the strands used to take corrosion potentials in the field and also drilled cores for chloride testing. The details of the potential and chloride testing are given in Section 4.1 and 4.3, respectively. Finally, the piles were testing to destruction in flexure. Following testing, strand samples were taken for tension testing (Section 5.2) and concrete cores were taken for compressive strength (Section 5.1).

The goal when selecting piles for recovery was to ensure that a wide range of corrosion damage and presumably a wide range of structural capacities were represented. The selections were based on the extent of spalling and rust staining visible during the inspection. Two cathodically protected piles were also selected for a total of 12 piles.

In January 2004 demolition of the bridge began with the removal of the deck slab and girders, which was completed before removal of the pile bents began. Removal of the pile bents entailed several steps. First, the cap beams were removed by cutting the tops of each pile with a "pile beaver". Figure 5a shows the bents after the cap beams had been removed. The "pile beaver" is a hydraulic shearing device (Figure 5b) that is either slipped over the exposed pile or fastened around the pile under the cap. The hydraulic actuators then push the cutting head through the pile, shearing the concrete and steel in a relatively clean manner. The next step was to use the pile beaver to cut the piles at the mud line for removal (Figure 5c and Figure 5d).

There was concern that the results of the structural testing would be adversely effected by the damage caused during pile removal. The cutting process, however, affected a relatively isolated area near the pile ends. Cracking and spalling of the concrete usually extended into the pile no more than 20-in. (Figure 5e).

(a)

(b)

(c)

(d)

(e)

Figure 5 – (a) Prestressed pile bents after cap removal; (b) Pile "beaver" used to cut the piles at the mud line; (c) Pile being lifted from the water after being cut; (d) Pile Recovery; (e) pile immediately after recovery. Note damage at end of pile from cutting.

4.1 IN SITU CORROSION POTENTIALS

Maintenance of the cathodic protection (CP) system had been abandoned some years earlier due to the impending bridge replacement. In addition, this particular CP design had not been used by FDOT in several years. To determine what portion of the CP system was still operational, corrosion and instant off potentials were taken on selected piles fitted with CP (Table 3). It was determined that all of the connections from the zinc mesh to the prestressing steel in the selected piles were deficient. The bulk anode connections, however, were intact, with the exception of Pile 40-4. Instant off values with the electrode in the water indicated that the bulk anode was still providing protection to the strands below the water line. Hartt, Kumria, and Kessler (1993) concluded that the application of cathodic polarization with potentials more negative than -900 mV$_{cse}$ (Copper sulfate electrode) may generate atomic hydrogen and lead to fracture. The polarization levels indicated by the instant-off potentials are such that hydrogen may be generated at the level of the prestressing steel. Consequently, it was decided to sample strands from one of the piles for hydrogen immediately after extraction. When the potentials were taken on these piles, it was noted that the top of CP jacket was approximately 3 feet above high tide.

Table 3 – Prestressing strand potential (volts) in reference to copper/copper sulfate electrode

Location	Pile 44 - 1		Pile 44 - 3		Pile 40 - 4		Pile 39 - 3	
	On	Instant Off	On	Instant Off	On*	Instant Off	On	Instant Off
In Water	-1.029	-1.016	-1.024	-1.012	-1.013	N/A	-1.024	-1.023
6-in. A.H.T.**	-0.645	-0.709	-0.721	-0.718	-0.844	N/A	-0.750	-0.742
1-ft A.H.T.	-0.529	-0.587	-0.579	-0.612	-0.649	N/A	-0.690	-0.665
2-ft A.H.T.	-0.362	-0.343	-0.488	-0.376	-0.644	N/A	-0.465	-0.459
3-ft A.H.T.	-0.251	-0.241	-0.495	-0.388	-0.487	N/A	-0.362	-0.386

* No instant off values are available because both of the anode connections (zinc sheet and bulk) were faulty on pile 40-4. The off potentials are noticeably high due to the extended coverage of arc sprayed zinc from the pile cap down toward the waterline.
**A.H.T. – Above High Tide

4.2 CORROSION POTENTIALS AFTER EXTRACTION

Corrosion potentials were measured on selected piles in the field prior to their extraction. Details of the testing are included in Appendix B. Corrosion potential values give an indication that the steel is at a potential that could lead to (or be an indication of) corrosion activity. Concrete moisture content and resistivity, among other things can have a significant effect on the potential readings. Furthermore, the potentials only provide an indication of the presence of corrosion activity and do not necessarily indicate corrosion rates.

The results of these tests are summarized in the plots shown in Figure 6, which show the corrosion potential relative to copper-copper sulfate electrode above the mean high water mark on the pile. Table 4 gives the range of potentials and their associated probability of occurrence. After the piles were extracted and moved to the FDOT Structures Laboratory, the electrical

continuity of the strands was checked against the strand used for the ground. Some of the noted data from piles 44-2, 32-3J, 40-3J were questionable due to lack of continuity.

The -350mV$_{CSE}$ demarcation on the plots provides an elevation below which corrosion activity was likely. Piles 39-2 and 40-3J have potentials more negative than -350mV$_{CSE}$ over most of the seven feet above MHW. Piles 40-4, 29-2, and 44-2 have potentials less negative than -350mV$_{CSE}$ over the height where measurements were taken, while pile 32-3J is split nearly evenly. These results will be related to the flexural capacities later in this report.
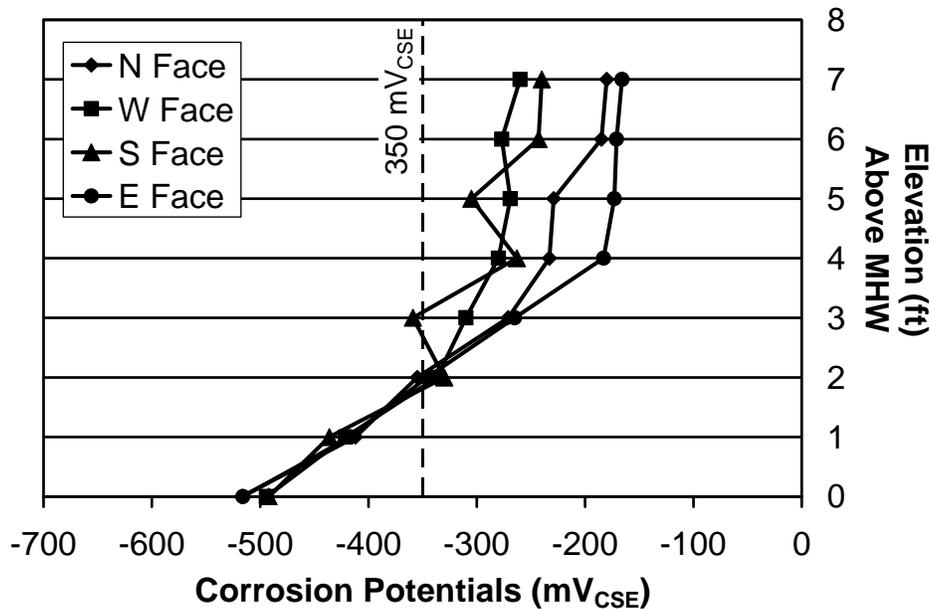
(a) Corrosion potentials at various heights of Pile 29-2
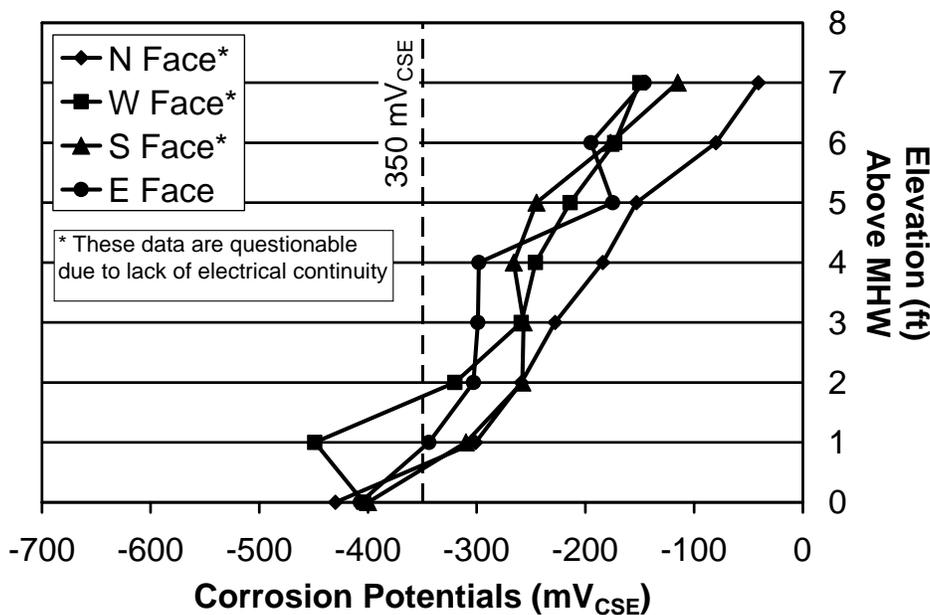
(b) Corrosion potentials at various heights of Pile 44-2
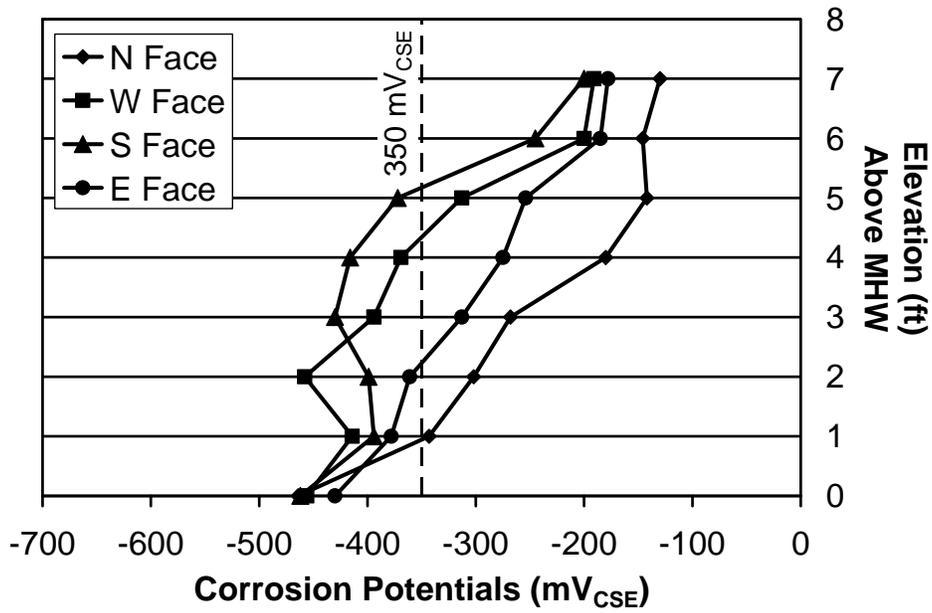
(c) Corrosion potentials at various heights of Pile 39-2
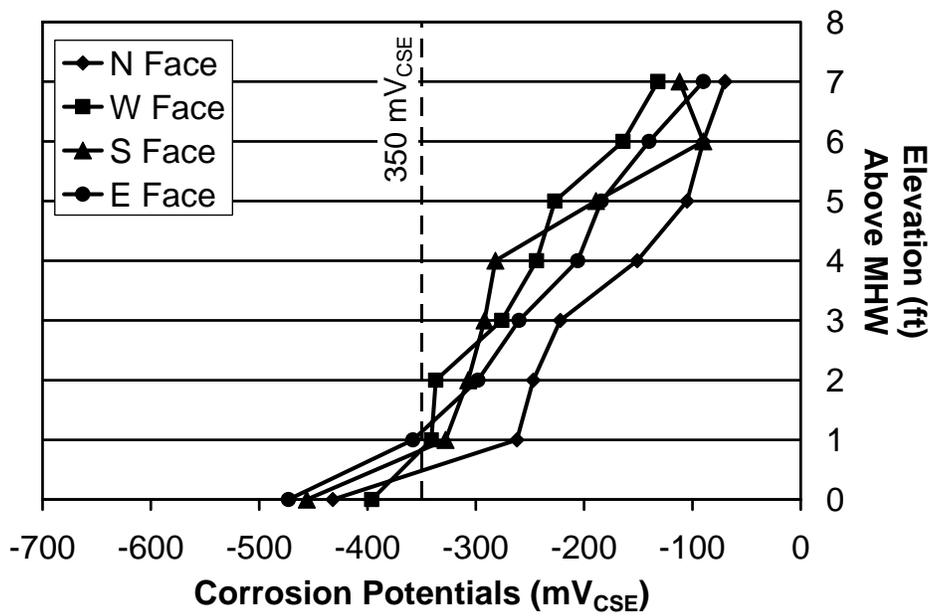
(d) Corrosion potentials at various heights of Pile 40-4
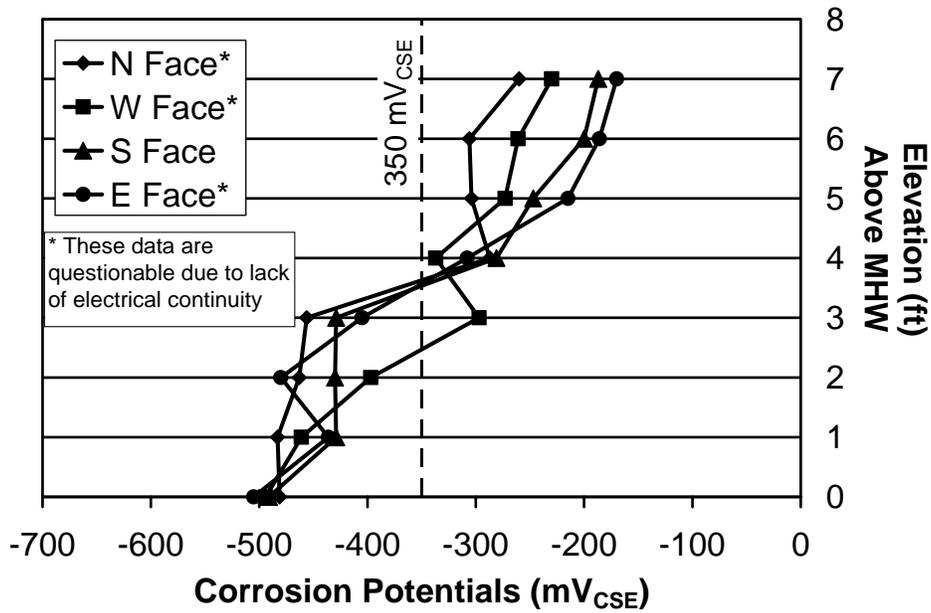
(e) Corrosion potentials at various heights of Pile 32-3J
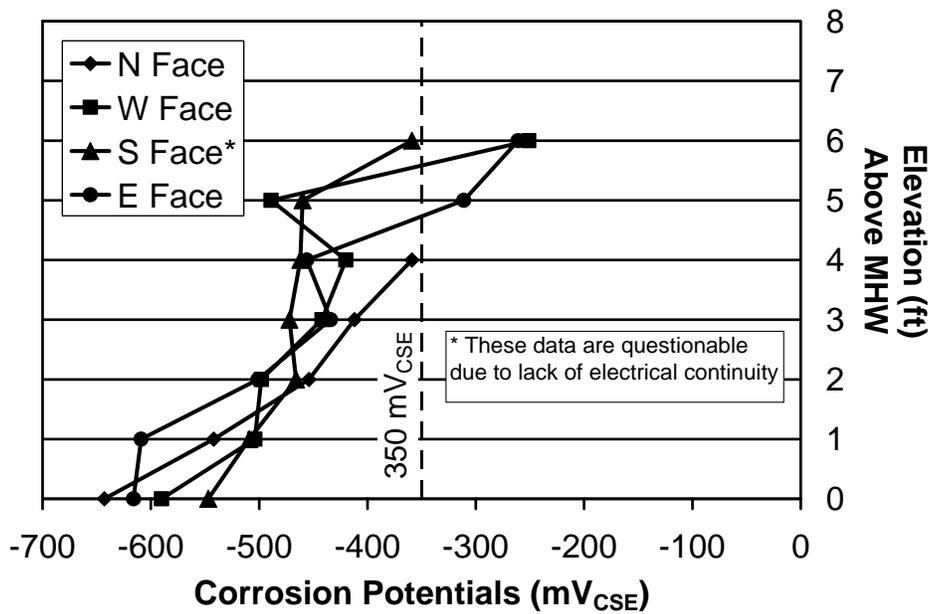
(f) Corrosion potentials at various heights of Pile 40-3J

Figure 6 – Corrosion potentials of selected piles. Measurements taken in the field.

Table 4 – Rating of corrosion activity based on potentials

Potential (mV vs CSE)	Probability of finding corrosion activity
-350 to -500	95%
-200 to -350	50%
< -200	5%

4.3 CHLORIDE TESTING

Cores were taken from two of the piles (32-3J and 44-2) to measure the chloride ion concentration of the concrete. The two piles were sampled while the piles were stored in the FDOT Structures Research Center awaiting flexural testing. Two-inch diameter cores were taken in four locations on their north face (as it was oriented in service). All cores were taken in sound concrete that contained no visibly apparent cracks, delaminations, spalls, or patching. The cores were drilled to 6 inches deep to ensure a minimum of 5 inch long cores. Figure 7 shows that the cores were distributed along the height of pile to include the submerged zone (6 feet below MHW), tidal zone (1 foot below MHW), splash zone (3 feet above MHW), and dry zone (7 feet above MHW). The tidal zone is the area between the low and high water marks and the splash zone is the area above the MHW that is subject to wetting and drying due to wave action and wicking of moisture.

The chloride profiles for each pile are plotted in Figure 8 and Figure 9. The *Florida Method of Test for Determining Low-Levels of Chloride in Concrete and Raw Materials Designation: FM 5-516* was used to determine the chloride ion concentrations in the samples. This method determines acid-soluble chloride concentration similar to *AASHTO Standard Test Method for Sampling and Testing for Chloride Ion in Concrete and Concrete Raw Material: T260-97 (2001)*. For the top 1 in. of concrete, ½ -in. thick slices were pulverized for titration, while 1-in. thick slices were used for the remainder of the depth.
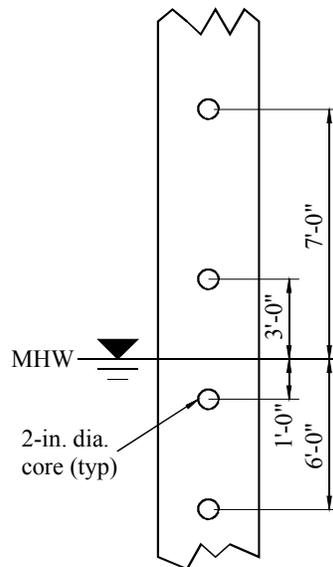
Figure 7 – Core location for chloride content sampling
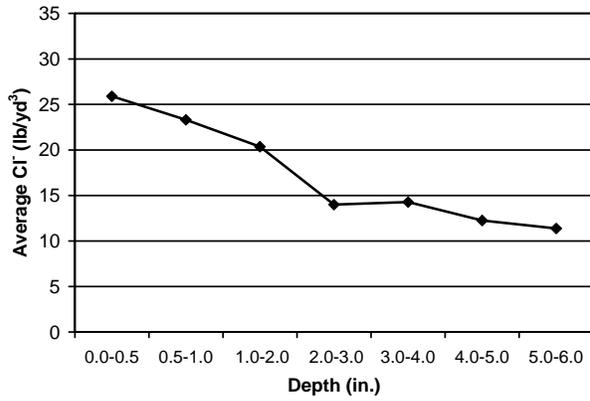
Submerged Zone
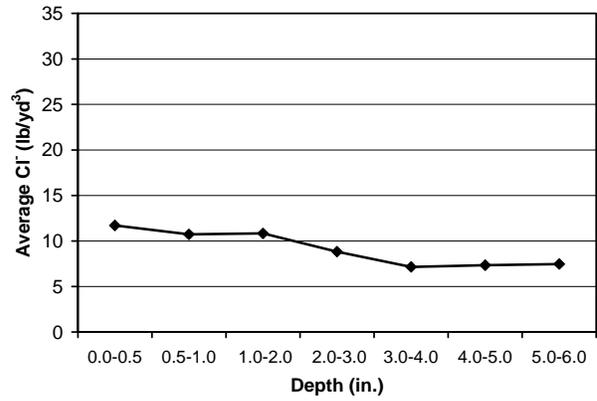
Tidal Zone
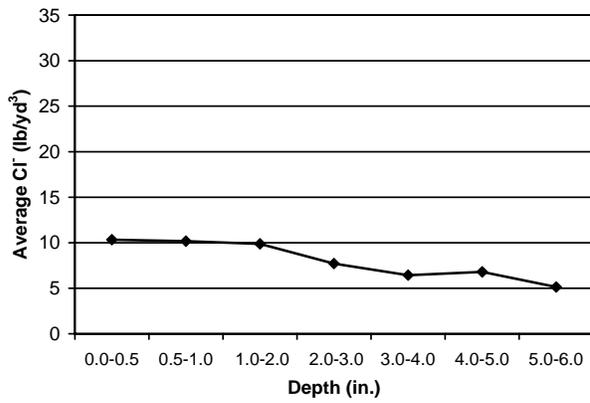
Splash Zone
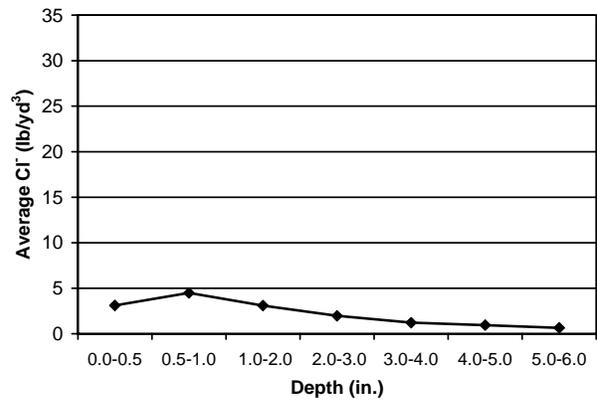
Dry Zone

Figure 8 – Chloride content, Pile 32-3J
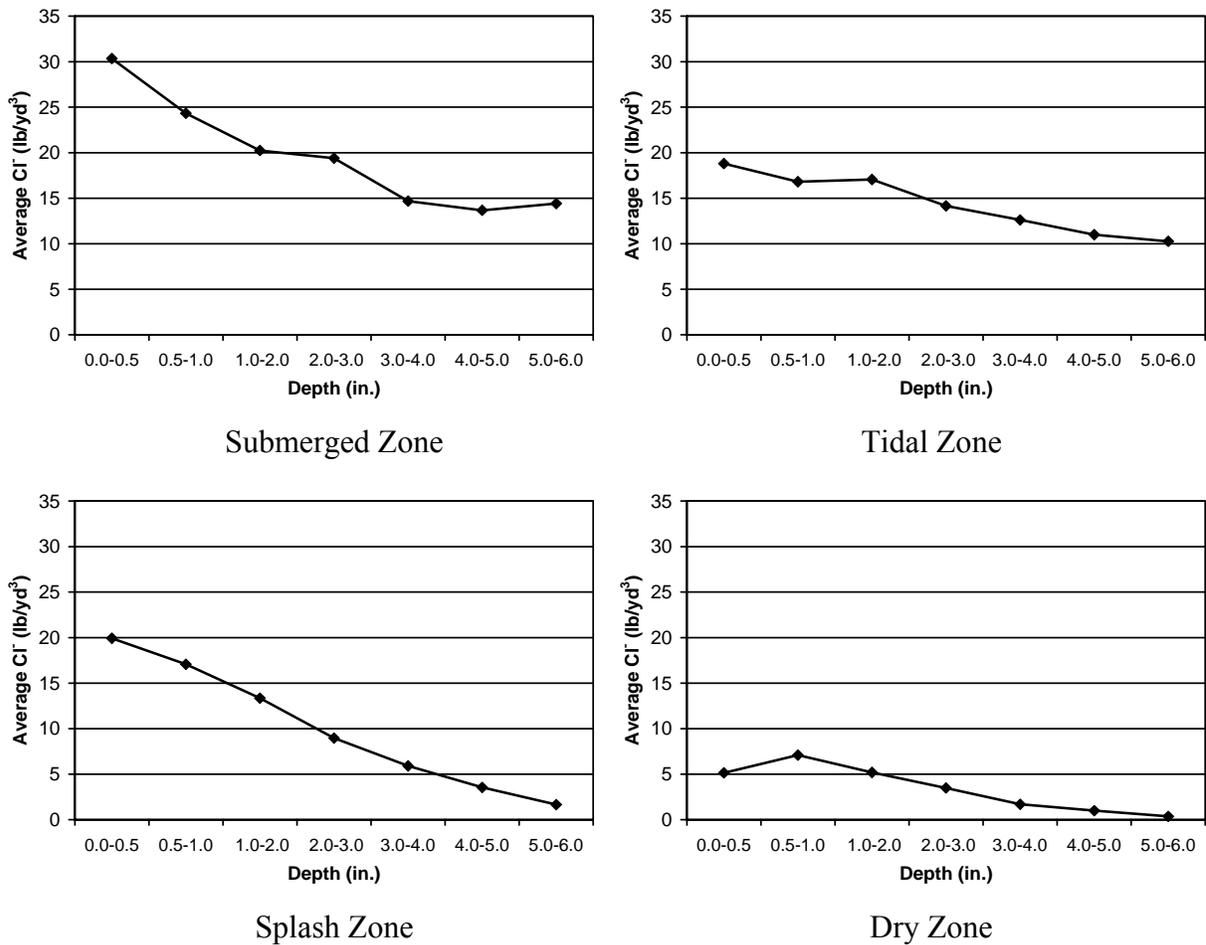
Figure 9 – Chloride content, Pile 44-2

The chloride profiles show that the greatest contamination occurs in the submerged portion of the pile where the concrete is continuously exposed to the salt water. The location of next greatest contamination is that of the tidal zone where the concrete is repeatedly submerged by the tidal fluctuation, followed by the splash zone and then the dry zone. Corrosion generally occurs in the splash zones due to the combination of chloride contamination and oxygen availability to support the corrosion reactions.

Table 5 shows selected values of chloride content in the splash zone of the two piles. The values have been converted to a percentage of the cement content assuming that the actual cement content is as listed in Table 1 (at 378 lbs./barrel). The splash zone is of interest because the simultaneous availability of moisture, chlorides and oxygen makes this area highly conducive to corrosion. When the chloride content exceeds the "chloride corrosion threshold", unacceptable corrosion may occur. This is assuming that the conditions necessary to support the corrosion reactions are in place such as the presence of oxygen and moisture. Although a single chloride corrosion threshold does not really exist, it is useful to compare the chloride contents measured in these piles with controlled laboratory tests. ACI 222 (1997) cites studies that have shown that threshold limits of 0.33% have been measured with values as low as 0.15%. More recently researchers (Alonso (2000)) reviewed nearly thirty papers for experimental values of chloride threshold and found that they ranged from 0.2% to 3.0% with most data below 1.5

---

percent. Clearly, the chloride ion concentration in these piles is unsurprisingly high considering the relatively low cement content, lack of pozzolan use, and long-term exposure to a severe environment. Visual inspection of the two piles and subsequent flexural testing, however, indicated that pile 44-2 was in better condition than that of 32-3J, even though the chloride contents were comparable. A jacket was installed on pile 32-3J in 1983, which perhaps contributed to the lower chloride levels at the 2 to 3-in. depth and the better visual rating.

Table 5 – Chloride content at the level of the steel in splash zone

Pile	Slice location (in.)	Chloride ion content	
		lbs/yd^3	% cwt
32-3J	2.0-3.0	7.7	1.3
	3.0-4.0	6.4	1.0
44-2	2.0-3.0	9.0	1.5
	3.0-4.0	5.9	1.0

4.4 PRESTRESSING STEEL CHEMISTRY

Two piles were sampled for both dissolved hydrogen and chemistry of the prestressing strand to determine if the bulk anode cathodic protection system (Figure 10) had been operating at sufficiently negative potentials to generate hydrogen. The chemical analysis was conducted using Leco combustion and dissolved hydrogen was determined using Optical Emission Spectroscopy.

The first pile sampled was 21-4, which was cut and pulled from the bay on May 27, 2004. The pile was placed on the demolition barge to allow samples of the prestressing strand to be taken for hydrogen testing. Although potentials were not taken following extraction of 21-4, inspection of the bulk anode indicated that the anode was still electrically connected to the strand and likely providing protection. The second pile was 44-2, which was sampled at the FDOT Structures Research Center after it had been tested in flexure. This pile did not have a cathodic protection system installed. Accordingly sampling of this pile was intended to provide background data on the dissolved hydrogen.

Strand sample locations for piles 21-4 and 44-2 are shown in Figure 11. Samples were pulled from a corner strand (C) and from a middle strand (M) at each of five locations along the length of the pile. Sampling started under the cathodic protection jacket and extended downward in three-foot increments. The samples are named according to their location on the pile with the first letter indicating vertical position and the second letter indicating horizontal position (as the pile was oriented in service). Saw cuts were made to a sufficient depth to allow a 10-in. long strand sample to be extracted without the use of prying tools that might contaminate the specimen (Figure 12). The wire samples to be tested were packed in dry ice and shipped to the testing laboratory within 3 hours of pile extraction to prevent out gassing of hydrogen during transit.

Figure 10 – Bulk zinc anode on pile 21-4
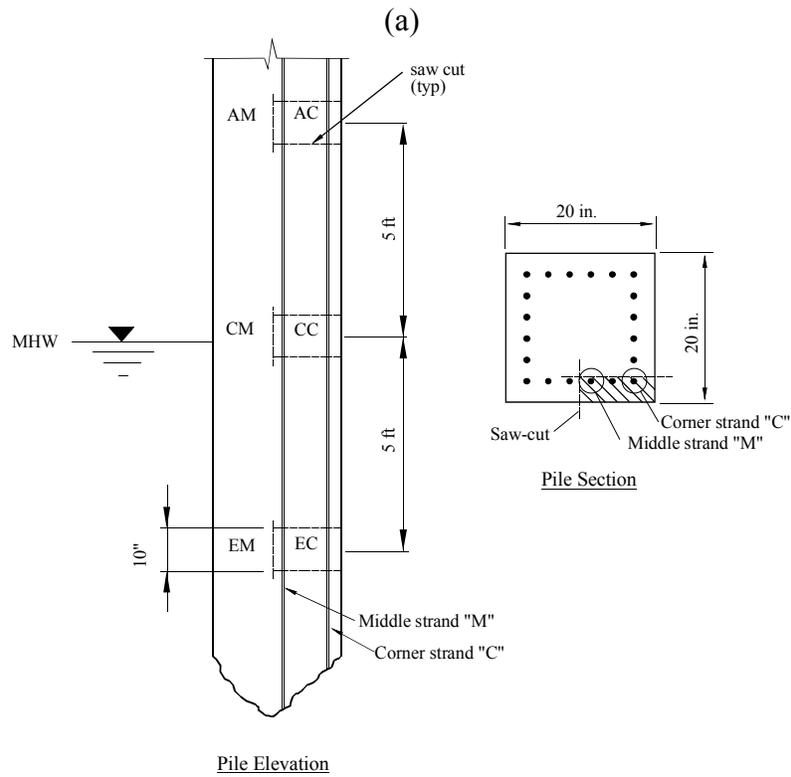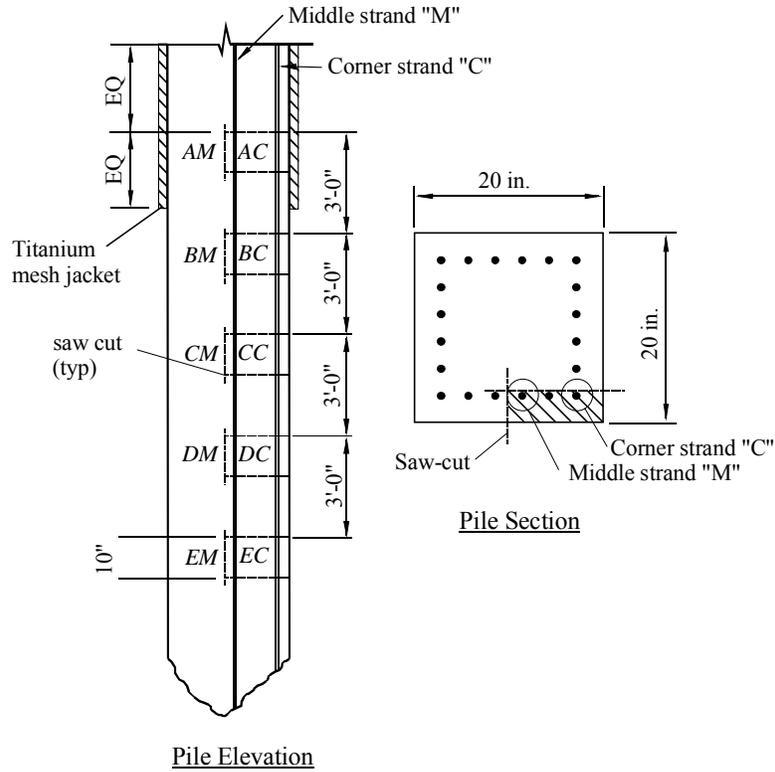
Figure 11 – Strand sampling locations (a) pile 21-4 and (b) pile 44-2

Figure 12 – Saw cut and strand removal

Strand samples taken from both piles generally exhibited light to moderate surface corrosion with spotty mild pitting (Figure 13a). The strand samples from Pile 21-4 showed corrosion primarily in the interstitial space between the outside and center wires. This pattern was consistent at all sample locations. In general, the cathodic protection system appeared to have done a reasonable job of protecting the reinforcement. Some of the strand samples pulled from pile 44-2 (Figure 13b) had surface corrosion on the outer wires. The strand shown in the figure exhibits some bleeding of corrosion product into the concrete as well as black corrosion product indicating a low oxygen environment. Note that the corrosion has the appearance of emanating from the tie wire.
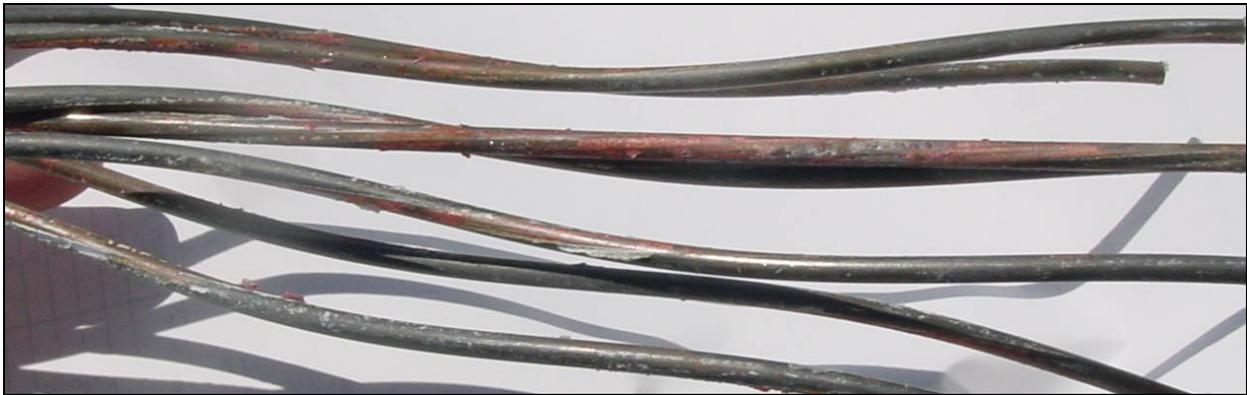
(a)

(b)

Figure 13 – Corrosion on strand pulled from (a) pile 21-4 (b) pile 44-2.

Dissolved hydrogen results for both piles are compared in Table 6. The "outer" designation indicates that the sample was taken from one of the six helical wires on the outside of the strand. The "inner" designation indicates that the sample was taken from the inner wire. Only outer wires were sampled for dissolved hydrogen in pile 44-2 since pile 21-4 showed much higher values in the outer wires. It is expected that as-drawn prestressing wire would have a background dissolved hydrogen content ranging from 0.2 ppm to as high as 1.0 ppm, most typically averaging around 0.6 to 0.7 ppm (Lewis (2006)). This compares well with the average background value of 0.92 measured in pile 44-2. Furthermore, the data from 21-4 show that, with the exception of sample CC, there appears to have been hydrogen charging of both center and outer wires via cathodic protection. Also, with the exception of the "E" values, the inner wires at each location appear to have somewhat lower dissolved hydrogen than the corresponding outer strand wires. This confirms that the outer wires tend to shield the inner wires, but do not completely protect them from charging.

Experience has shown that these levels of dissolved hydrogen measured in pile 21-4 can cause embrittlement problems in some high-strength wires (Lewis (2006)). There was no evidence from visual examination or flexural testing (discussed later in the report) of embrittlement problems in the piles that had cathodic protection. It is suspected that the stabilization process used on stress-relieved or low-relaxation strand redistributes residual drawing stresses in the wire rendering the wire much less susceptible to hydrogen damage.

The results of the chemical analysis are given in Table 7.

Table 6 – Dissolved hydrogen results (ppm)

Location:	Pile 21-4		Pile 44-2
	Outer wire	Center wire	Outer wire
AM	1.7	1.4	0.8
AC	2.7	2.2	0.8
BM	1.4	-	-
BC	2.5	-	-
CM	2.3	1.7	1.0
CC	0.9	0.4	1.4
DM	2.2	-	-
DC	2.9	-	-
EM	1.5	1.5	0.5
EC	-	-	1.0
Average	2.0	1.4	0.92

Table 7 – Chemical analysis

Element	Pile 21-4		Pile 44-2	
	AC-Outer (%)	AM-Outer (%)	AM-Outer (%)	AM-Outer (%)
C	0.75	0.73	0.72	0.73
Mn	0.66	0.68	0.68	0.60
P	0.020	0.009	0.009	0.010
S	0.023	0.018	0.018	0.023
Si	0.18	0.25	0.25	0.16
Cu	0.09	0.08	0.06	0.06
Ni	0.04	0.03	0.03	0.03
Cr	0.08	0.06	0.07	0.06
Mo	< 0.01	< 0.01	< 0.01	< 0.01
Al	< 0.01	< 0.01	-	-
Ti	< 0.01	< 0.01	-	-

5   MATERIAL PROPERTIES

5.1   CONCRETE STRENGTH

Two four-in. diameter cores were taken from pile 31-1 to determine concrete strength. The cores were taken at each end of the pile and were oriented parallel with the pile axis. Table 8 gives the test values. The compressive strengths were conducted on dry samples.

Table 8 – Compressive strength of cores taken from pile 31-1

Location	Compressive Strength (psi)
Above waterline	6,400
Below waterline	6,100

5.2   STRAND TENSION TESTING

Tension testing was conducted on undamaged strand samples recovered from Pile 44-2 on February 17, 2005. Detailed test data are included in Appendix E. The ultimate strength and modulus values are reported in Table 9. The data indicate that the strand meets the mechanical requirements of ASTM A416.

Table 9 – Steel Strength and Modulus

Sample Number	1	2	3	4	5	AVG	ASTM A416
Strength (ksi)	264.5	262.7	259.1	259.1	261.8	261.5	>250
Elongation (%)	7.8	7.8	8.5	8.1	7.8	8.0	>3.5%
Yield point at 1% elongation	235	232.9	227.5	229.3	237.5	232.4	>229
Modulus of Elasticity (ksi)	27,800	28,200	28,500	30,400	28,000	28,580	n/a

6 PILE RATING

Bridge inspectors rely largely on visual inspections to evaluate the condition of bridge substructures. Although some State departments of transportation have employed nondestructive evaluation methods to complement visual inspection, widespread use of these nondestructive technologies has been limited, and visual inspection remains the most widely used method of reporting bridge conditions in a standardized format.

A visual rating system was devised and used to rate the capacity of the 12 piles tested in this research. This rating system was based on the FDOT inspection guidelines for Commonly Recognized Structural Elements (CoRe). Table 10 shows the numerical rating and condition state descriptions taken from the FDOT Bridge Inspectors Field Guide – Structural Elements (2000). To supplement the guide and to enable direct estimation of capacity, the estimated loss of capacity shown in the table was developed.

Table 10 – Damage definitions

CoRe Rating*	Severity of Damage	Condition State*	Estimated Loss of Capacity
1	Not Damaged	Pile shows little of no deterioration. There may be discoloration, efflorescence, and/or superficial cracking but without affect on strength and/or serviceability.	0 – 5 %
2	Slightly Damaged	Minor Cracks, spalls, and scaling may be present and there may be exposed reinforcing with no evidence of corrosion. There is no exposure of the prestress system.	6 – 15 %
3	Damaged	Moderate cracks, spalls, scaling and some delaminations may be present. There may be minor exposure but no deterioration of the prestress system. Corrosion of non-prestressed reinforcement may be present but loss of section is incidental and does not significantly affect the strength and/or serviceability of either the element or bridge	16 – 30 %
4	Severely Damaged	Severe cracks, spalls, scaling, delaminations, and corrosion of non-prestressed reinforcement are prevalent. There may also be exposure and deterioration of the prestress system (manifested by loss of bond, broken strand or wire, failed anchorages, etc). There is sufficient concern to warrant a review to ascertain the impact on the strength and/or serviceability of either the element or the bridge	> 31 %
* Ratings and condition state description taken from FDOT Bridge Inspectors Field Guide – Structural Elements, March 13, 2000.			

The loss in capacity is relatively low until the CoRe rating reaches a level 4. This is because the rating system appears to be designed such that ratings of 3 or less do not have a significant impact on the capacity of the structure. If an element receives a rating of 4, however, then additional review of the structural capacity of the element or bridge is warranted. Consequently, the maximum loss of capacity for a rating of 3 was, somewhat arbitrarily, chosen to be 30 percent.

A UF graduate student (in the structural engineering program) who was unfamiliar with the results of the flexural testing was chosen to rate the piles using only the photos and notes taken of the piles in the water by FDOT divers prior to extraction. The researchers felt that this would give an independent evaluation of the piles. It should be noted that the graduate student had no previous formal inspection training. Table 11 shows a list of the 12 piles and their corresponding visual rating. In a few cases the rating number was subdivided.

Piles 44-3CP and 44-1CP were cathodically protected. Piles 33-4J and 32-3J were jacketed and they showed significant and severe damage respectively. Piles 29-2 and 44-2 were rated as being in the best condition, while piles 32-3J and 40-2 as being the worst. The rest of the piles, including the cathodically protected piles, were visually rated between these extremes.

Table 11 – Visual rating results

Pile	Pile Rating
29-2	1
31-1	2
32-3J	4
33-4J	3
39-2	1.5
40-2	2
40-3J	4
40-4	3
44-1CP	2
44-2	1
44-3CP	3
44-4	2

(J) concrete jacket, (CP) cathodically protected

7 FLEXURAL TESTING

7.1 FLEXURAL TEST SETUP

Following recovery and transporting to the FDOT Structures Research Center, the piles were cleaned and tested to failure in a four-point bending test. The objective of the flexural testing was to simulate lateral load such as a barge impact and further to determine quantitatively the reduction in flexural capacity caused by the corrosion of the prestressing strands.

The four-point bending test was chosen to create an area of constant moment and zero shear under the transfer beam (See Figure 14). Rather than apply the load at the mid length of each pile, the center of the splash zone was selected as the location of loading such that the weakest portion of the pile carried the highest moment. This would also be the likely location of

an impact from a drifting barge. The splash zone was marked during inspection of the bridge as the 4-ft. zone between 1-ft. and 5-ft. above MHW. The load application point also varied relative to the end of each pile due to the irregular nature of the removal process. Table 12 gives the span, *L*, the position of the spreader beam, *a* and *b,* and the effective depth, *d*, to the bottom layer of prestressing strand (see Figure 2). The effective depth was measured at each end of the pile and averaged. If significant damage was noted, however, at a location other than the center of the splash zone, the transfer beam was then centered directly over the damage.
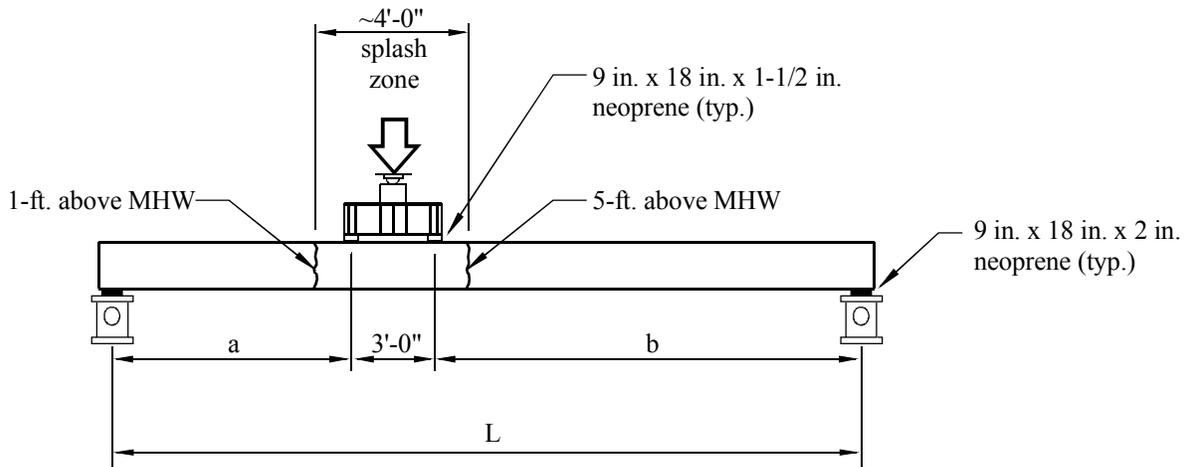
(a)

(b)   (c)

Figure 14 – Flexural test setup (a) dimensions and details; (b) photograph of pile ready to test; (c) photograph of spreader beam

Table 12 – Pile dimensions and details

Pile	a (ft)	b (ft)	L (ft)	d (in)
29-2	19.1	13.9	36.00	17.25
31-1	7.2	17.5	27.67	17.5
32-3J	7.5	18.5	29.00	17.25
33-4J	9.5	18.5	31.02	17.25
39-2	17.2	12.8	33.00	17
40-2	11.5	9.5	24.00	17.75
40-3J	10.0	8.0	21.00	16.5
40-4	13.5	11.3	27.83	17.25
44-1CP	13.5	7.5	24.00	17.25
44-2	10.5	12.5	26.04	16.5
44-3CP	11.5	7.0	21.50	17
44-4	11.0	6.5	20.50	17.75

The load was transferred from the spreader beam to the pile through two 1½-in. thick reinforced neoprene bearing pads. The pile was supported on two biaxial clevis load cells, which measured both horizontal thrust and vertical support reactions (See Figure 15). Load was also measured with a load cell at the load application point.

Figure 15 – Biaxial clevis load cell

The piles were instrumented with 14 displacement transducers (DT) placed at selected locations along their spans (Figure 16). Because the splash zone and the immediate surrounding area were of the most interest, and would experience the peak curvature deflection, the DTs were more closely spaced in those regions.

An 11 ft. length of the west face (as oriented in the test frame) centered under the transfer beam was whitewashed to improve crack visibility during loading. Within this whitewash zone, ten of the fourteen DTs were used. Three DTs were evenly spaced under the transfer beam 3-in. from the east edge of the pile (Figure 17). Since the load was never placed exactly at midspan,

the remaining DTs were proportioned such that 6 would be on the shorter side of the span, and 5 would be on the remaining, longer part of the span (Figure 18). This method provided deflections measurements necessary to map the hinging expected to occur around the load point.

Figure 16 – Instrumentation for flexural testing

Figure 17 – DT placement within the splash zone

Figure 18 – DT placement at pile ends

7.2 SHEAR TEST SETUP

Preliminary structural calculations indicated that the decision to center the load in the splash zone resulted in a short shear span (load point placed close to one of the supports) in some of the test set-ups. There was concern that these piles might fail in shear rather than flexure. To determine the actual shear capacity, a shear test was conducted on pile 39-2 immediately after it was tested in flexure. Pile 39-2 was chosen to test first because its long length and relatively centered splash zone ensured that a flexural failure was likely.

After successfully testing pile 39-2 in flexure, a second test was conducted on the portion of the pile that was out of the water and above the splash zone, thereby ensuring that corrosion damage was minimal and that the damage from the flexural test would not affect the results. The shear test setup is shown in Figure 19. Instrumentation included one DT at the load point and one at each support. The test was conducted at a load rate of 10 kips per minute.
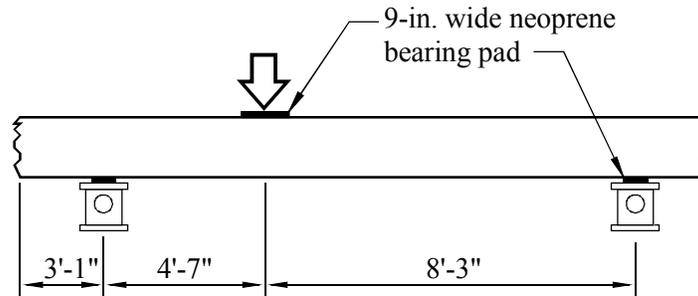
Figure 19 – Shear test setup on pile 39-2.

7.3 TESTING PROCEDURES

The hydraulic system was set to load the pile at approximately five to seven kips per minute until failure occurred. Load control was used up to strand yield or rupture after which displacement control was used. Piles continued to be loaded until they were deemed to be unstable, which was generally a result of the loss of the compression zone or rupture of strands or both.

8 Results and Discussion

8.1 FLEXURAL TESTS

Twelve precast prestressed concrete piles were load tested in flexure to failure. The failure mode of each pile was dominated by flexure near the load point. Generally, as loading was initially increased, cracks became visible in the high moment region at a load of approximately 10 kips. As loading approached the pile capacity, audible strand wire rupture or slip or both occurred.

Pile behavior at flexural capacity was typified by extensive flexural cracking, compression zone crushing, strand and wire rupture or slipping, or some combination thereof. Four piles failed from compression zone crushing only, and did not have any ruptured strands (see Figure 20). Three of these failures occurred within the area between the load points. The other pile crushed just outside of a load point. Piles 44-1CP and 44-3CP failed from strand rupture alone (Figure 21). Three strand breaks appear to have occurred in each pile. The remaining six piles failed due to a combination of compression zone crushing and rupture or debonding (Figure 22). Each of these piles showed crushing in the compression zone. Five of them crushed between the two load points, as expected. The sixth pile crushed just outside of one of the load points.

Figure 20 – Compression zone crushing and flexural cracking in pile 44-2

Figure 21 – Strand rupture of pile 44-3CP.

Figure 22 – Combination of strand rupture and crushing of compression zone on pile 40-3J. Spalling seen on bottom of pile was caused by corrosion of the strand in service.

Relative comparison of the load-displacement plots is of little value since each pile was tested with a different span. They do, however, provide an indication of the general aspects of the behavior of the piles under load. Figure 23 shows the load-deflection response for pile 40-4, and is what would be expected from an undamaged pile. The pile initially responded in a linear manner until cracking and strand yielding caused a reduction in stiffness. Load continued to increase up to the ultimate capacity when the compression zone failed. This pile reached a

flexural capacity comparable to that measured in the shear test. No strands ruptured during this test as indicated by the smooth and continuous load deflection response.
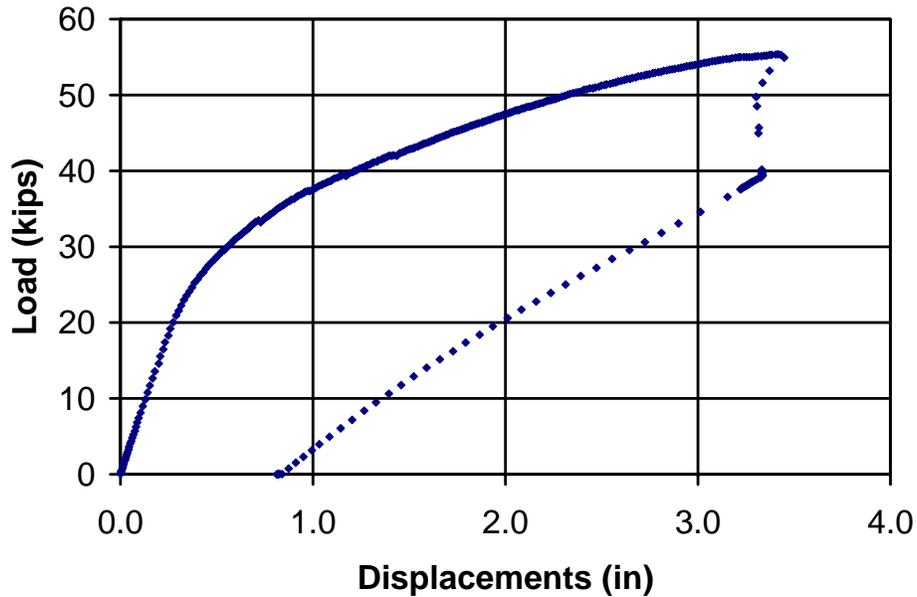
Figure 23 – Pile 40-4 load displacement response

In many of the tests, the pile capacity was controlled by strand rupture or slip or both. Figure 24 shows the load-displacement behavior for pile 32-3J. Denoted on the plot are the locations where drops in load corresponded to audible sounds video-recorded during testing. These sounds are attributed to either strand rupture or slip since they are associated with a sharp reduction of load. Video recordings of each test were reviewed to determine the number of breaks or slips noted in each test. These are presented along with the failure mode in Table 13.
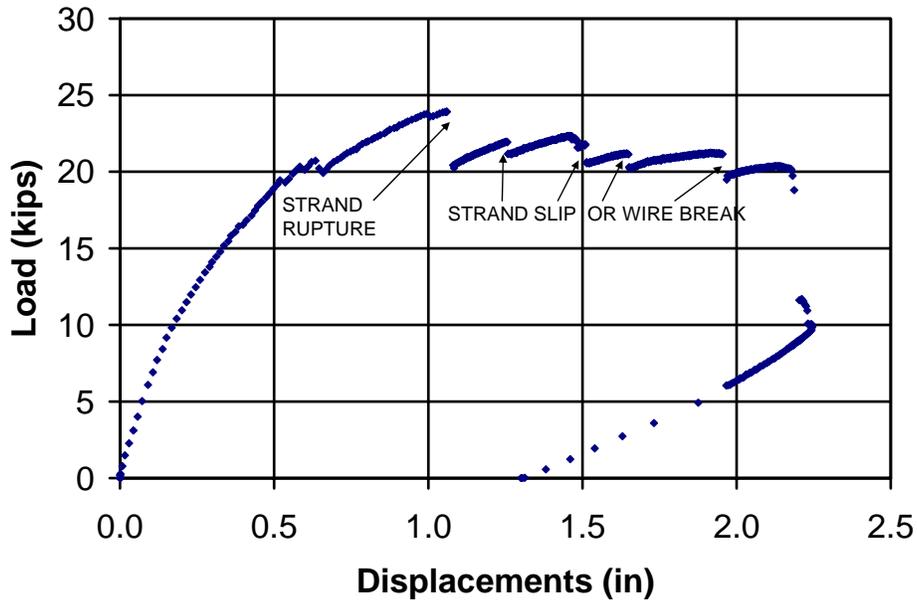
Figure 24 – Pile 32-3J load-displacement response

Table 13 – Wire or breaks or slips per pile

Pile	Existing Condition	Failure Mode*	Wire/Strand Breaks, or Slips
29-2	No visible damage	C	0
31-1	No visible damage	CR	2
32-3J	Missing chunk of concrete in tension zone with cracking	CR	6
33-4J	Missing chunk of concrete on tension face	C	0
39-2	No visible damage	CR	6
40-2	Large spall exposing corroded strands	CR	2
40-3J	5-ft. crack ~ 3-in. above bottom of pile	CR	2
40-4	No visible damage	C	0
44-1CP	No visible damage	R	3
44-2	No visible damage	C	0
44-3CP	No visible damage	R	6
44-4	24-in. crack about 2-in. above bottom of pile	CR	5

* C – Compression failure; R – strand or wire rupture; CR – combination of compression and rupture.

The peak measured load from each test was used along with the support geometry to calculate the experimental maximum flexural capacity (M_E) while also accounting for self-weight (Table 14). The moments are also normalized to the calculated moment capacity of the cross-section (M_C), which represents a rated or calculated capacity against which the loss of capacity due to corrosion can be compared. For example, an M_E / M_C ratio of 0.52 indicates that pile 32-3J has lost 48% of its rated capacity due to corrosion. Details of the procedures used to calculate the moment capacity are presented in the next section.

Table 14 shows that most of the piles maintained at least 70% of their rated capacity. The four exceptions are piles 39-2, 32-3J, 44-3CP and 40-3J. Pile 40-3J, the worst case, retained only 31% of its undamaged capacity. The cathodically protected piles, 44-3CP and 44-1CP, showed a significant loss of structural capacity by retaining 53% and 79% of their original capacity, respectively. This was likely due to damage sustained prior to installation of the CP system because there were no outward signs of significant corrosion noted on either pile after the structural testing.

Table 14 – Moment capacity normalized to calculated capacity

Pile	M_E (kip-ft)	M_E / M_C
29-2	366	1.08
31-1	259	0.76
32-3J	175	0.52
33-4J	372	1.10
39-2	224	0.66
40-2	256	0.76
40-3J	106	0.31
40-4	385	1.14
44-1CP	267	0.79
44-2	355	1.05
44-3CP	178	0.53
44-4	282	0.83
M_C	339	1.00
Shear test on 39-2	341	1.01

8.2   CORROSION POTENTIALS AND FLEXURAL CAPACITY

It is rare to have both flexural capacity and corrosion potential data from actual field structures. Determining if the corrosion potential can be related to the tested flexural capacity would be useful in conducting field inspections of existing structures. The lower the measured corrosion potential, the more likely corrosion has occurred. Corrosion will cause section loss resulting in a reduction of the flexural capacity. Although the half-cell test measures only corrosion potential and not corrosion rate, it can still be useful in determining the severity of the corrosion by examining the length of pile over which the corrosion potentials are very negative.

Figure 25 shows a compilation of the average corrosion potentials from all tested piles. Each plot represents the average of the corrosion potentials on all four faces for a particular

elevation including only those data in which electrical continuity of the ground connection was confirmed. The plot clearly indicates that some of the piles have very negative potentials over most of their height. Pile 40-3J, for example, has readings more negative than -350 mV up to nearly 6 ft. above MHW. This pile retained only 31% of its calculated capacity. Conversely, pile 44-2 has only one reading more negative than -350mV near the MHW line and retained more than 100% of its calculated capacity. As the length of pile in the splash zone that has very negative readings increases it appears that the flexural capacity decreases.
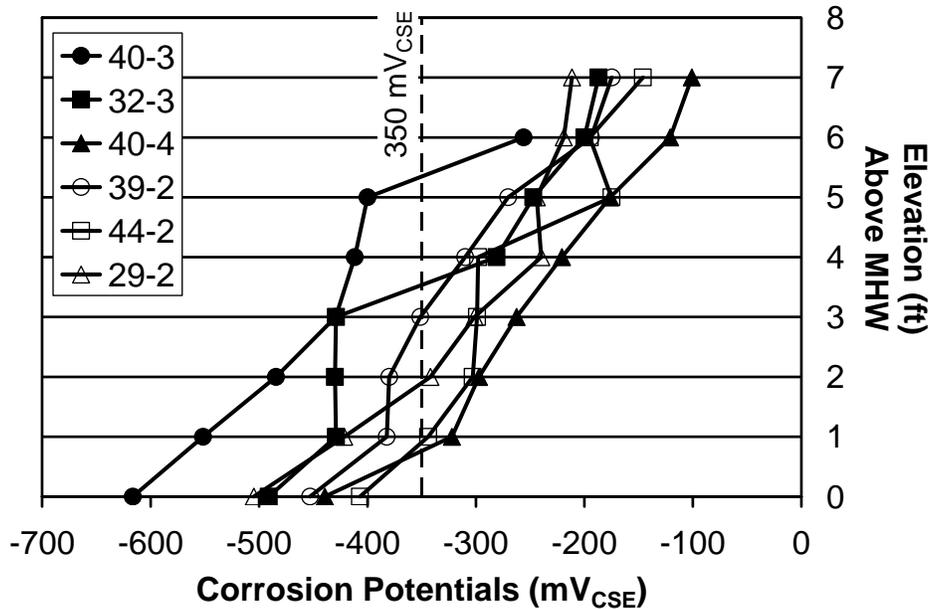
Figure 25 – Compilation of the average corrosion potential of the tested piles.

Figure 26 illustrates this trend. The normalized moment capacities are shown on the vertical axis and the horizontal axis shows the length of pile above the mean high water over which the measured corrosion potentials are less than -350 mV$_{CSE}$. There appears to be a linear relationship between the measured corrosion potential and flexural capacity that is quite strong ($R^2 = 0.92$). Visual inspection of the strand after the flexural test indicated that corrosion was most severe at the base of the splash zone (just above the MHW) and would taper in intensity as the distance from the MHW was increased. Field observations also confirm that the corrosion tends to migrate upward on the pile through the splash zone, which supports the behavior illustrated by the plot. The plot can be summarized as follows. When the average corrosion potential was less than -350 mV$_{CSE}$ over an approximate height of:

- 1 ft. above the MHW, then 100% of the pile capacity remained.
- 3 ft. above the MHW, then approximately 68% of the pile capacity remained.
- 5 ft. above the MHW, then approximately 32% of the pile capacity remained.
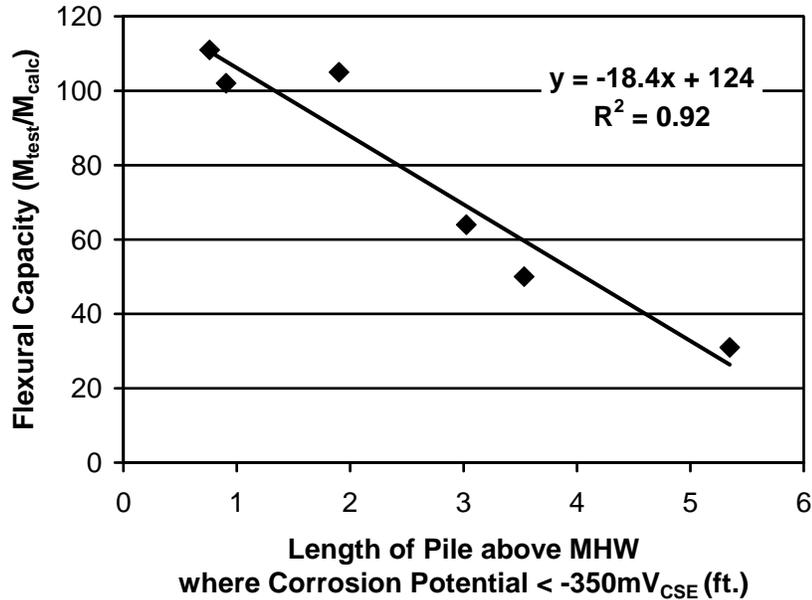
Figure 26 – Relationship between flexural capacity and corrosion potential

9 Post-Test Evaluation

Following flexural testing, piles 44-3CP (cathodically protected), 32-3J (concrete jacket), and 44-2 were excavated to inspect the strands in the splash zone. Figure 27 shows the piles after excavation. Concrete was removed from the face that carried the extreme flexural tension during flexural testing, which was oriented to coincide with the splash zone. Strands were examined for corrosion and wire breaks. Generally, moderate to severe corrosion was noted on the prestressing strands. In some cases the prestressing strands were completely consumed by corrosion as can be seen in the top two strands in Figure 28. Figure 29 shows a range of corrosion. The top two strands are severely corroded while the bottom four strands have corrosion ranging from light to severe as the strands enter the splash zone. The portion of the pile above the splash zone when it was in service is to the left of the figure.

Severe corrosion was also noted in strand that appears to have been used for pick up points during pile construction and handling. Pick up points were noted in both 32-3J and 44-2. Figure 29 shows an example in which the pick-up point strand and pile strand have been nearly completely consumed by corrosion. The pick-up point strand, however, was in bright condition away from the pile strand and farther into the pile. Corrosion at these locations likely was initiated by chloride intrusion along the pick-up point strands where they exited the pile. The fact that the pick-up point was located in the splash zone accelerated this behavior.

Figure 27 – Piles being excavated to examine corroded strand.

Figure 28 – Pile 32-3J after excavation. Wire breaks are circled.

Figure 29 – Severely corroded strand from pick up point on Pile 32-3J. Prestressing strand in this area has been completely consumed by corrosion. Moderate to severe corrosion on the remaining strands as they enter the splash zone.

Figure 30 shows pile 44-3CP after excavation. The repair material used to replace the original concrete that spalled due to corrosion appears darker and devoid of coarse aggregate. The patch was reinforced with a galvanized steel welded wire fabric, which did not have significant corrosion (Figure 31). Closer inspection of the prestressing strand showed that there was significant loss of cross-section at the time of the repair. Figure 31 shows the severe elongated pitting associated with corrosion of prestressing strand. The pits are filled with grout indicating that the corrosion products were likely mechanically removed before patching. Corrosion product was present on the remainder of the prestressing strands to varying degrees. Figure 32 shows four of the strands from the bottom strand layer of pile 44-3CP highlighting the variation in corrosion severity across the width. The top strand has light to moderate surface corrosion. The strand below it has moderate to significant corrosion with some significant pitting. The bottom two strands have severe corrosion with significant loss of cross-section and have rupture where they intersect a flexural crack in the concrete.

Unfortunately, it was not possible to differentiate between corrosion that occurred before and after the 1994 installation of the cathodic protection system. If the strand is assumed to have been cleaned to bright condition during the 1994 repairs, then the corrosion that occurred since then was minimal, indicating that the cathodic protection system provided some protection while it was operational.

Generally, in concrete that has been patched due to corrosion, local corrosion cells will form between the uncontaminated patch material and the contaminated surrounding concrete causing the reinforcement in the concrete surrounding the patch to corrode at an accelerated rate.

This phenomenon is known as the halo effect. The cathodic protection system provides protection to the reinforcement surrounding the patched area, which otherwise would become the anode to the newly passivated reinforcement under the patch. FDOT personnel indicated that the CP system in this bridge had a very short service life due to hurricanes and other ambient conditions that accelerated the splash-zone anode consumption (Lasa 2006). It is possible that some corrosion occurred after the anode in the splash zone was consumed.

Furthermore, informal observations made during the pile selection process indicated that the piles with CP systems generally had fewer spalls and less outward signs of corrosion damage that those piles that did not. In conclusion, the CP likely did provide protection for the prestressing strand, but the duration and extent is not known.

Figure 30 – Pile 44-3CP after excavation. Darker concrete is patch material placed during the 1994 repairs.

Figure 31 – Interface between existing pile concrete and patch material. Galvanized steel mesh was used in patch. Prestressing strand in foreground appears to have had significant section loss before repair.

Figure 32 – Strand in bottom of pile 44-3CP. Corrosion severity increases in intensity from top to bottom. Wire breaks are distributed along a major flexural crack in the more heavily corroded strands.

Figure 33 shows the behavior of a severely corroded strand when loaded to rupture. The wires generally ruptured at varying locations along the length of the strand. In contrast, Figure 34 shows the rupture pattern of an uncorroded strand taken from the piles in which the individual wire ruptures occur in very close proximity to each other. Furthermore, each wire exhibits the ductile necking and cup/cone fracture surface.

Figure 33 – Typical rupture pattern of severely corroded prestressing strand exhibiting fingernail splitting.

Figure 34 – Failure mode of uncorroded prestressing strand sample taken from pile 44-2. Ductile necking of the cross section and cup/cone fracture surface are shown.

10 Moment Curvature Analysis

To better understand the structural capacity, ductility, and flexural behavior of the piles, a moment-curvature plot was developed for each pile. The sectional moment-curvature relationship was developed from the experimental deflection data for each pile to obtain insight into the flexural behavior and particularly the formation of plastic hinges and associated ductility. Moment curvatures that are not measured directly can be generated by differentiating the deflection data twice. To smooth the accumulation of error that occurs with double differentiation, a curve is generally fit to the deflection profile. The curve equation is then differentiated twice to determine curvature. When a plastic hinge forms, however, curve fitting becomes less desirable due to the discontinuity of the deflection profile in the hinge region. Consequently, numerical differentiation was performed directly to obtain the curvatures at selected load intervals. The sectional curvature to be plotted was based on the maximum curvature (generally occurring near the load point) at the peak measured moment. The peak

curvatures at or adjacent to that location were used in all other points for a particular pile. Figure 35 shows the results of the moment-curvature analysis. Although this method compounds error and results in somewhat distorted curvature profiles, the results are still insightful. Individual plots are included in Appendix D.

Each plot in Figure 35 also shows a theoretical moment curvature, which was calculated using strain compatibility along with the material properties obtained from tests on concrete cores and prestressing strand coupons pulled from the piles following the structural tests. Table 15 shows the properties used to calculate the moment curvature relationship. The average compressive strength of the two cores taken from pile 31-1 was used along with an average effective depth of 17.19 in. Average mechanical properties of the strands were also used to derive the moment curvature.
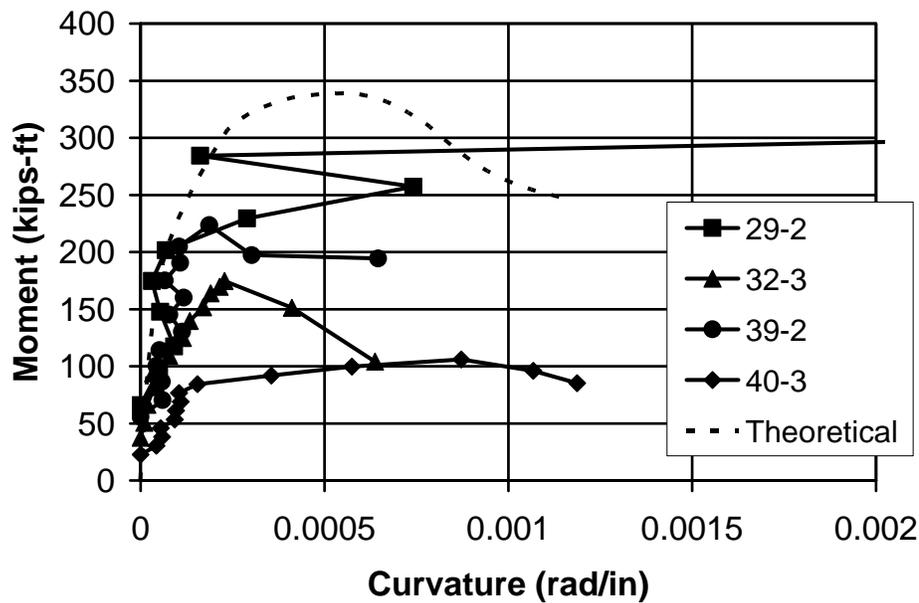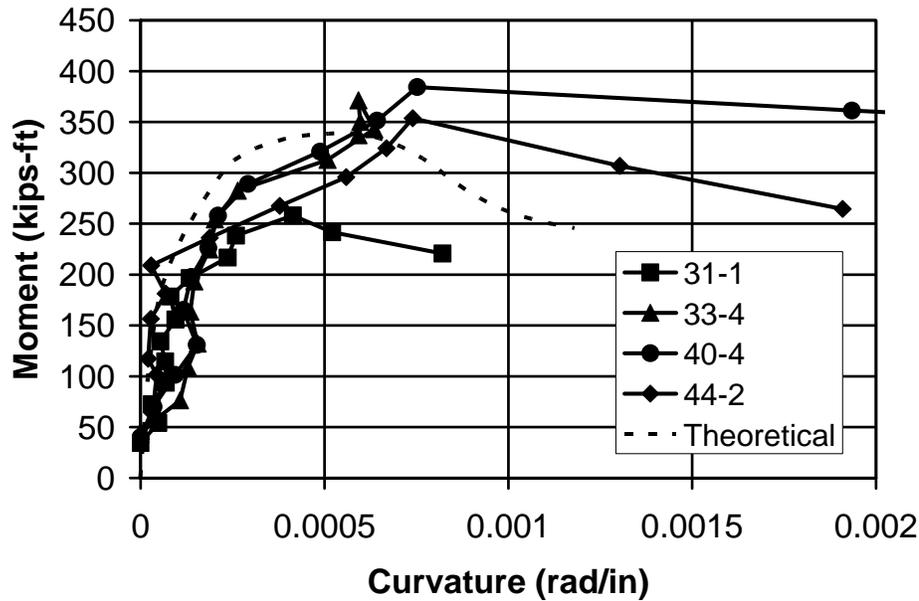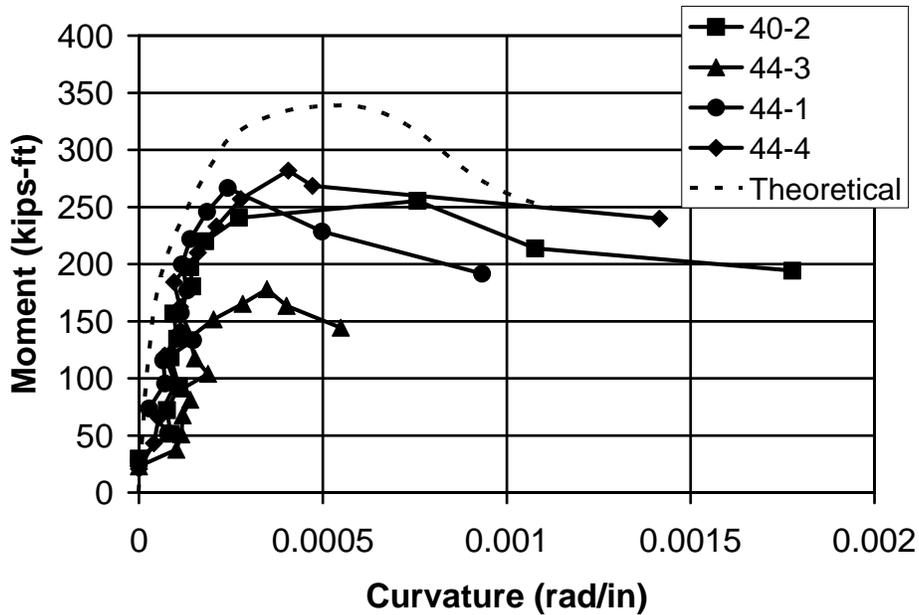
Figure 35 – Actual vs. theoretical moment-curvatures

Table 15 – Section and materials properties used in moment curvature analysis.

Concrete	
Compressive Strength	6,250 psi
Effective depth d	17.19 in.
Prestressing Strand	
Tensile strength	261.5 ksi
Yield at 1% elongation	232.4 ksi
Elongation	8%
Modulus of elasticity	28,580 ksi

The two piles that had strand rupture with no significant crushing of the compression zone also happen to be the piles that had cathodic protection (Table 13). This raises the question of whether hydrogen charging from the cathodic protection system could have contributed to the rupture of the strands before crushing occurred. To test this hypothesis, the moment curvature plots were used to generate ductility factors for each of the piles. Because the piles were not loaded to collapse, the terminal curvature is somewhat arbitrary. One measure of ductility is to compare the curvature at 90% of the peak moment capacity on the backside of the curve with the curvature at the peak moment capacity. This is defined as follows:

$$\mu_\phi = \frac{\phi_{ME}}{\phi_{0.9ME}}$$

Equation 1

where μ_ϕ is the curvature ductility factor, ϕ_{ME} is the curvature when the pile is at its peak moment, $\phi_{0.9ME}$ is the curvature when the moment is at 90% of the peak moment. Table 16 shows

the values for all piles except 33-4J, for which the curvature ductility factor could not be calculated because of the irregularity of the moment curvature diagram. The other ductility factors tend to vary between 1.13 and 3.63. Based on this comparison, there does not appear to be a significant loss of ductility in the CP piles when compared with the other piles. For example, pile 44-1CP has a ductility factor that is greater than all but two other piles, while 44-3CP has a ductility factor greater than only two other piles. The reduced ductility of pile 44-3CP is mirrored by the reduced flexural capacity, which may have been due to severe corrosion occurring prior to the installation of CP. In addition, there are several piles that have comparable ductility factors such as 40-3J and 44-2. In summary, there is no clear trend that would indicate that hydrogen embrittlement has affected the capacity or ductility of these piles.

Table 16 – Curvature ductility determined from the moment curvature plots.

Pile	ϕ_{ME} (rad/in.)	$\phi_{0.9ME}$ (rad/in.)	μ_ϕ	Normalized Ductility
29-2	0.0121	0.013697	1.13	0.80
31-1	0.000414	0.000648	1.57	1.11
32-3J	0.000228	0.000361	1.59	1.12
33-4J	n/a	n/a	n/a	n/a
39-2	0.000187	0.000282	1.51	1.07
40-2	0.000872	0.00107	1.23	0.87
40-3J	0.000758	0.000954	1.26	0.89
40-4	0.000752	0.002732	3.63	2.57
44-1CP	0.000241	0.000422	1.75	1.24
44-2	0.00074	0.000954	1.29	0.91
44-3CP	0.000348	0.000417	1.24	0.87
44-4	0.000406	0.000964	2.37	1.68
Calculated	0.00057	0.000806	1.41	1.00

11 Comparison of Ratings

The visual rating, flexural capacity, and ductility of each pile were compared to determine if visual inspection correlated with the remaining capacity and ductility. The raw data from the two ratings are shown in Table 17. The visual ratings were normalized assuming that a rating of 1 corresponds to a pile that has 100% of its design capacity remaining. Similarly, a pile with a rating of 4 would have 25% of its original capacity. Moment capacity and ductility were normalized to their respective calculated values.

Figure 36 shows the data plotted in order of increasing moment capacity to give a visual impression of the distribution of capacity loss that these piles experienced. Several of the piles retained their full capacity while the most damaged pile lost nearly 70% of its capacity.

The figure also shows the normalized visual rating for each pile. For piles 32-3J, 33-4J, and 40-4 the visual inspection significantly underestimated the tested pile capacity. Two of these piles were jacketed, which will impede visual inspection. Conversely, visual inspection significantly overestimated the capacity in only one pile (39-2).

Both cathodically protected piles, 44-3CP and 44-1CP, had visual ratings that were comparable to the rated capacity. Based on limited exploratory excavations of the cathodically protected piles it is unclear how much protection was provided to the piles since the system was installed in 1994. The excavations did indicate, however, that on at least one of the piles, the corrosion prior to the installation of the CP system was severe. Based on this observation and that there was little outward signs of continued corrosion, it is likely that most of the corrosion occurred before repair and installation of the cathodic protection system.

Figure 37 shows a comparison of the visual ratings and the ductility factors calculated from the experimental data. Ductility appears to be relatively constant with the exception of 44-4 and 40-4. Consequently, no clear relationship between visual ratings used in this research and the ductility factors was found.

Application of the visual inspection criteria and normalization of the data can be somewhat subjective. It is, however, useful to examine the ability of the visual inspection to predict the flexural capacity of the piles. In 7 of the 12 piles (58%) the normalized visual rating was within 10% of the normalized moment capacity. In only one pile (8%) was the capacity overestimated and in the remainder of the piles (34%) the capacities were underestimated by the normalized visual ratings.

Table 17 – Comparison of visual ratings, moment capacity, and ductility

Pile Designation	Normalized Moment Capacity	Normalized Ductility Factor	Visual Rating	Normalized Visual Rating
29-2	1.08	0.80	1	1
31-1	0.76	1.11	2	0.75
32-3J	0.52	1.12	4	0.25
33-4J	1.10	n/a	3	0.5
39-2	0.66	1.07	1.5	0.875
40-2	0.76	0.89	2	0.75
40-3J	0.31	0.87	4	0.25
40-4	1.14	2.57	3	0.5
44-1CP	0.79	1.24	2	0.75
44-2	1.05	0.91	1	1
44-3CP	0.53	0.87	3	0.5
44-4	0.83	1.68	2	0.75
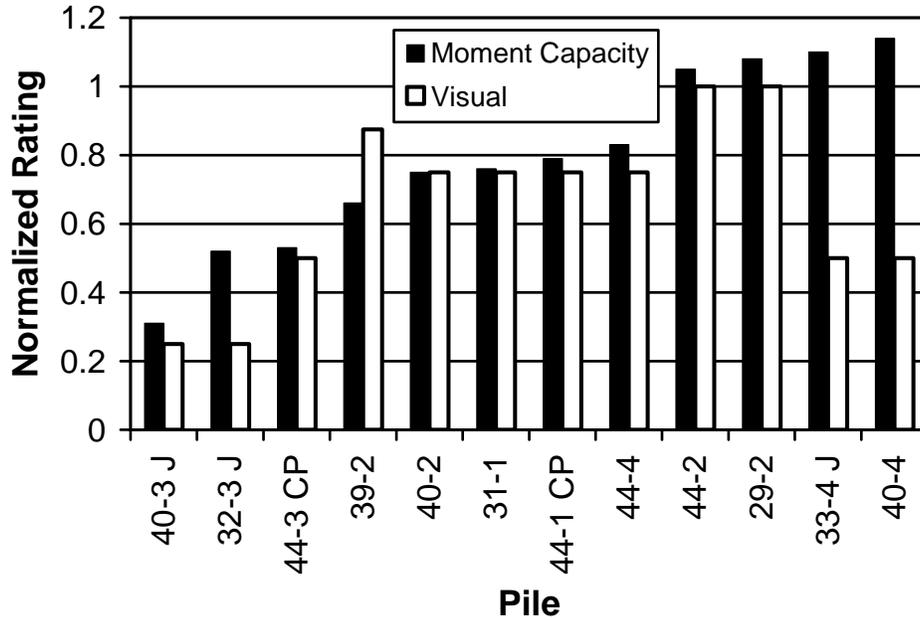
Figure 36 – Comparison of visual rating with experimental moment capacities
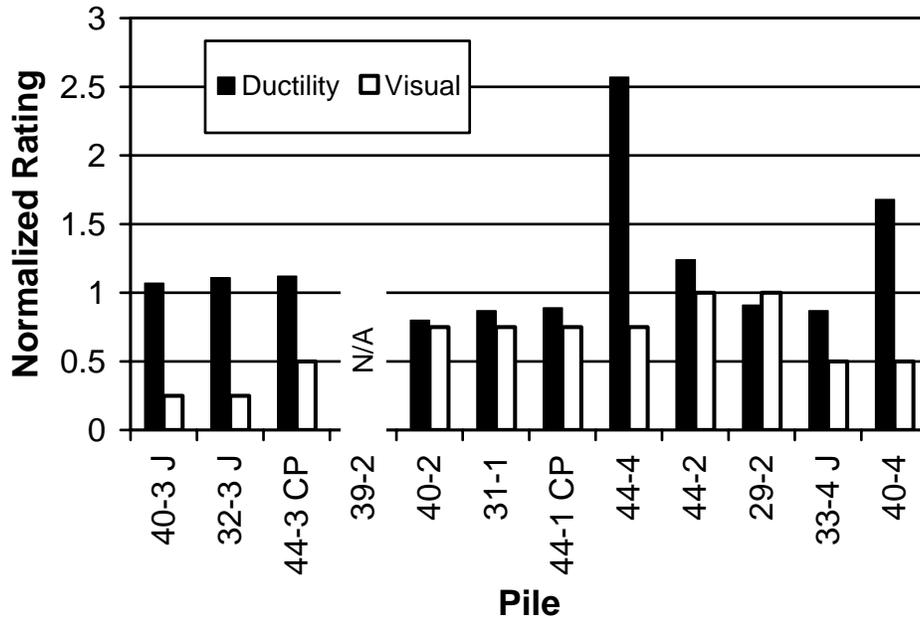
Figure 37 – Comparison of visual rating with experimental ductility

12 Escambia Bay Bridge Pile Tests

Precast post-tensioned cylinder piles from the Escambia Bay bridge carrying route I-10 were tested to determine flexural capacity. The piles were taken from the piers that were damaged by Hurricane Ivan in 2004. The bridge was constructed in 1964. Figure 38 shows the piles as recovered from the bay. The photo shows the top end of the pile, which has been filled with concrete to connect to the cap beam. The connection was made by six mild steel reinforcing bars. Figure 39 shows the opposite end of the piles. The cylinder piles were approximately 36-in. diameter with a 5-in. thick wall. Twelve post-tensioning tendons were evenly spaced around the perimeter at the mid-thickness of the cylinder wall. Each tendon had 10 0.192-in. diameter parallel prestressing wires surrounded by prestressing grout (Figure 40). The number of wires in the tendons was increased to twelve in the region near the connection to the cap beam. It appears that the tendon passages were cast into the cylinder piles without the use of a conduit.

The piles were tested in the cantilever fixture shown in Figure 41. The specimens were clamped with the use of concrete saddles and tied to the strong floor and structural steel fixtures. A concentrated load was then applied monotonically to the tip of the pile until capacity was reached failure. Displacements and load were recorded during testing.

The moment displacement plots are shown in Figure 42 through Figure 44. The plots were generated from the displacement of deflection gage at the outer most point on the cantilever. Movement in the fixture, which contributed to the tip displacement was removed by subtracting the rigid body motion measured by the displacement transducers mounted over the support. Difficulty with the fixture on the first test required that the specimen be unloaded. The second loading then was taken to the pile capacity. Behavior of the three piles was similar in that the wires of the tendons slipped, giving the "saw-tooth" shape to the plots after capacity had been reached. Wires may have also been yielding, but is unconfirmed because they were not instrumented.

Figure 38 – Three piles prior to testing, view of filled end of pile.

Figure 39 – Open end of pile

Figure 40 – Prestressing tendon from cylinder pile. Note grout surrounding wire with no evidence of conduit.

Table 18 shows the peak loads reached by each pile along with the span used to calculate the moments shown in the plots and the peak moment shown in the table. The flexural capacity of the specimens was estimated using strain compatibility procedures and assumptions of material properties. Assuming a modulus of elasticity of 28,000 ksi; a residual prestress of 145 ksi; a concrete strength of 5.0 ksi (taken from the original construction drawings); and a wire diameter of 0.192 inches (taken from the original construction drawings) and an assumed wire ultimate strength of 250 ksi, the calculated moment capacity of the section (M_C) is 863 kip-ft. The peak moments are normalized using the calculated capacity and show a reserve capacity of up to 27 percent. It is apparent that the 40-years of exposure in Escambia Bay did not cause significant deterioration of the flexural capacity of the cross-section. This was confirmed by localized excavation and visual inspection of selected tendons in the region just below the filled portion of the pile.
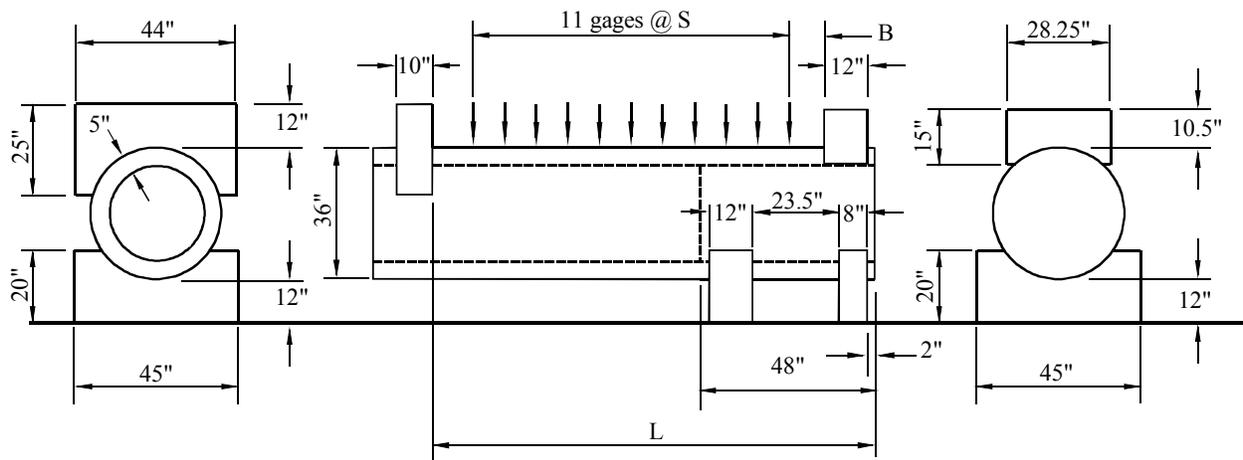
Specimen	Dimensions (in.)		
	L	S	B
CP1	121.5	10	4
CP2	119.25	10	4
CP3	155	13.75	3

(a) Schematic Drawing

(b) Photograph of test setup

Figure 41 – Cylinder pile test setup
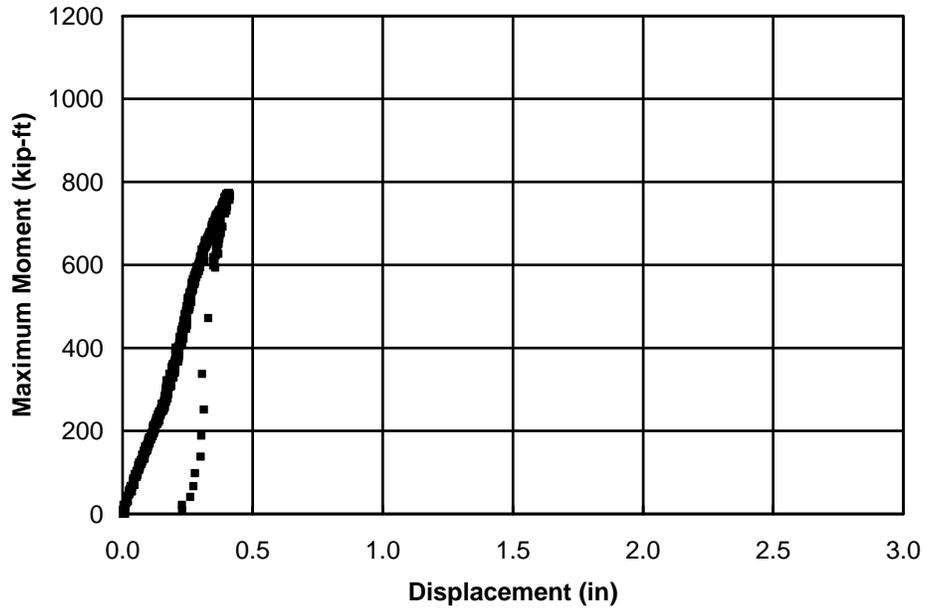
(a) Initial loading
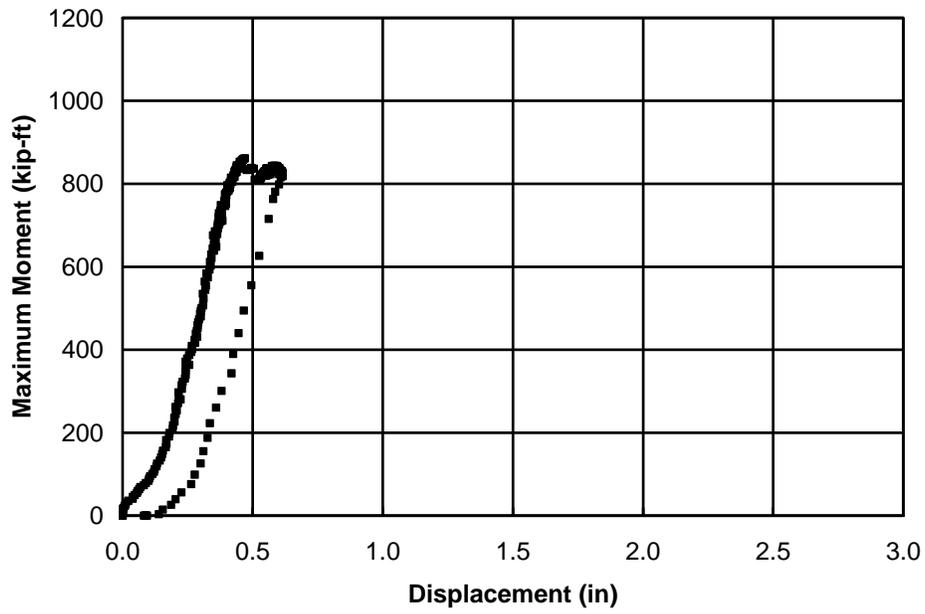
(a) Second loading

Figure 42 – Load deflection response of CP1
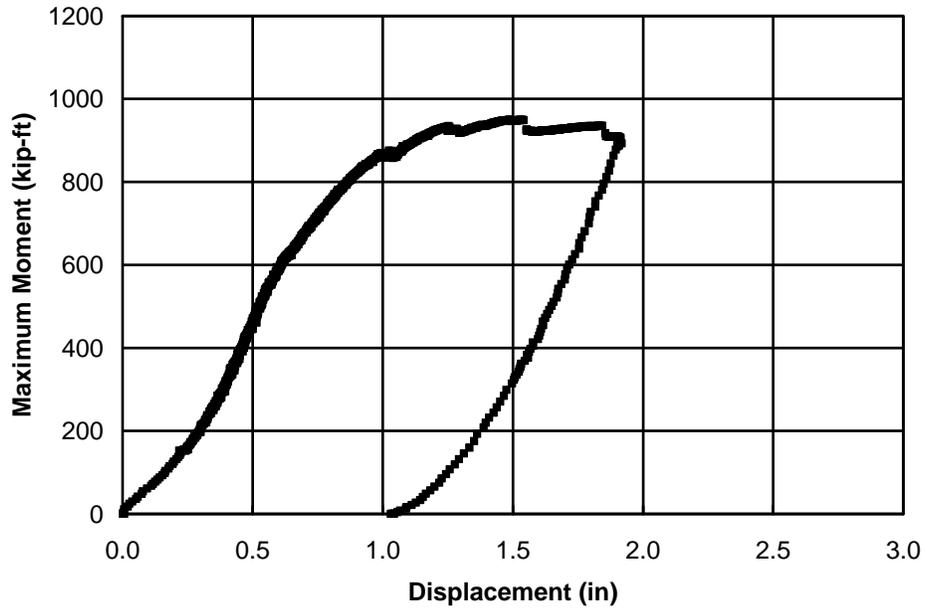
Figure 43 – Load deflection response CP2
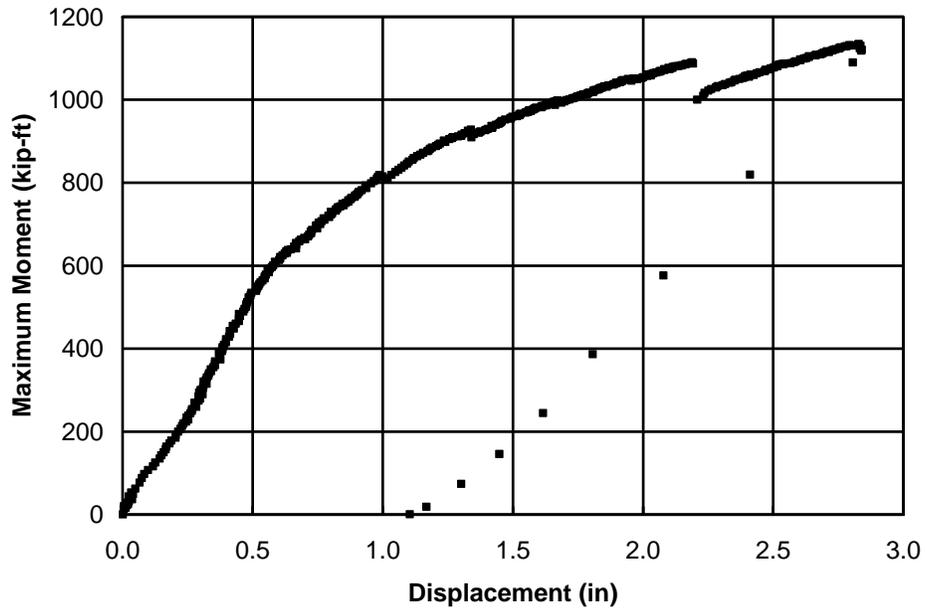
Figure 44 – Pile deflection response CP3

Table 18 – Escambia Bay pile capacities

Pile	Maximum Load Capacity (kips)	Span (in.)	Measured Moment (M_E) (kip-ft)	M_E/M_C
CP1	120	87	870	1.01
CP2	135	84.75	953	1.10
CP3	110	120.5	1100	1.27

13 Summary and Conclusions

This report presents the results of a series of tests aimed at evaluating the existing capacity of precast pretensioned concrete piles that had been in service in a harsh salt-water environment for approximately 40 years. In 2004 the Bryant Patton Bridge over Apalachicola Bay in the Florida panhandle was replaced with a new bridge. During demolition of the existing structure, twelve prestressed concrete piles with varying levels of corrosion damage were recovered. Two of the selected piles were equipped with a cathodic protection that had been installed in 1994 as part of a repair project involving most of the piles supporting the bridge. The prestressing strand from a third recovered cathodically protected pile was sampled for dissolved hydrogen to determine the potential for hydrogen embrittlement. Visual inspections were conducted by District Two Florida Department of Transportation (FDOT) divers on the selected piles before they were removed. Following recovery of the piles, they were cleaned and tested to failure in a four-point bending test. The piles were also sampled for chloride content of the concrete and half-cell potential of the prestressing steel. Visual ratings were assigned to each pile by the researchers based on photographs and notes taken by FDOT district 2 field personnel during their site visit. The ratings were normalized to allow comparison with the tested flexural capacities of the piles. The conclusions can be summarized as follows:

- Flexural test results indicated that some of the piles had severe reduction in capacity while others had no loss of capacity when compared to the calculated capacity. For example, in the most extreme case, the pile was able to carry only 31% of its calculated capacity. Some piles, however, were able to sustain loads higher than the rated capacity. Reduction in flexural capacity was due primarily to the section loss sustained as a result of corrosion damage to the prestressing strand. There was no apparent reduction in concrete strength.
- In 7 of the 12 piles (58%) the normalized visual rating was within 10% of the normalized moment capacity. In only one pile (8%) was the capacity overestimated and in the remainder of the piles (34%) the capacities were underestimated by the normalized visual ratings.
- Visual ratings underestimated the capacities of the concrete jacketed piles.
- The flexural capacities of the two cathodically protected piles were 53% and 79% of the calculated flexural capacity. It was not clear, however, from the post-test excavation how much of the corrosion had occurred since the CP system had been installed. There appeared to have been some protection provided by the cathodic protection system based on limited visual observations, but the duration and extent is not known.

- Severe corrosion was also noted in strand that appeared to have been used for pick up points during pile construction and handling. Corrosion at these locations likely was initiated by chloride intrusion along the pick-up point strand where it exited the pile.
- Corrosion potentials measured on selected piles were related to the flexural capacity. When the average corrosion potential was less than -350 mV$_{CSE}$ over an approximate height of: 1 ft. above the mean high water (MHW), then 100% of the pile capacity remained; 3 ft. above the MHW, then approximately 68% of the pile capacity remained; 5 ft. above the MHW, then approximately 32% of the pile capacity remained.
- The dissolved hydrogen content averaged 2.0 ppm for the outer wires and 1.4 ppm for the inner wires of prestressing strands from a cathodically protected pile. The hydrogen content of the outer wires of a strand from an unprotected pile averaged of 0.92 ppm. It is expected that as-drawn prestressing wire would have a background dissolved hydrogen content ranging from 0.2 ppm to as high as 1.0 ppm, most typically averaging around 0.6 to 0.7 ppm. This compares well with the average background value of 0.92 measured in the unprotected pile and indicates some charging of the protected pile. These results also indicate that the outer wires tend to shield the inner wires, but do not completely protect them from charging.
- To investigate the effect of the elevated levels of hydrogen on the mechanical properties of the strand, a ductility factor for each pile was calculated from the flexural test results. The factor was calculated by taking the ratio of the curvature at peak capacity to the curvature at 90% of capacity based on deflection data gathered during the flexural testing. One of the cathodically protected piles had a ductility factor greater than all but two unprotected piles, while the other had a ductility factor greater than only two of the unprotected piles. This same pile also had a comparable reduction in flexural capacity, which may have been due to severe corrosion occurring prior to the installation of cathodic protection. In summary, there was no clear trend indicating that hydrogen embrittlement had affected the capacity or ductility of the CP piles.

Three precast post-tensioned cylinder piles from the Escambia Bay bridge carrying route I-10 were also tested to determine flexural capacity. The piles were taken from piers that were damaged by Hurricane Ivan in 2004. The bridge was constructed in 1964. The following can be concluded from these tests:

- All three piles retained at least their calculated flexural capacity.
- No significant corrosion was noted on the prestressing wire during post-test excavation.

14 Recommendations

This research is a unique combination of materials and structural testing that provides previously unavailable information on the performance of precast, pretensioned concrete piles that are located in severely corrosive environments. We expect that the results of this research will be used to improve inspection and rating of the existing FDOT bridge inventory. Indeed, FDOT District 2 is currently evaluating and improving their pile inspection and evaluation protocol and has made use of the information contained in this document. We expect that an improved understanding of the relationship between the pile condition and structural capacity will allow an improvement in the efficiency of the repair and replacement programs.

Visual rating of structural elements is inherently subjective. Even though our visual rating of the piles related reasonably well to the flexural capacity, it is our intent that the results of this research be used to improve visual inspection techniques. The strong relationship between the corrosion potentials and flexural capacity noted in this research appears to offer a promising addition to the current inspection techniques. Corrosion surveys are currently a routine inspection technique that includes measurement of corrosion potentials.

We also recommend that the use of strand for lift points be re-evaluated. In one of the specimens, significant corrosion was found in the area of one of these lifting loops. As the Department moves to higher performance concrete and expectations of longer service lives, these details must be evaluated to ensure that localized corrosion in these areas does not undermine the expected performance.

15 REFERENCES

ACI Committee 222 (1996), "Corrosion of Metals in Concrete," American Concrete Institute, 30 pp.

Alonso, C., Andrade, C., Castellote, M., Castro, P. (2000), "Chloride Threshold Values to Depassivate Reinforcing Bars Embedded in a Standardized OPC Mortar," Cement and Concrete Research, v 30, n 7, Jul, 2000, p 1047-1055.

Hartt, W. H., Kumria, C. C., and Kessler, R. J. (1993), "Influence of Potentials, chlorides, pH, and Precharging Time on Embrittlement of Cathodically Polarized Prestressing Steel," Corrosion, V.49, No.5, pp.387 – 385.

Lasa, Ivan, Personal Correspondence, May 26, 2006.

Lewis, R. O., Personal Correspondence, March 15, 2006.

FDOT (2000), "Florida Department of Transportation Bridge Inspectors Field Guide – Structural Elements," March 13, 2000.

16 Appendix A – FDOT District 2 Inspection
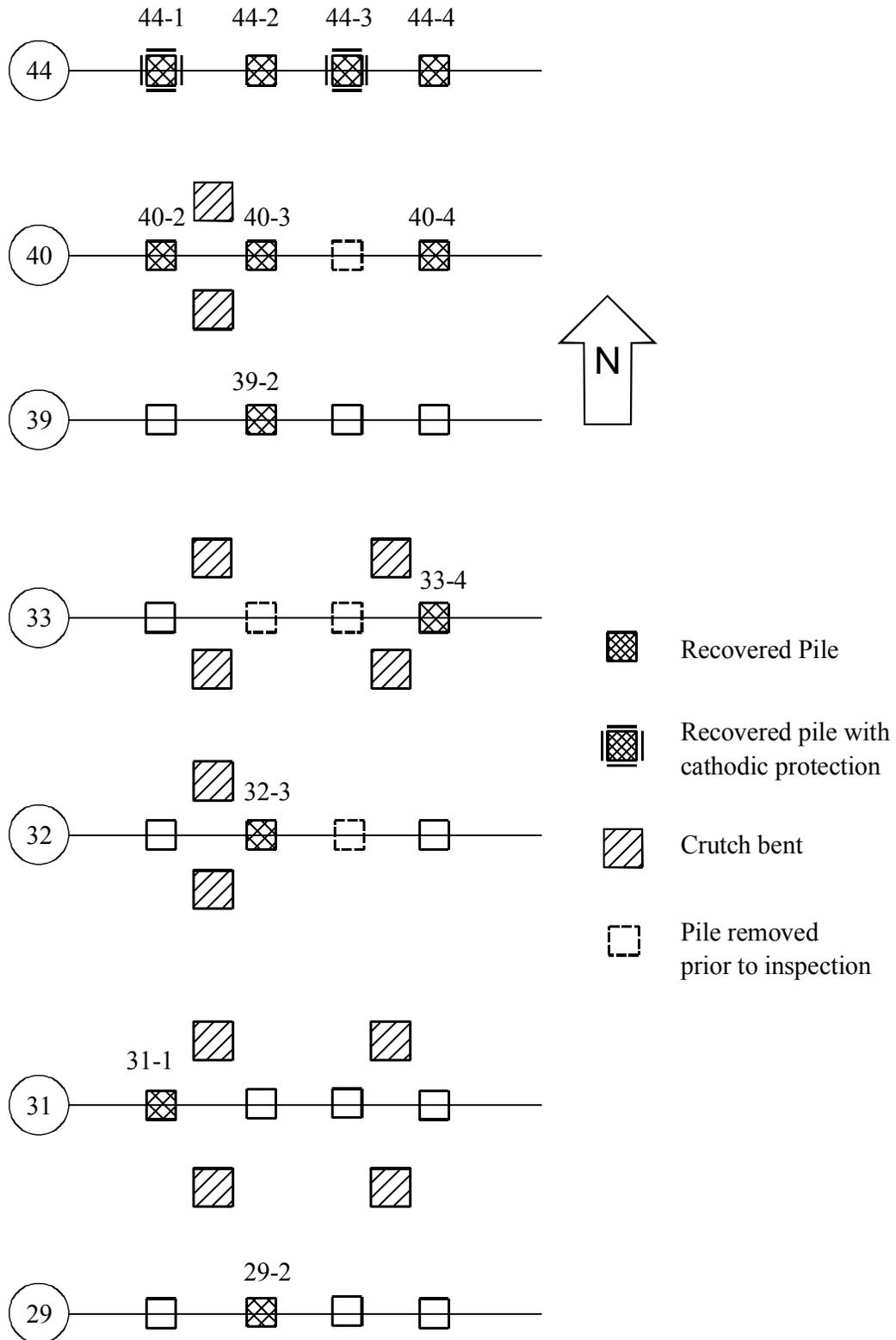
Figure 45 – Pile Setup

1   NORTH FACE PILE 29-2

2   SOUTH FACE PILE 29-2

3   SOUTH FACE BENT 29

4   SOUTH FACE OF BENT 31

5   SOUTH FACE PILE 31-1

6   NORTH FACE PILE 31-1

7

NORTH FACE PILE 31-1

8

NORTH FACE PILE 31-1

9

SOUTH FACE BENT 32

10

SOUTH FACE PILE 32-3J

11

NORTH FACE PILE 32-3J

12

SOUTH FACE PILE 32-3J

13 SOUTH FACE PILE 32-3J

14 SOUTH FACE BENT 33

15 SOUTH FACE PILE 33-4J

16 NORTH FACE PILE 33-4J

17 NORTH FACE PILE 33-4J

18 SOUTH FACE BENT 39

19 SOUTH FACE PILE 39-2

20 NORTH FACE PILE 39-2

21 SOUTH FACE BENT 40

22 NORTH FACE BENT 40

23 SOUTH FACE PILE 40-2

24 SOUTHEAST CORNER PILE 40-3J

25

NORTHEAST CORNER PILE 40-3J

26

NORTHEAST CORNER PILE 40-3J

27

SOUTH FACE BENT 44

28

SOUTH FACE BENT 44

29

NORTH FACE BENT 44

30

NORTHWEST CORNER PILE 44-4

PILE DEFICIENCIES IN TIDAL ZONE

PILE	FACE / CORNER	DIMENSIONS	REMARKS
29-2			No deficiencies noted
31-1	South	24″ x hairline	Vertical crack
	West	28″ x 1/32″	Vertical crack
	North	34″ x 1/8″	Vertical crack w/CBO
	East	34″ x 1/16″	Vertical crack w/CBO
	Southwest		Minor spall
	Northwest		Minor spall
32-3J	Southeast	6′6″ x 12″ x 2″	Spall with one heavily deteriorated exposed strand 24″ long extending to grout of partially removed jacket
	South	3′ x 9″	Incipient spall
	West	40″ x 1/8″	Vertical crack
	North	38″ x 1/8″	Vertical crack w/CBO
33-4J			Remaining grout of partially removed jacket has multiple cracks and spalls
39-2	South	29″ x 1/16″	Vertical crack
	Southwest		Epoxy patch
	East	44″ x 1/8″	Vertical crack w/CBO above tidal zone
	West		Four epoxy patches
40-2	Northwest		Minor spall
	Northeast	37″ x 7″	Incipient spall w/CBO above tidal zone
	Southeast	38″ x 8 ½″	Incipient spall w/CBO above tidal zone
	South	7′ x 3/8″	Vertical crack w/CBO
40-3J	West	63″ x 3/8″	Vertical crack w/CBO, most of jacket grout removed
	South & East	4′ x 18″ each face	Delaminated from 1′ above MHW to 5′ above MHW
	East	47″ x 13″ x 2 ¼″	Spall chipped away with two heavily deteriorated strands 16″ long. Delaminated area extends around 7″ into North face
40-4	Northwest		Epoxy patch above tidal zone
	East		Two epoxy patches
	Northeast		Minor spall
	Southeast		Minor spall
44-1CP	West		Epoxy patch, impressed current jacket in-place
44-2	West		Two epoxy patches
44-3CP	East		Two epoxy patches, impressed current jacket in-place
44-4	East		Three epoxy patches
	Northeast		One epoxy patch

	North	45″ x 3/16″	Vertical crack
	West	49″ x 1/16″	Vertical crack w/CBO
	Northwest	28″ x 7″	Incipient spall

CBO = Corrosion Bleedout
MHW = Mean High Water

Note: Pile 32-3J original Pile 32-2; Pile 40-2 original pile 40-1; Pile 40-3J original pile 40-2. See attached sketches for pile layout.

17 Appendix B – Corrosion Potentials

Concorr Florida, Inc. under contract with FDOT conducted a corrosion evaluation survey of piles 29-2, 44-2, 39-2, 40-4, 32-3, and 40-3 on May 19, 2004. The following data sheets include information gathered during their field visit. Delamination, cover, and corrosion potentials are reported.

Piling 29-2

Delamination Survey Results

Delamination Survey Results (show dimensions and location, including elevations)

North Face	West Face	South Face	East Face
No Damage on this Face.	No Damage on this Face.	No Damage on this face	36"↑ ←9→ Patched Core holes. ←12→ 27"↑ High Tide mark

NDT Concrete Cover Measurements: 2.5", 2.25", 2.56", 2.9", 3.10", 3.5"
Original Cover on Exposed Steel: 2-3/4"

Corrosion Potential and Concrete Resistivity Measurements (see diagram for strand numbering)

Elevation, ft *	Corrosion Potentials, mV CSE				Concrete Resistivity, Kohm-cm
	N Face Strand 17	W Face Strand 12	S Face Strand 6	E Face Strand 2	W Face
0	-517	-499	-492	-516	31.9
1	-412	-421	-436	-417	89
2	-355	-337	-330	-346	59
3	-271	-310	-359	-265	62
4	-233	-280	-263	-183	65
5	-229	-269	-305	-173	58
6	-185	-277	-243	-171	60
7	-180	-260	-240	-166	66
8					
9					
10					

*0 is at the water line.
Strand used for ground 18, elevation of ground if drilled hole was used 40"

6 ← ... → 11

Strand Numbering

1 ← ... → 16

N Face
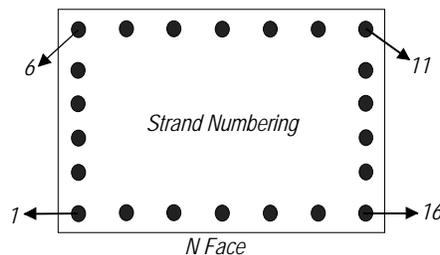
Piling 44-2				
Delamination Survey Results				
North Face	West Face	South Face	East Face	

North Face	West Face	South Face	East Face
No Damage on this Face	No Damage on this Face	No Damage on this Face	No Damage on this Face

NDT Concrete Cover Measurements: 2.0", 2.25", 2.5", 2.8", 2.7", 2.1"
Original Cover on Exposed Steel: 2.0"

Corrosion Potential and Concrete Resistivity Measurements (see diagram for strand numbering)

Elevation, ft *	Corrosion Potentials, mV CSE				Concrete Resistivity, Kohm-cm
	N Face Strand 19[1]	W Face Strand 11[1]	S Face Strand 8[1]	E Face Strand 5	E Face
0	-430	-216/-404	-400	-407	17.2
1	-301	-449	-310	-344	23.3
2	-259	-320	-258	-303	36.2
3	-228	-259	-257	-299	52.9
4	-184	-246	-266	-298	56.9
5	-153	-214	-245	-175	60.3
6	-080	-173	-177	-195	65.8
7	-041	-150	-115	-146	69.1
8	-038	-144	-110	-140	71.3
9					
10					

*0 is at the water line.
Strand used for ground 5, elevation of ground if drilled hole was used 36"

[1] Data Questionable since strand tested is discontinuous from ground used. There were only five discontinuous strands and one of them was used as the ground.

Strand Numbering

6

11

1

16

N Face
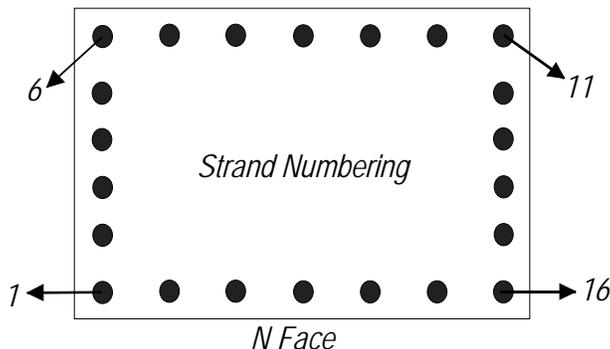
Piling 39-2			
Delamination Survey Results			
Delamination Survey Results (show dimensions and location, including elevations)			
North Face	West Face	South Face	East Face

Delam ~91"

15

20"

2' slots at From Water Line (Hish)

Class III
3/4" Long.
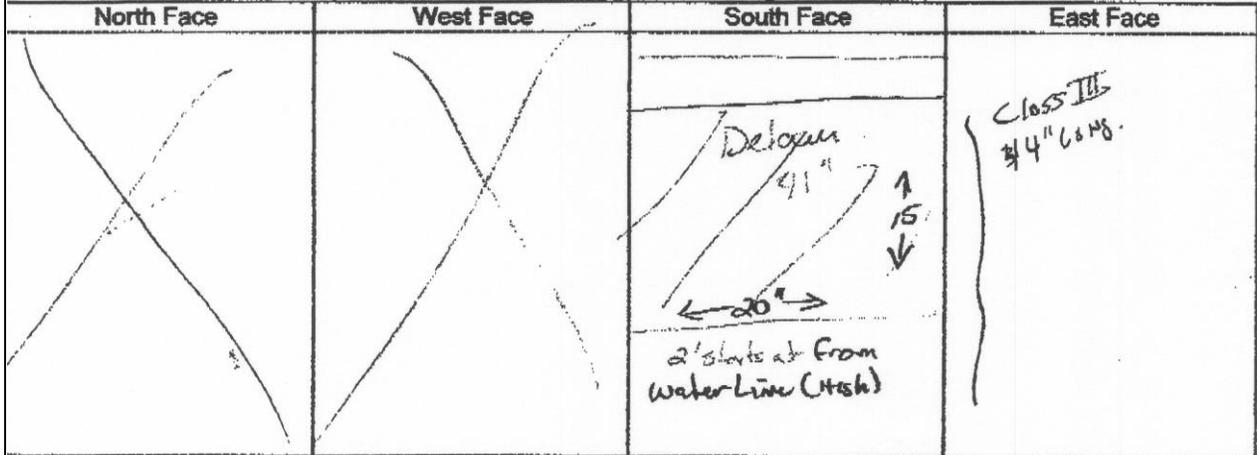
NDT Concrete Cover Measurements: 2.5", 2.95", 2.9", 2.65", 3.1", 3.3"
Original Cover on Exposed Steel: 2.5"

Corrosion Potential and Concrete Resistivity Measurements (see diagram for strand numbering)

Elevation, ft *	Corrosion Potentials, mV CSE				Concrete Resistivity, Kohm-cm
	N Face Strand 18	W Face Strand 12	S Face Strand 8	E Face Strand 6	E Face
0	-464	-456	-462	-430	43.1
1	-343	-414	-394	-378	26.1
2	-302	-458	-399	-361	29.4
3	-268	-394	-430	-313	30.6
4	-180	-369	-416	-275	63.1
5	-142	-313	-372	-254	44.3
6	-146	-200	-245	-185	63.7
7	-130	-191	-200	-178	68.1
8					
9					
10					

*0 is at the water line.
Strand used for ground 6, elevation of ground if drilled hole was used 48"

Strand Numbering

6

11

1

16

N Face
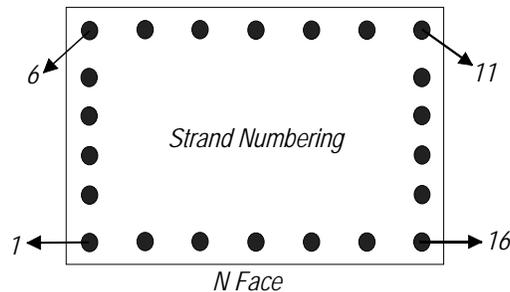
Piling 40-4			
Delamination Survey Results			
North Face	West Face	South Face	East Face
No Damage on this Face	No Damage on this Face	No Damage on this Face	No Damage on this Face

NDT Concrete Cover Measurements: 2.5", 2.65", 2.7", 3.0", 3.1", 3.25"
Original Cover on Exposed Steel: 3.25"

Corrosion Potential and Concrete Resistivity Measurements (see diagram for strand numbering)

Elevation, ft *	Corrosion Potentials, mV CSE				Concrete Resistivity, Kohm-cm
	N Face Strand 20	W Face Strand 7[1]	S Face Strand 5[1]	E Face Strand 6	W Face
0	-432	-396	-456	-473	50.9
1	-262	-341	-328	-358	54
2	-247	-337	-307	-298	68.1
3	-222	-276	-292	-260	67.4
4	-151	-244	-282	-206	65
5	-105	-227	-189	-184	70.6
6	-090	-164	-090	-140	70.9
7	-070	-132	-112	-090	70.8
8	-066	-121	-088	-090	72.6
9					
10					

*0 is at the water line.
Strand used for ground 6, elevation of ground if drilled hole was used 48"

[1] These strand numbers may not be correct.

Strand Numbering

N Face
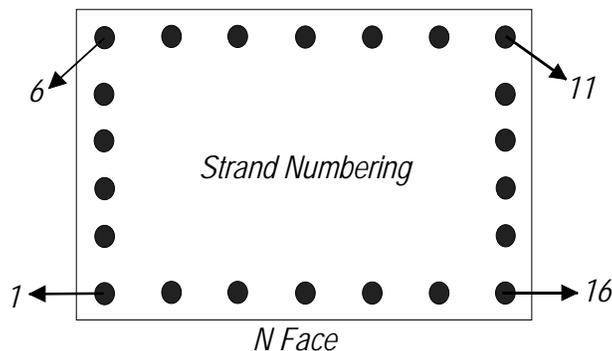
Piling 32-3J

Delamination Survey Results

Delamination Survey Results (show dimensions and location, including elevations)

North Face	West Face	South Face	East Face
No Damage	3' up, 2" s out from concrete jacket 2' class II crack 23' DELAM	INSIPICNT spall 5' Delam ← =12" → 7/4"	Delam - 33" (3-5) area 2½ foot up half of all concrete jacket exist.

High water line
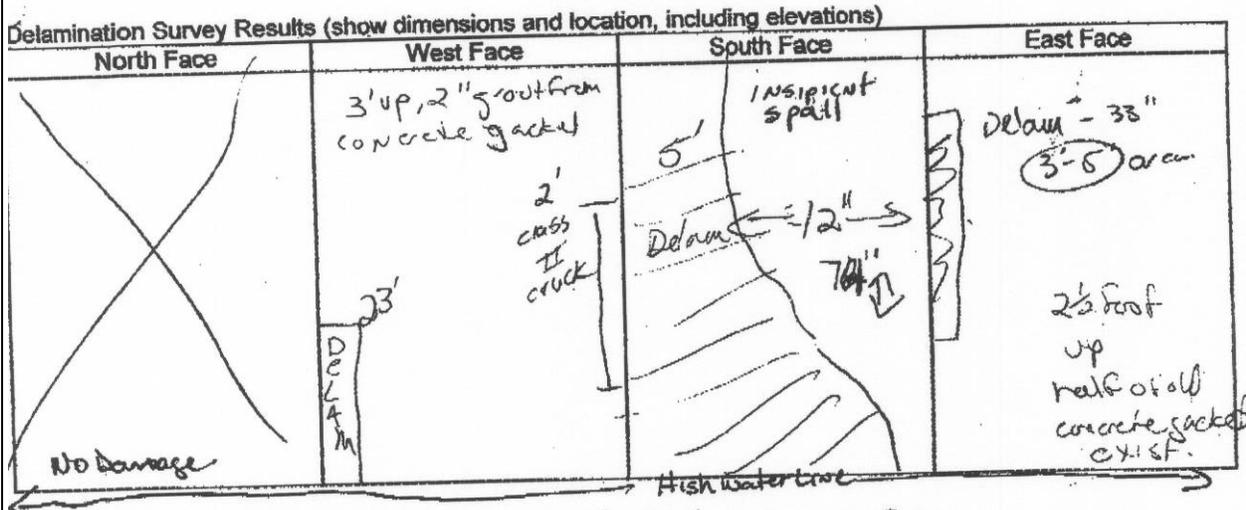
NDT Concrete Cover Measurements: 2.7", 2.9", 2.95", 2.8", 2.5", 3.0"
Original Cover on Exposed Steel: 3.0", 3.0", 2.75"

Corrosion Potential and Concrete Resistivity Measurements (see diagram for strand numbering)

Elevation, ft *	Corrosion Potentials, mV CSE				Concrete Resistivity, Kohm-cm
	N Face Strand 17[1]	W Face Strand 12[1]	S Face Strand 9	E Face Strand 5[1]	W Face
0	-481	-494	-491	-505	9.0
1	-483	-461	-429	-436	6.8
2	-463	-397	-430	-480	10.8
3	-456	-297	-429	-405	17.2
4	-287	-337	-281	-308	23.7
5	-304	-273	-247	-215	25.1
6	-306	-261	-200	-186	32.5
7	-260	-230	-187	-170	35.3
8					
9					
10					

*0 is at the water line.
Strand used for ground 9, elevation of ground if drilled hole was used 43"

[1] Data Questionable since strand tested is discontinuous from ground used. There were only six discontinuous strands and one of them was used as the ground.

Strand Numbering

N Face

6   11
1   16
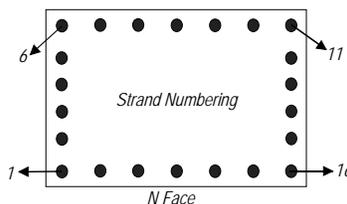
Piling 40-3J

Delamination Survey Results
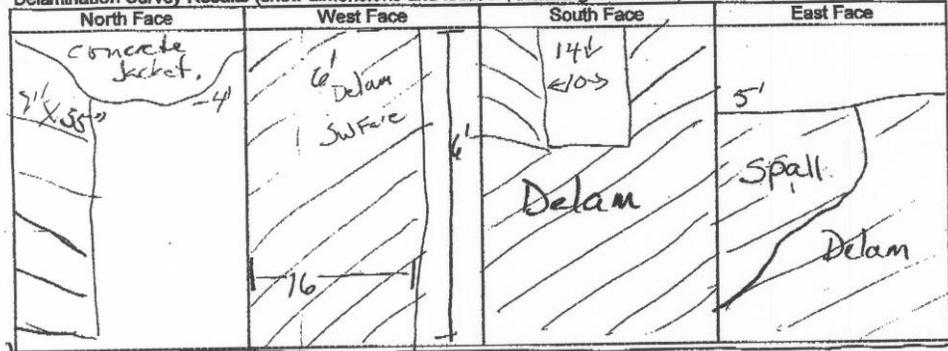
NDT Concrete Cover Measurements: 2.45", 2. 5", 2.25", 2.6", 2.7", 2.65"
Original Cover on Exposed Steel: 2-7/8", (2-3/4", 3.00") Exposed bars

Corrosion Potential and Concrete Resistivity Measurements (see diagram for strand numbering)

Elevation, ft *	Corrosion Potentials, mV CSE				Concrete Resistivity, Kohm-cm
	N Face Strand 18	W Face Strand 12	S Face Strand 6[1]	E Face Strand 1	W Face
0	-643	-590	-547	-616	925
1	-542	-504	-509	-609	9.2
2	-454	-498	-466	-501	8.2
3	-412	-442	-472	-434	16.6
4	-359	-420	-462	-456	16.3
5		-489	-460	-311	14.9
6		-251	-359	-261	29
7					
8					
9					
10					

*0 is at the water line.
Strand used for ground 5, elevation of ground if drilled hole was used__.

[1] Data Questionable since strand tested was discontinuous from ground used.
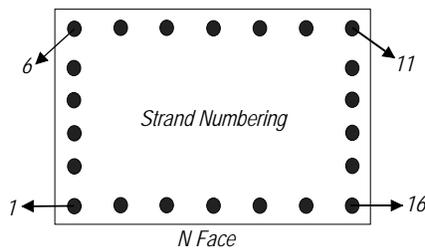
18 Appendix C – Chloride Analysis Results

Florida Department of Transportation

CORROSION RESEARCH LAB

CHLORIDE TEST RESULTS

SUBMITTED BY: Bill Scannell			TESTED BY: PSI				
LAB NUMBER: 4549 - 4578			REPORT DATE: January 27, 2005				
LAB #	**SAMPLE #**	**DESCRIPTION**	**TEST #1**	**TEST #2**	**TEST #3**	**AVG. Cl⁻**	**Cl⁻ RANGE**
		BRYANT GRADY PATTON BRIDGE					
		BRIDGE#490003					
4565	32-3-N-1-A	0.0-0.5	11.456	11.876	11.816	11.716	0.420
4566	32-3-N-1-B	0.5-1.0	10.781	10.858	10.528	10.722	0.330
4567	32-3-N-1-C	1.0-2.0	10.931	10.781	10.801	10.838	0.150
4568	32-3-N-1-D	2.0-3.0	8.775	8.928	8.795	8.833	0.153
4569	32-3-N-1-E	3.0-4.0	7.201	7.118	7.151	7.157	0.083
4570	32-3-N-1-F	4.0-5.0	7.341	7.365	7.324	7.343	0.041
4571	32-3-N-1-G	5.0-6.0	7.452	7.714	7.267	7.478	0.447
4572	32-3-N-3-A	0.0-0.5	10.261	10.289	10.475	10.342	0.214
4573	32-3-N-3-B	0.5-1.0	10.319	10.084	10.120	10.174	0.235
4574	32-3-N-3-C	1.0-2.0	9.917	9.988	9.735	9.880	0.253
4575	32-3-N-3-D	2.0-3.0	7.819	7.730	7.602	7.717	0.217
4576	32-3-N-3-E	3.0-4.0	6.311	6.485	6.518	6.438	0.207
4577	32-3-N-3-F	4.0-5.0	6.813	6.911	6.677	6.800	0.234
4578	32-3-N-3-G	5.0-6.0	5.050	5.090	5.268	5.136	0.218
4579	32-3-N-6-A	0.0-0.5	25.747	25.975	25.973	25.898	0.228
4580	32-3-N-6-B	0.5-1.0	23.342	23.273	23.304	23.306	0.069
4581	32-3-N-6-C	1.0-2.0	20.490	20.211	20.372	20.358	0.279
4582	32-3-N-6-D	2.0-3.0	14.128	13.946	13.902	13.992	0.226
4583	32-3-N-6-E	3.0-4.0	14.310	14.392	14.117	14.273	0.275
4584	32-3-N-6-F	4.0-5.0	12.297	12.319	12.133	12.250	0.186
4585	32-3-N-6-G	5.0-6.0	11.428	11.318	11.383	11.376	0.110
4586	32-3-N-7-A	0.0-0.5	3.130	3.094	3.130	3.118	0.036
4587	32-3-N-7-B	0.5-1.0	4.387	4.458	4.624	4.490	0.237
4588	32-3-N-7-C	1.0-2.0	3.065	3.122	3.102	3.096	0.057
4589	32-3-N-7-D	2.0-3.0	1.944	1.973	2.002	1.973	0.058
4590	32-3-N-7-E	3.0-4.0	1.220	1.231	1.209	1.220	0.022
4591	32-3-N-7-F	4.0-5.0	0.931	0.976	0.938	0.948	0.045
4592	32-3-N-7-G	5.0-6.0	0.656	0.686	0.642	0.661	0.044

*** ALL READINGS ARE IN LBS/YD³ ***

Florida Department of Transportation

JEB BUSH	State Materials Office	JOSÉ ABREU
GOVERNOR	5007 NE 39th Avenue, Gainesville, FL 32609	SECRETARY
	Phone (352) 955-6695, Fax (352) 955-6689	

CORROSION RESEARCH LAB

CHLORIDE TEST RESULTS

SUBMITTED BY: Bill Scannell			TESTED BY: PSI				
LAB NUMBER: 4579 - 4606			REPORT DATE: January 27, 2005				
LAB #	SAMPLE #	DESCRIPTION	TEST #1	TEST #2	TEST #3	AVG. Cl⁻	Cl⁻ RANGE
		BRYANT GRADY PATTON BRIDGE					
		BRIDGE#490003					
4593	44-2-N-1-A	0.0-0.5	18.569	18.985	18.884	18.813	0.416
4594	44-2-N-1-B	0.5-1.0	16.492	16.927	17.017	16.812	0.525
4595	44-2-N-1-C	1.0-2.0	17.062	16.861	17.247	17.057	0.386
4596	44-2-N-1-D	2.0-3.0	14.018	14.111	14.355	14.161	0.337
4597	44-2-N-1-E	3.0-4.0	12.435	12.630	12.794	12.620	0.359
4598	44-2-N-1-F	4.0-5.0	11.067	10.961	10.957	10.995	0.110
4599	44-2-N-1-G	5.0-6.0	10.260	10.596	9.963	10.273	0.633
4600	44-2-N-3-A	0.0-0.5	20.062	19.933	19.801	19.932	0.261
4601	44-2-N-3-B	0.5-1.0	16.966	16.973	17.258	17.066	0.292
4602	44-2-N-3-C	1.0-2.0	13.277	13.447	13.320	13.348	0.170
4603	44-2-N-3-D	2.0-3.0	8.979	8.879	9.026	8.961	0.147
4604	44-2-N-3-E	3.0-4.0	5.999	5.866	5.866	5.910	0.133
4605	44-2-N-3-F	4.0-5.0	3.739	3.550	3.374	3.554	0.365
4606	44-2-N-3-G	5.0-6.0	1.652	1.648	1.655	1.652	0.007
4607	44-2-N-6-A	0.0-0.5	30.239	30.746	30.042	30.342	0.704
4608	44-2-N-6-B	0.5-1.0	24.310	24.339	24.339	24.329	0.029
4609	44-2-N-6-C	1.0-2.0	20.436	20.041	20.261	20.246	0.395
4610	44-2-N-6-D	2.0-3.0	19.451	19.161	19.585	19.399	0.424
4611	44-2-N-6-E	3.0-4.0	14.732	14.610	14.703	14.682	0.122
4612	44-2-N-6-F	4.0-5.0	13.604	13.630	13.777	13.670	0.173
4613	44-2-N-6-G	5.0-6.0	14.549	14.298	14.404	14.417	0.251
4614	44-2-N-7-A	0.0-0.5	5.122	5.115	5.198	5.145	0.083
1615	44-2-N-7-B	0.5-1.0	7.310	7.203	6.771	7.095	0.539
4616	44-2-N-7-C	1.0-2.0	5.223	5.175	5.191	5.196	0.048
4617	44-2-N-7-D	2.0-3.0	3.536	3.462	3.454	3.484	0.082
4618	44-2-N-7-E	3.0-4.0	1.672	1.745	1.666	1.694	0.079
1619	44-2-N-7-F	4.0-5.0	1.013	0.958	1.021	0.997	0.063
4620	44-2-N-7-G	5.0-6.0	0.371	0.384	0.355	0.370	0.029

*** ALL READINGS ARE IN LBS/YD³ ***

19 Appendix D – Detailed Description of Structural Testing

29-2

Pre-Test Condition
Minimal to no damage was visible on this pile.

Pre-Test Photos

Post-Test Condition
First crack appeared at 14 kips. Concrete 6 in below the top face of the pile just north of the north load point was crushed severely. Flexural cracks were present after unloading

Post-Test Photos
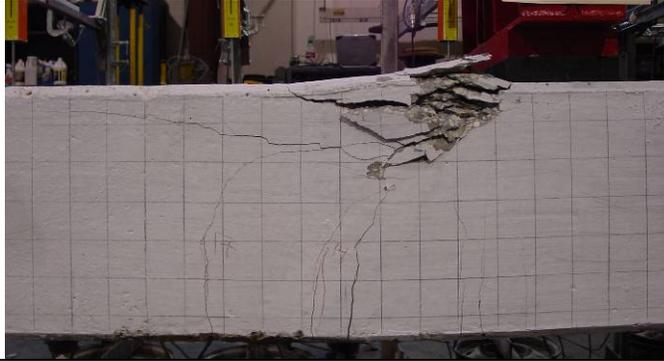
Load Deflection Plot
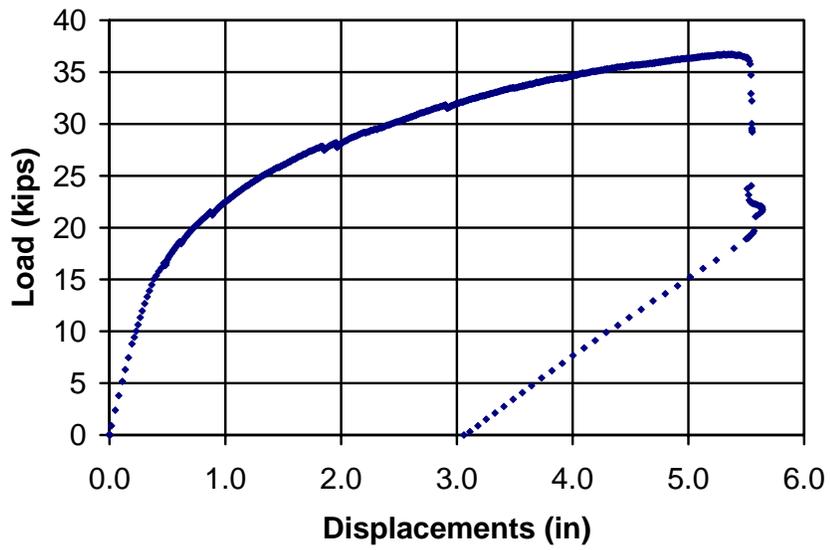
Moment Curvature Plot
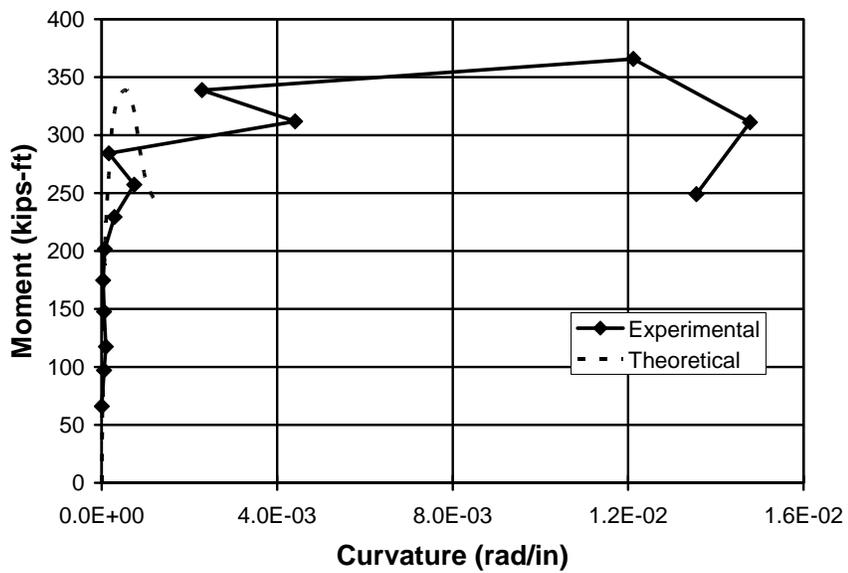
31-1

Pre-Test Condition
Minimal damage was visible on the pile.
Pre-Test Photos
Post-Test Condition
First crack appeared at 28 kips. The compression zone concrete was only slightly crushed. The pile showed compression zone crushing to a limited extent. The flexural cracks mostly closed after unloading.
Post-Test Photos
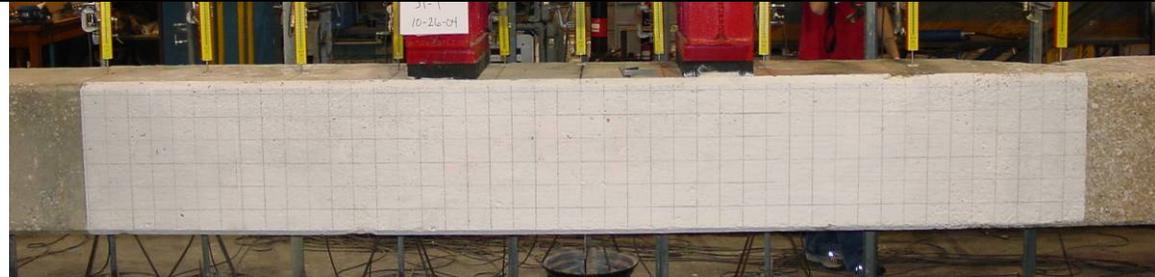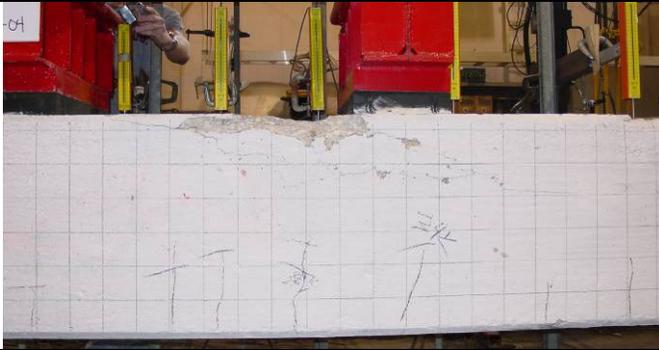
Load Deflection Plot
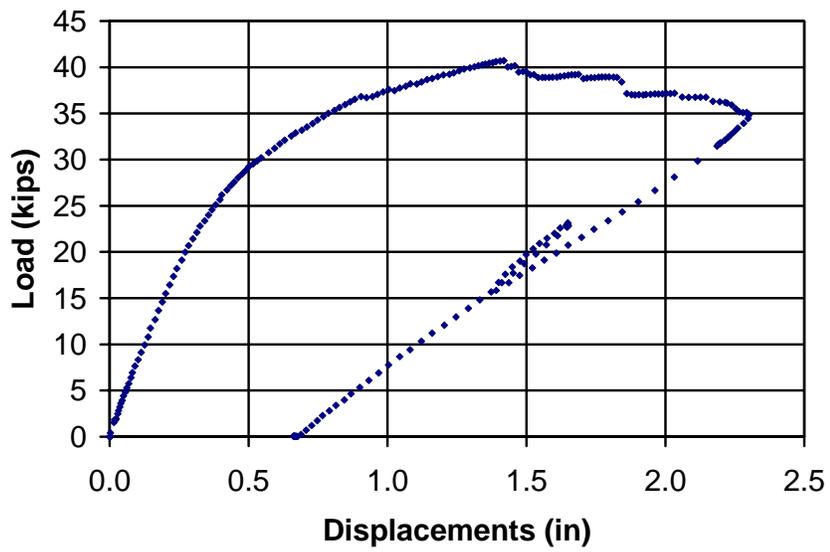
Moment Curvature Plot
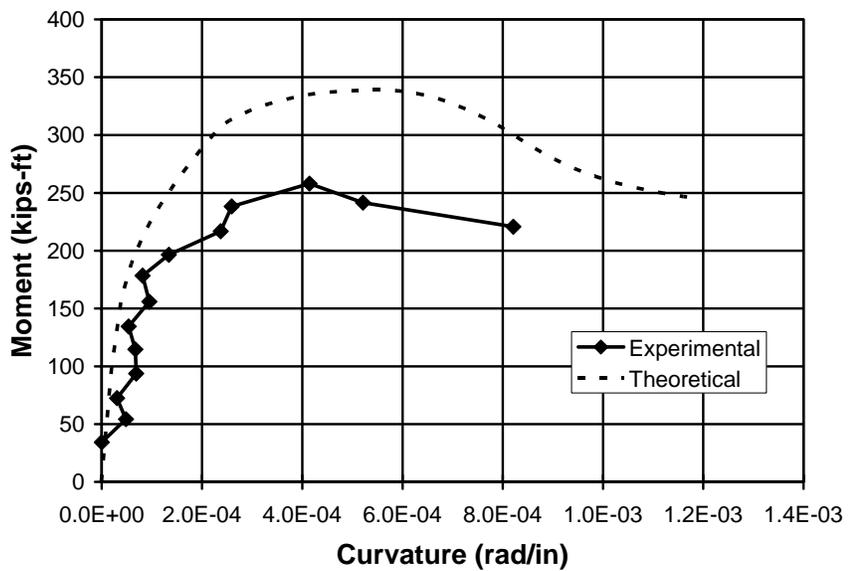
32-3J

Pre-Test Condition
Severe spalling, corrosion and strand damage were visible. Under the northern load application point, the bottom west corner had spalled off to expose the steel strands which were completely rusted through and had debonded from the concrete.

Pre-Test Photos

Post-Test Condition
The first crack occurred at 10 kips. The failure of this pile included a long horizontal crack from the north to the south support. Flexural cracks were also emanating from the missing concrete section in the tension zone. The concrete just to the south of the south load point was crushed in compression. The concrete in the tension region of the splash zone was removed after testing. All of the strands in this location were severely corroded. Five of the six strands had been corroded completely through and all of the wires broken.

Post-Test Photos

Load Deflection Plot
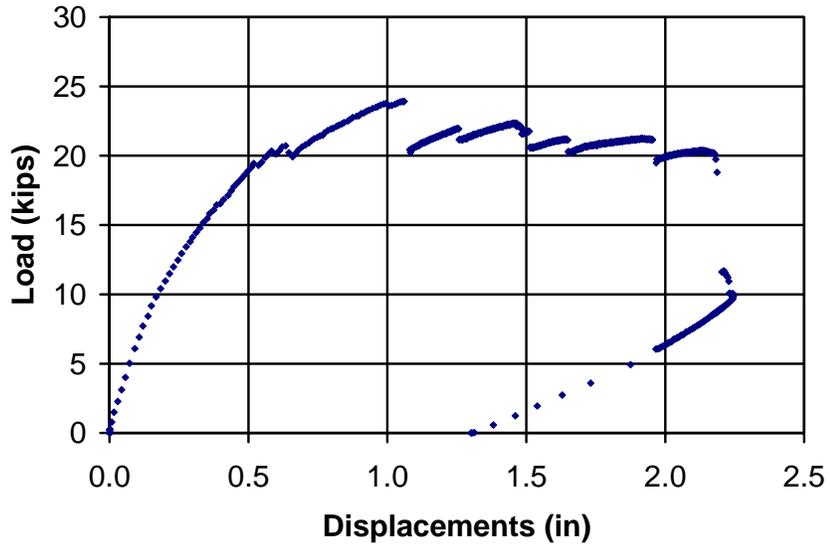
Moment Curvature Plot
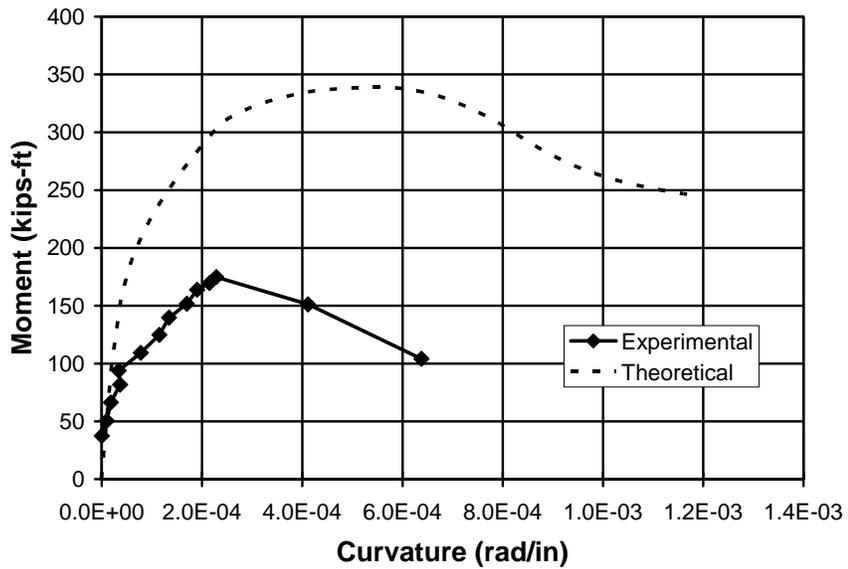
33-4J

Pre-Test Condition

Concrete had spalled off from the bottom west corner of the cross section under the north loading point. Strands were exposed and rust was visible.

Pre-Test Photos

Post-Test Condition

There were flexural cracks visible on the pile. The concrete in the compression zone was only slightly crushed at the completion of the test.

Post-Test Photos

OCT 21 2004

Load Deflection Plot
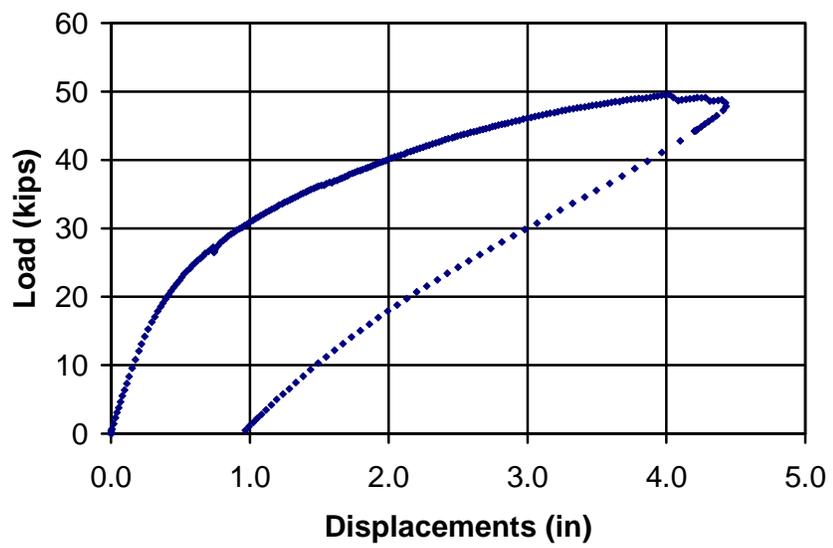
Moment Curvature Plot
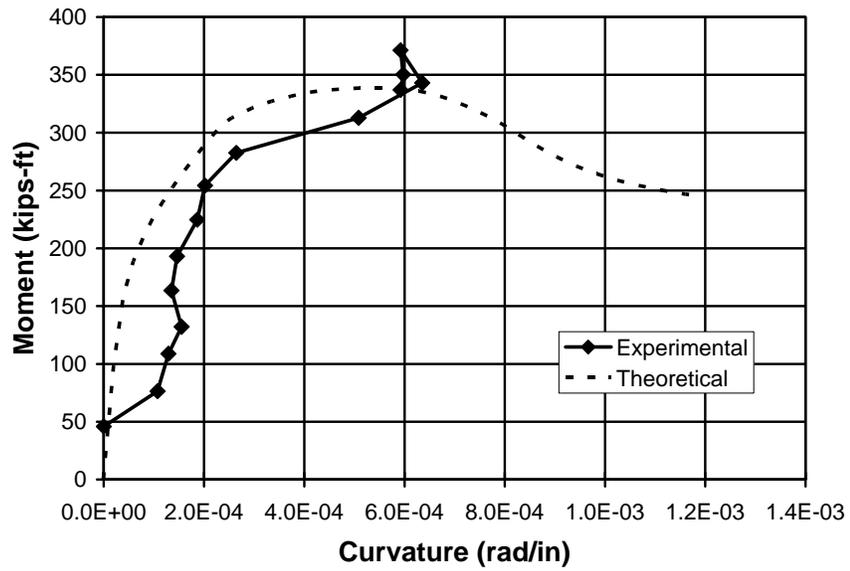
39-2

Pre-Test Condition

Minimal damage was visible on the majority of the pile. However, one crack was visible at the bottom of the west face of the pile, under the northern load point. The crack was approximately 30" long, running parallel with the bottom layer of steel at approximately 3" from the bottom edge.

Pre-Test Photos
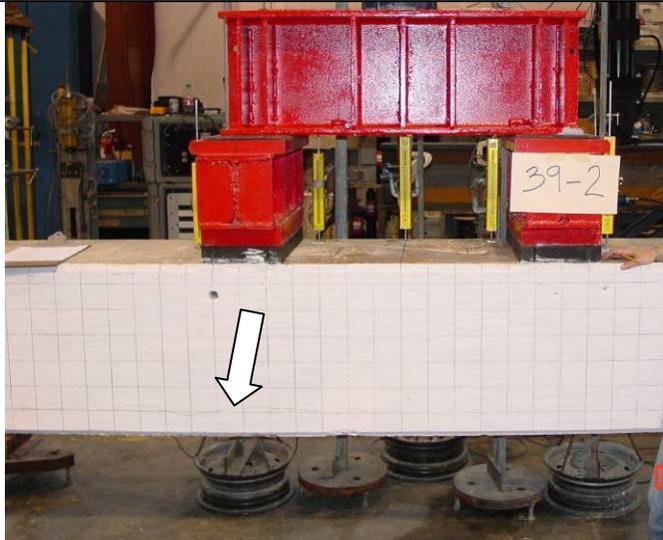
Post-Test Condition

First crack appeared at 10 kips. Concrete 4 in below the top face of the pile began to crush. Flexural cracks emanating from one major crack just below the north support. This crack caused a large piece of concrete on the bottom face of the west corner to come off. This revealed corroded strands. After testing, the concrete in the tension zone of the pile was removed. This revealed that all of the strands had broken wires and one of the strands was severely damaged by corrosion. All of the strands had corrosion damage.

Post-Test Photos
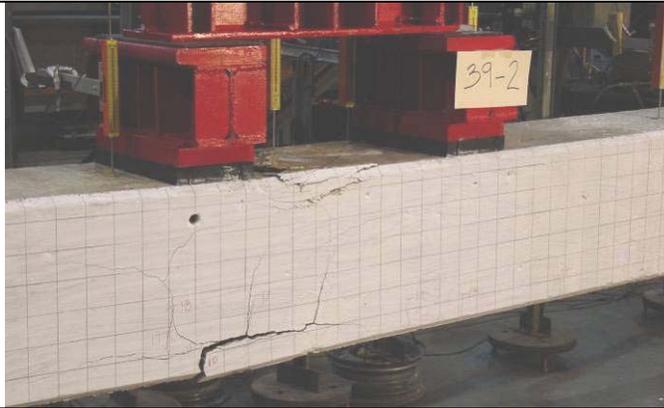
Load Deflection Plot
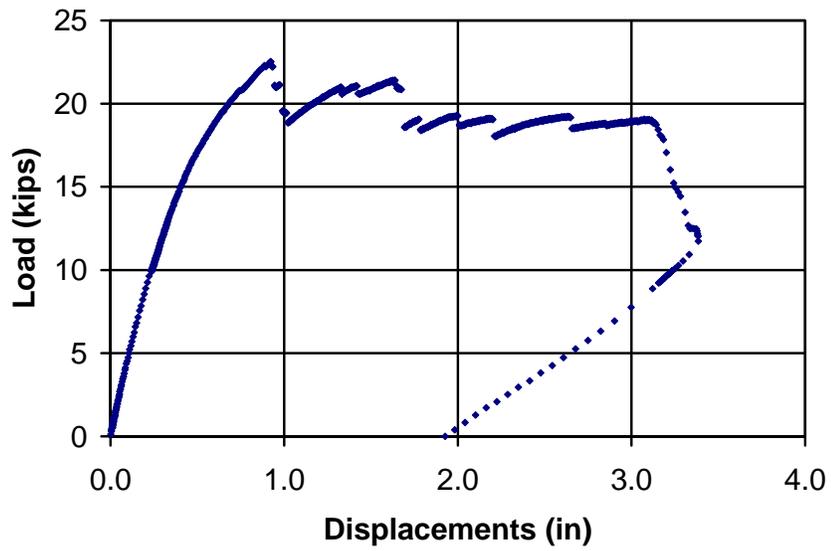
Moment Curvature Plot
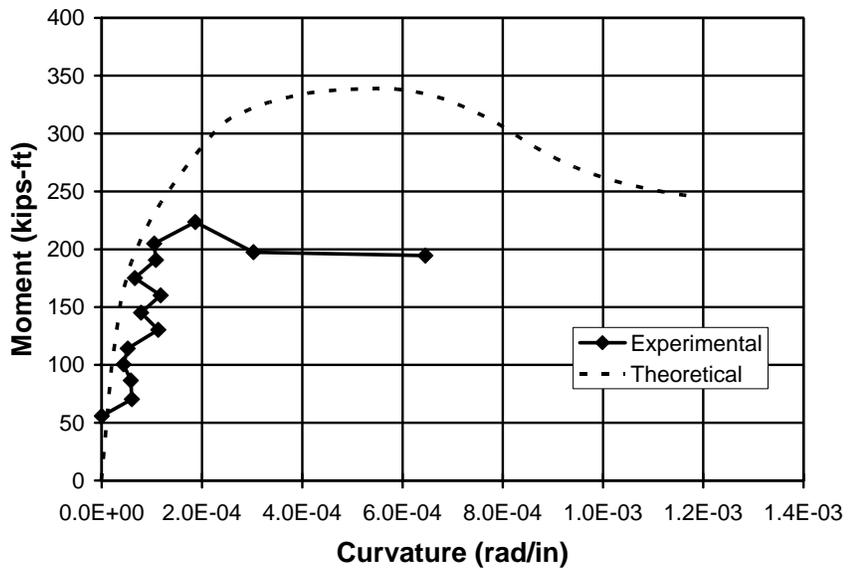
40-2

Pre-Test Condition
Cracks up to eight feet long were visible at the bottom side of the pile on both east and west faces. The crack was approximately 3" to 4" above the bottom edge of the pile. Rust staining was visible through the crack on the east face of the pile.

Pre-Test Photos

Post-Test Condition
Cracking first appeared on this pile at 15 kips. Many flexural cracks were emanating off of the horizontal crack. Eventually all of the concrete below the horizontal crack fell off. This revealed that all of the strands were severely corroded and all the strands were broken. Crushing of the compression zone occurred between the load points. A dip in the load-deflection plot between 1" and 1.5" deflection may relate to the concrete falling off.

Post-Test Photos

Load Deflection Plot
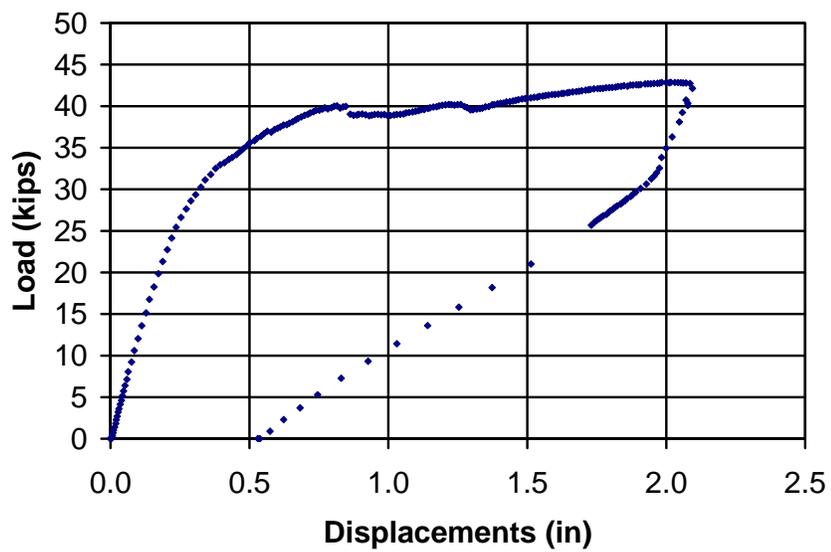
Moment Curvature Plot
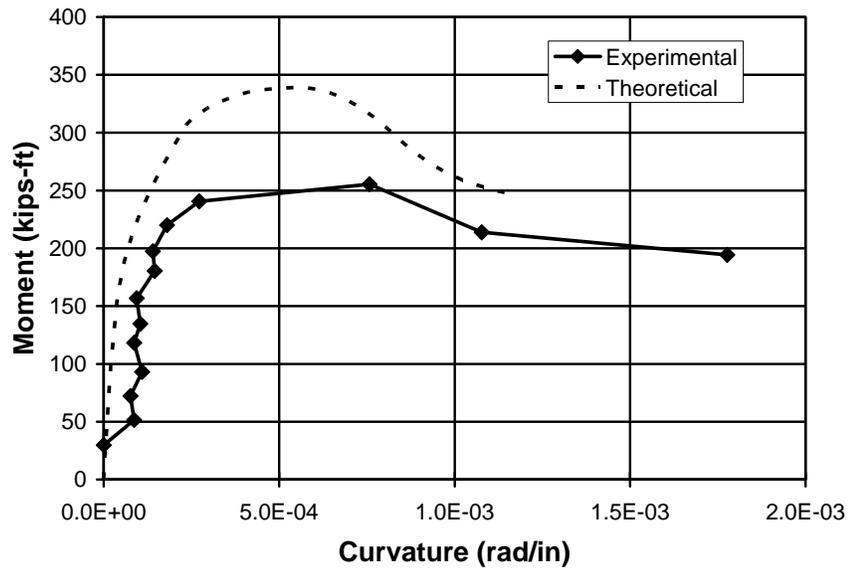
40-3J

Pre-Test Condition
Severe damage and spalling was evident on this pile. The bottom face of the cross section was missing prior to testing. Each strand on the bottom face of the pile was completely rusted through, had debonded and some were no longer intact. On the east face of the pile, a gap of approximately 12 in. wide and 12 in. high exposed another strand, which was also rusted and had debonded. Spalling and rust staining were extensive.
Pre-Test Photos

Post-Test Condition

First crack appeared at 12 kips. Flexural cracks appeared mostly under the North load point. The concrete of the top face began to crush. Large pieces of concrete spalled off on the east side of the pile exposing more corroded strands.

Post-Test Photos

Load Deflection Plot
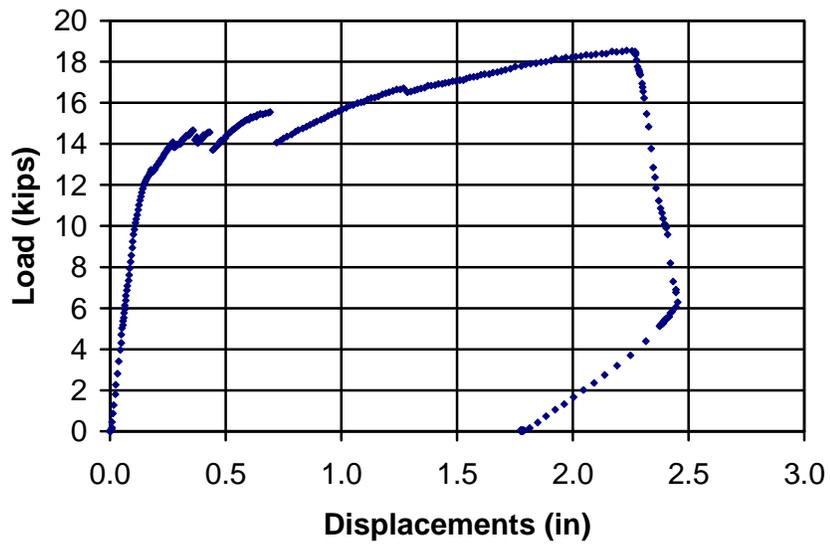
Moment Curvature Plot
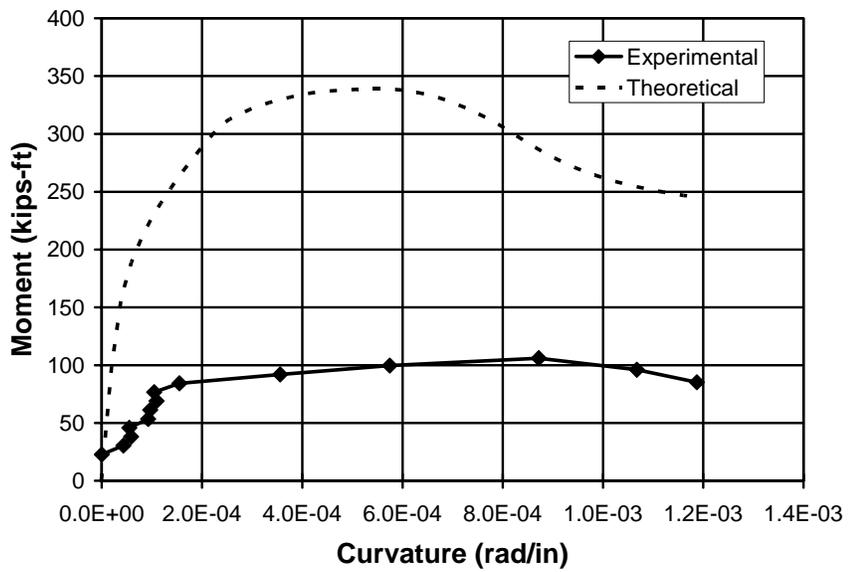
40-4

Pre-Test Condition

Some damage was evident on this pile. One vertical crack was visible on the west face of the pile in the middle of the splash zone. Some concrete spalling and subsequent patching was also evident.

Pre-Test Photos

Post-Test Condition

First crack appeared at 10 kips. Concrete on the top face of the pile, in between the load points was crushed. Flexural cracks were present but were not very large.

Post-Test Photos

Load Deflection Plot
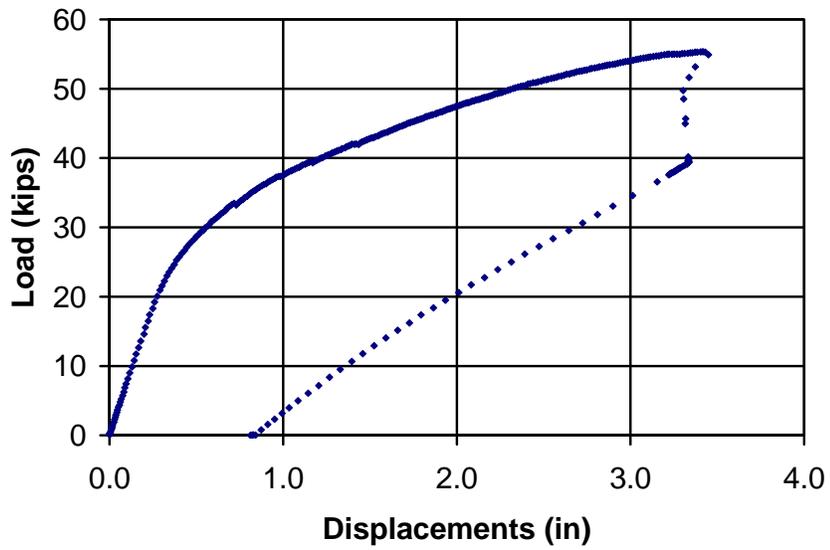
Moment Curvature Plot
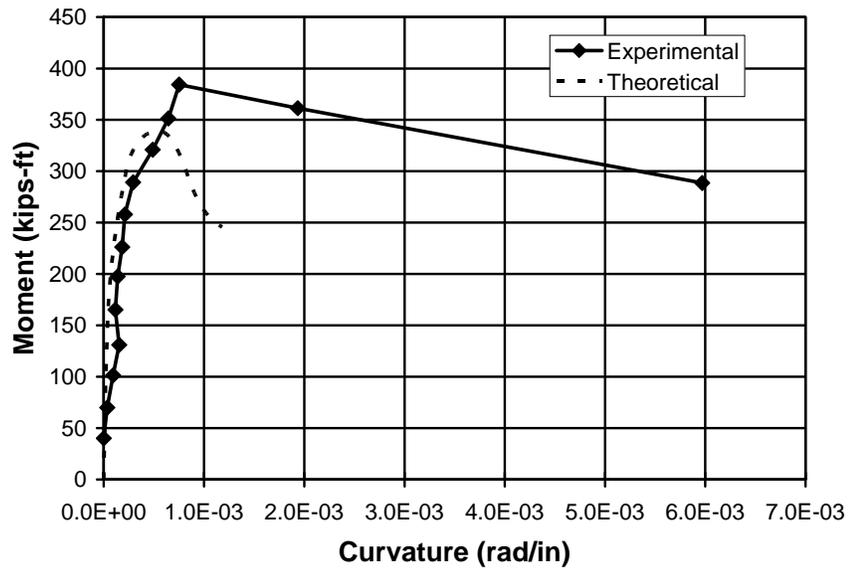
44-1CP

Pre-Test Condition
There were some small holes visible on the exterior of the pile, and minimal damage aside from one area on the bottom west corner approximately 2 ft. north of the north load point where a piece of concrete had chipped off.

Pre-Test Photos

Post-Test Condition
First crack appeared at 14 kips. The pile had multiple flexural cracks. One large flexural crack extended up from just under the north load point. The concrete on the top face was not crushed.

Post-Test Photos

Underside of pile (bottom face of cross section)

Load Deflection Plot
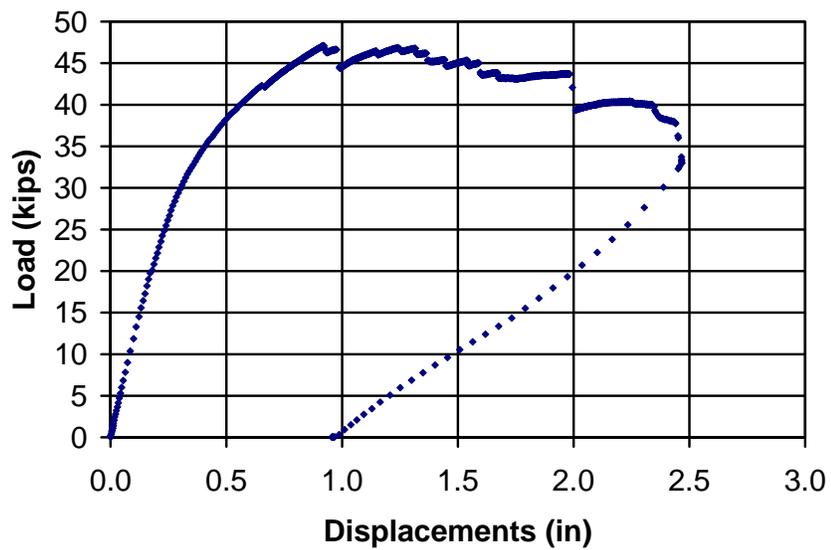
Moment Curvature Plot
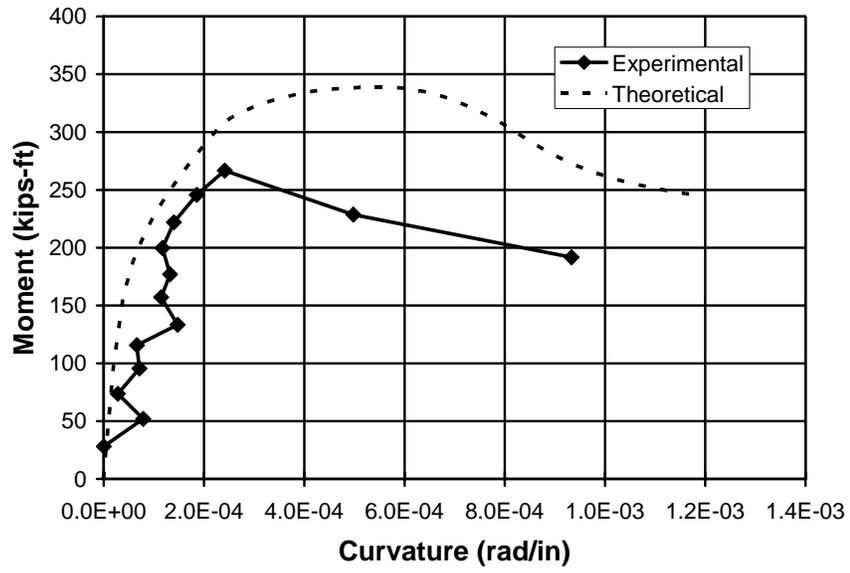
44-2

Pre-Test Condition
Minimal damage was visible in the splash zone of the pile.

Pre-Test Photos

Post-Test Condition
The first crack appeared at 24 kips. This pile had multiple flexural cracks within the splash zone. The concrete under the north support crushed. After testing, the cover was taken off the bottom face (tension zone) strands. There were a few broken wires but none of them were corroded very badly.

Post-Test Photos

Load Deflection Plot
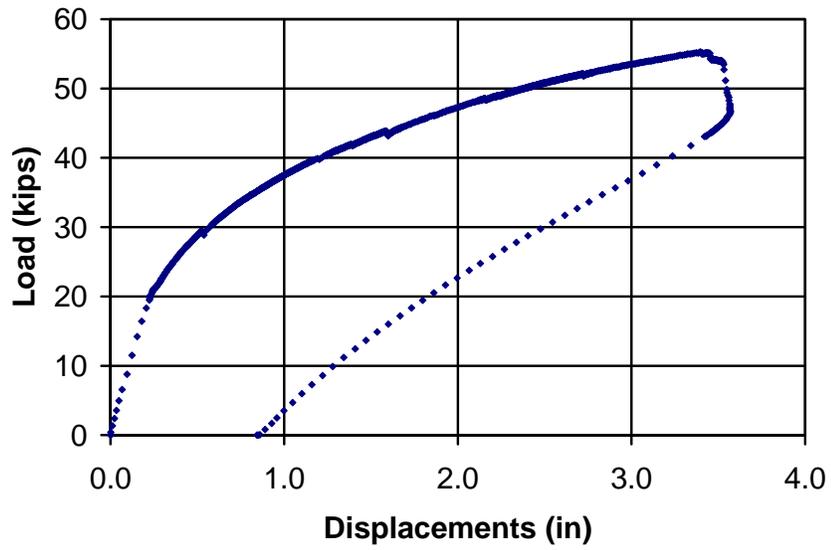
Moment Curvature Plot
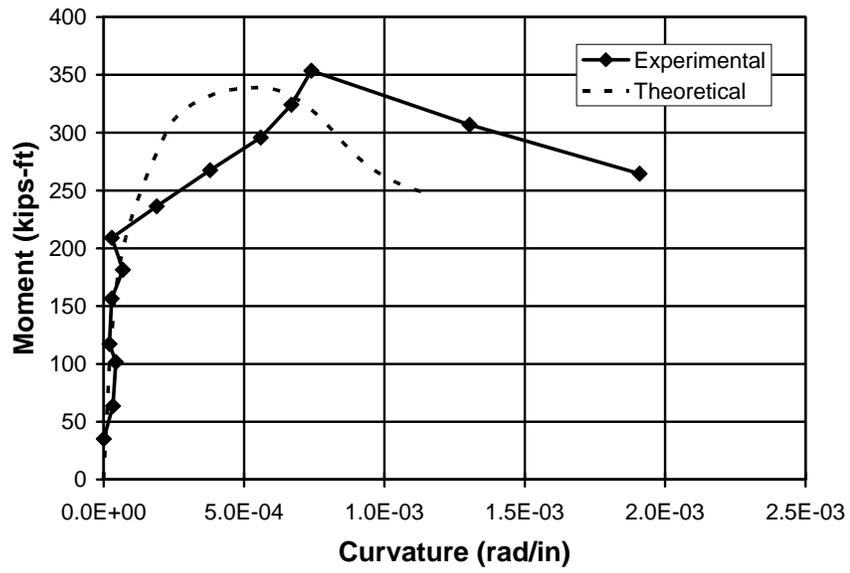
44-3CP

Pre-Test Condition
Minimal to no damage was visible on this pile.

Pre-Test Photos

Post-Test Condition
First crack appeared at 10 kips. A very large flexural crack opened up about midway between the north and south load points. This was the only crack visible and was approximately ¼ in wide after the load was removed. The crack extended through the bottom face of the pile to the east face. Removal of the tension face concrete revealed that this pile had been patched. The strands in this pile were also severely corroded. Many of the strands were completely corroded.

Post-Test Photos

Load Deflection Plot
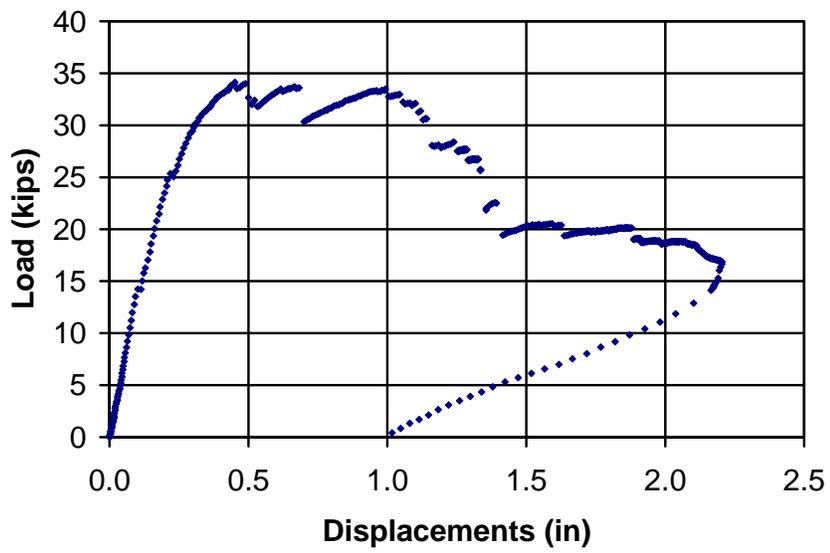
Moment Curvature Plot
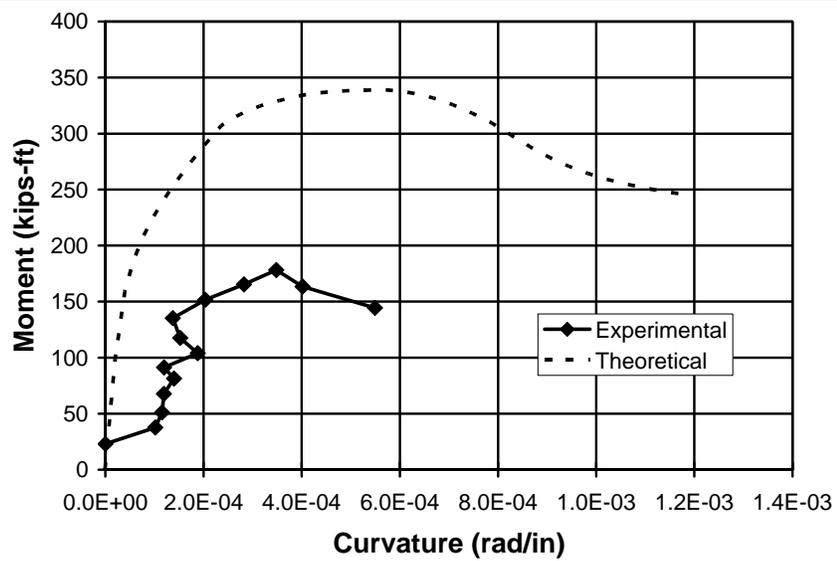
44-4 (No photos available)

Load Deflection Plot
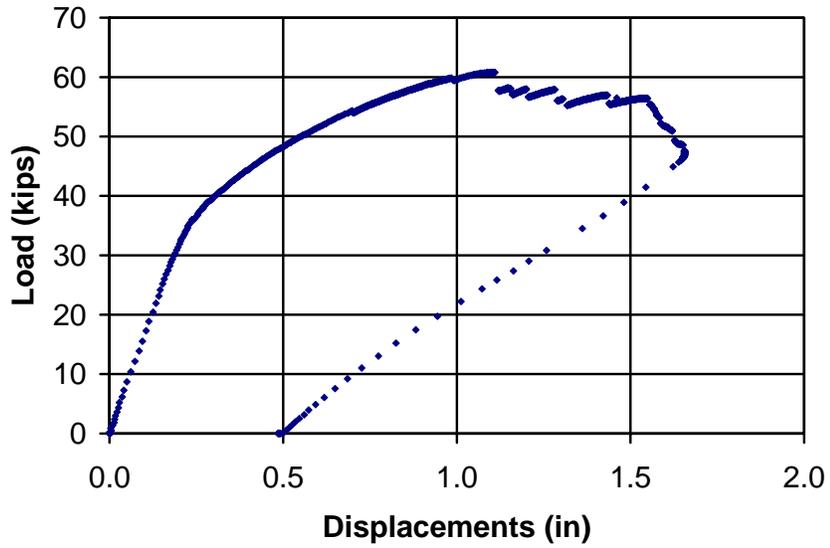
Moment Curvature Plot
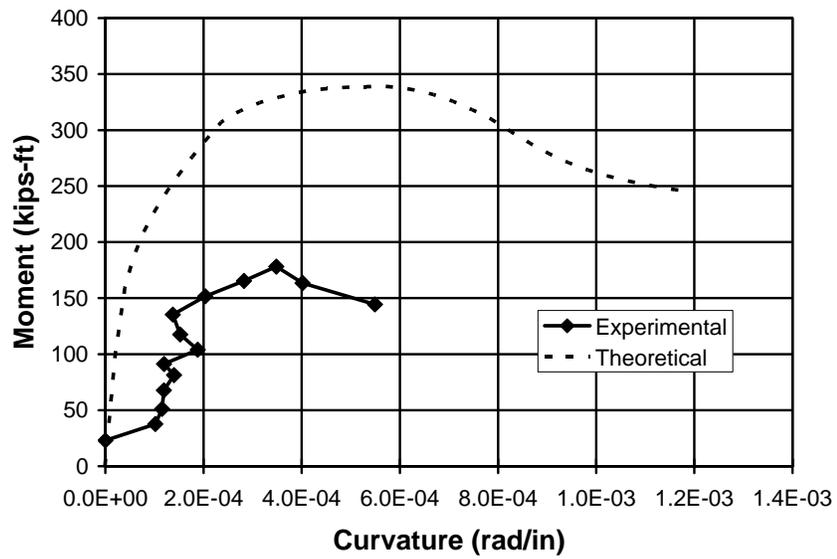
20 Appendix E – Prestressing Strand Tests

Physical Laboratory Raw Data Worksheet	Seven Wire Strand ASTM 416	Revised / Effective Date: 12/27/04 By: J. Fitzgerald	Page 1 of 1

Lims Number					
Project Number	St. George FS				
Sample Number	1	2	3	4	5
Ident.	7/16	7/16	7/16	7/16	7/16
Total Load	29100	28900	28500	28500	28800
Yield @ 1%	25850	25680	25030	25220	26120
Wt / 1000'	N/A	N/A	N/A	N/A	N/A
Elong %	7.8	7.8	8.5	8.1	7.0
Area	.110	.110	.110	.110	.110
Dia.	0.426	0.425	0.427	0.425	0.426
Inner Dia.	0.146	0.145	0.145	0.144	0.146
Outer Dia.	0.141	0.141	0.141	0.141	0.141
Diff	.005	.004	.004	.063	.005
Length	48"	48"	48"	48"	48"
Weight (g)	N/A	N/A	N/A	N/A	N/A
Grip Length	29.5	29.5	29.5	29.5	29.5
Ruler #1	30.0	30.0	30.0	30.0	30.0
Ruler #2	32.0	32.0	32.2	32.1	32.0
MOE	27.8	28.2	38.5	30.4	28.0
Date	2/17/05	2/17/05	2/17/05	2/17/05	2/17/05
Name	RD	RD	RD	RD	RD

K:\Physical Lab\Raw Data\Raw Data Sheets\New Forms\Cable.doc

Florida Department of Transportation
State Materials Office
Gainesville, Florida

CABLE
Program #189,779-R3

Lab No.:	
Project No.:	St George Island
Sample No.:	1
Material No.:	540
Size:	7/16
Grade:	270
Date Tested:	02/17/05
Coil No.:	
Ultimate, lbf:	29100
EUL @ 1, lbf:	25850
Modulus, psi:	27800000
CS Area, in²:	.110
:METRIC :	
Ultimate, kN:	129.4
EUL @ 1, kN:	115.0
Modulus, MPa:	191800
CS Area, mm²:	71.24
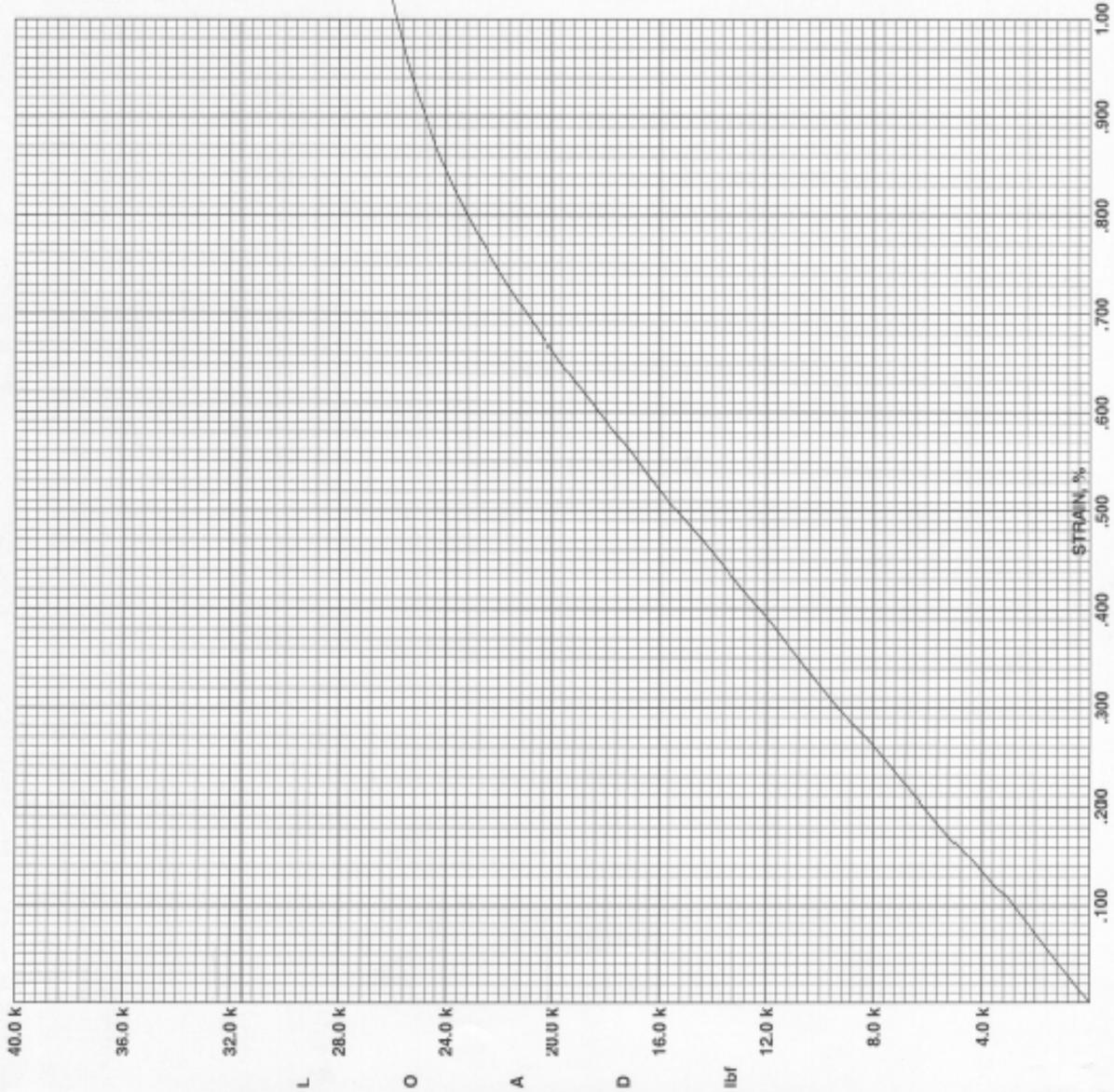
Specimen Break
Feb 18, 2005 2:46:31 PM

Florida Department of Transportation
State Materials Office
Gainesville, Florida

CABLE
Program #189,779-R3

Lab No.:	
Project No.:	St George Island
Sample No.:	2
Material No.:	540
Size:	7/16
Grade:	270
Date Tested:	02/17/05
Coil No.:	
Ultimate, lbf:	28900
EUL @ 1, lbf:	25620
Modulus, psi:	28200000
CS Area, in²:	.110
:METRIC :	
Ultimate, kN:	128.6
EUL @ 1, kN:	113.9
Modulus, MPa:	194400
CS Area, mm²:	71.10
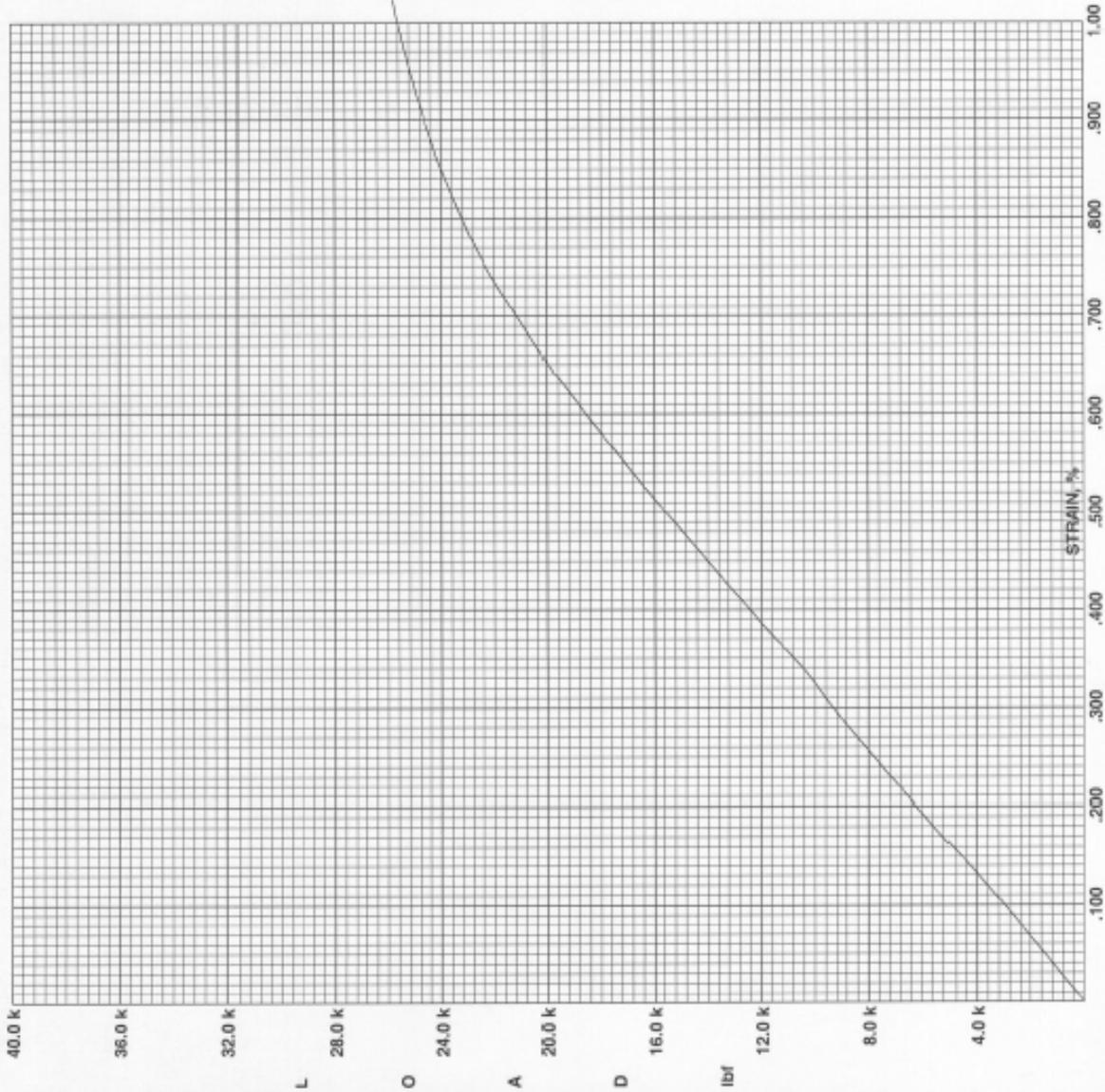
Specimen Break
Feb 18, 2005   2:55:38 PM

STRAIN, %

Florida Department of Transportation
State Materials Office
Gainesville, Florida

CABLE
Program #189,779-R3

Lab No.:
Project No.:   St George Island
Sample No.:   3
Material No.:   540
Size: 7/16
Grade: 270

Date Tested: 02/17/05
Coil No.:

Ultimate, lbf: 28500
EUL @ 1, lbf: 25030
Modulus, psi: 285000000
CS Area, in²: .110
:METRIC :
Ultimate, kN: 126.6
EUL @ 1, kN: 111.4
Modulus, MPa: 196400
CS Area, mm²: 71.10
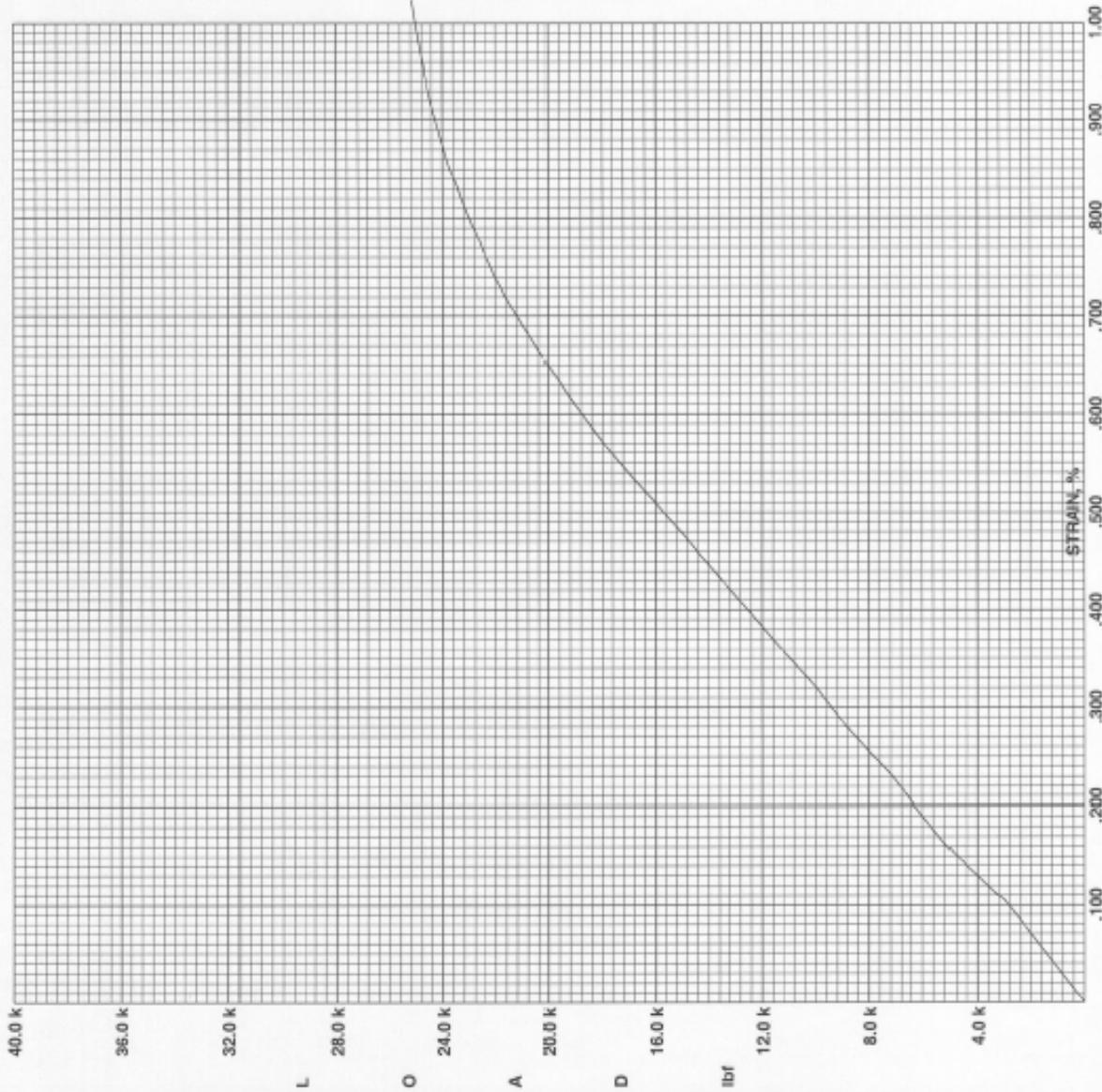
Specimen Break
Feb 18, 2005   3:03:00 PM

STRAIN, %

.100 .200 .300 .400 .500 .600 .700 .800 .900 1.00

4.0 k 8.0 k 12.0 k 16.0 k 20.0 k 24.0 k 28.0 k 32.0 k 36.0 k 40.0 k

lbf

L O A D

Florida Department of Transportation
State Materials Office
Gainesville, Florida

CABLE
Program #189,779-R3

Lab No.:	
Project No.:	St George Island
Sample No.:	4
Material No.:	540
Size:	7/16
Grade:	270
Date Tested:	02/17/05
Coil No.:	
Ultimate, lbf:	28500
EUL @ 1, lbf:	25220
Modulus, psi:	30400000
CS Area, in²:	.110
:METRIC :	
Ultimate, kN:	126.9
EUL @ 1, kN:	112.2
Modulus, MPa:	210000
CS Area, mm²:	70.95
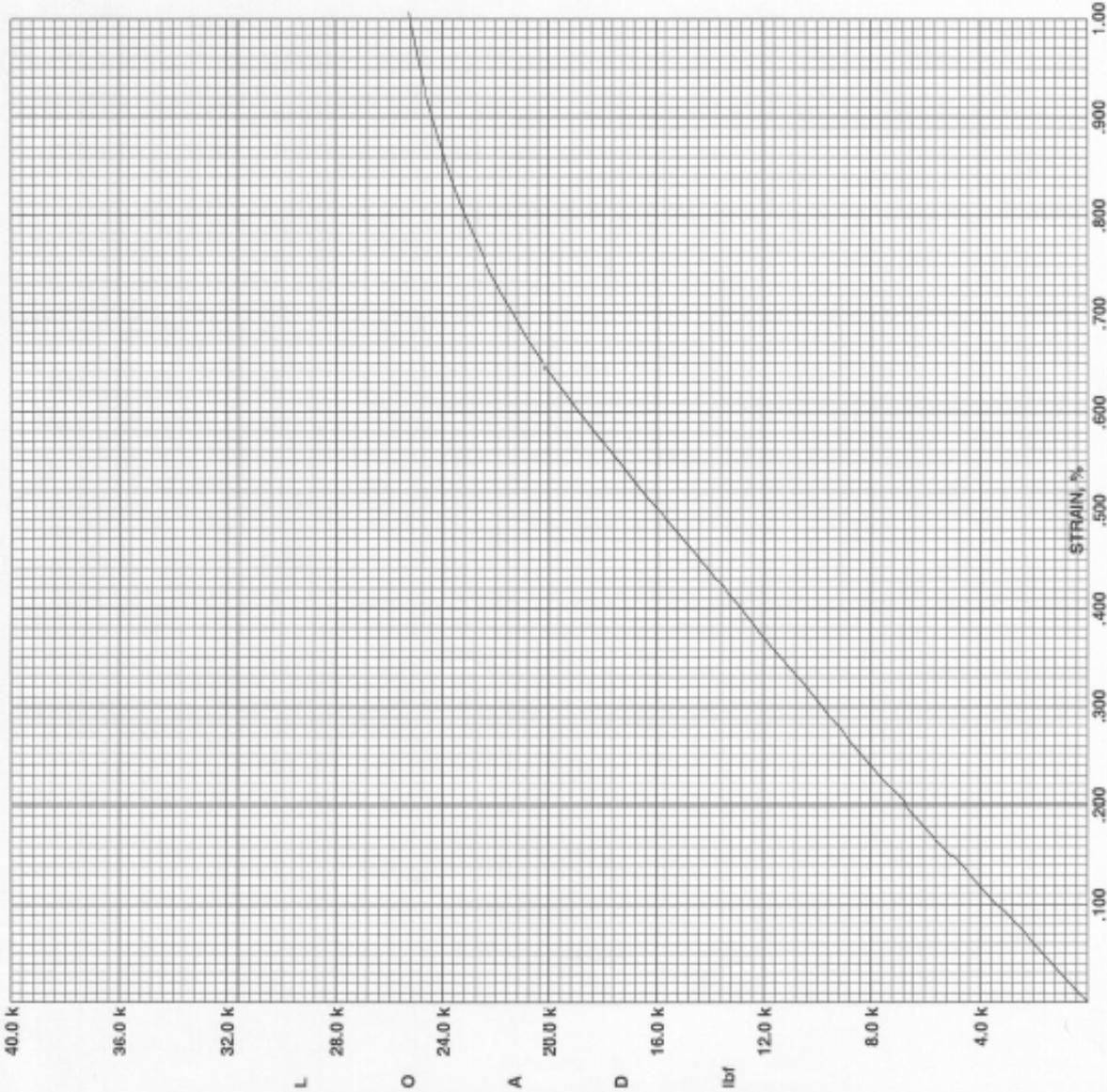
Specimen Break
Feb 18, 2005   3:09:16 PM

Florida Department of Transportation
State Materials Office
Gainesville, Florida

CABLE
Program #189,779-R3

Lab No.:	
Project No.:	St George Island
Sample No.:	5
Material No.:	540
Size:	7/16
Grade:	270
Date Tested:	02/17/05
Coil No.:	
Ultimate, lbf:	28800
EUL @ 1, lbf:	26120
Modulus, psi:	2.8E+07
GS Area, in²:	.110
:METRIC :	
Ultimate, kN:	128.0
EUL @ 1, kN:	116.2
Modulus, MPa:	193200
CS Area, mm²:	71.24
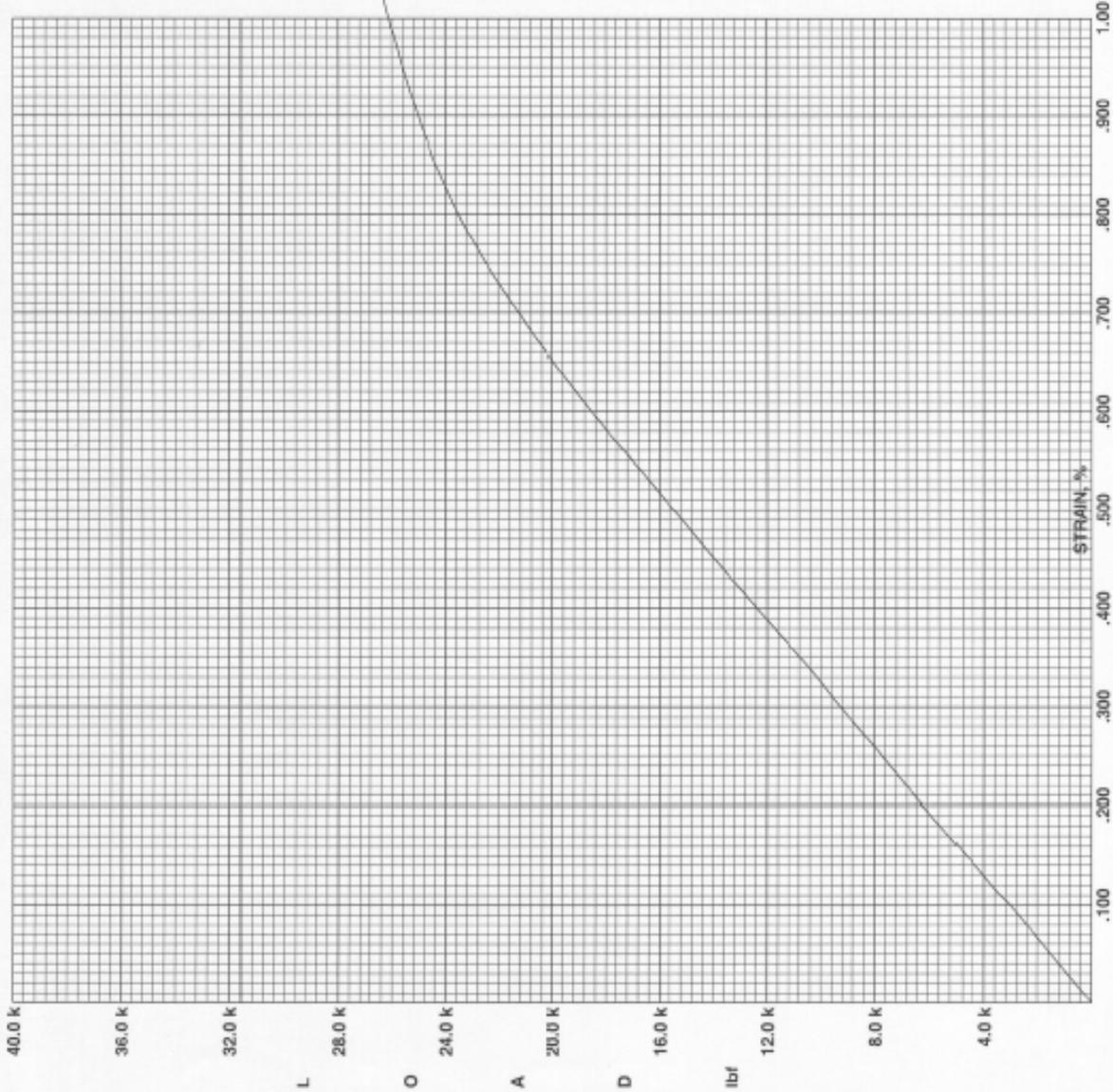
Specimen Break
Feb 18, 2005 3:15:44 PM